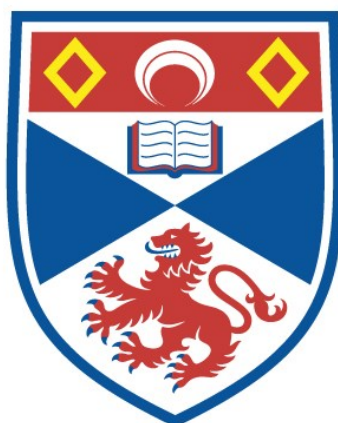# LAMINAR CONTRIBUTIONS OF SUPERFICIAL LATERAL ENTORHINAL CORTEX TO EPISODIC MEMORY

Brianna Vandrey

A Thesis Submitted for the Degree of PhD
at the
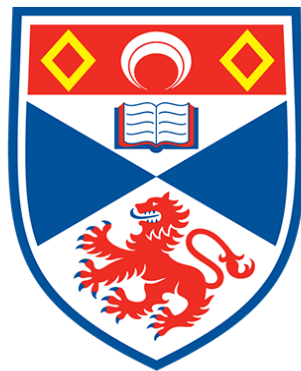University of St Andrews

2018

Laminar Contributions of Superficial Lateral Entorhinal Cortex to Episodic Memory

Brianna Vandrey

This thesis is submitted in partial fulfilment for the degree of

Doctor of Philosophy (PhD)

at the University of St Andrews

June 2018

Candidate's declaration

I, Brianna Vandrey, do hereby certify that this thesis, submitted for the degree of PhD, which is approximately 39,000 words in length, has been written by me, and that it is the record of work carried out by me, or principally by myself in collaboration with others as acknowledged, and that it has not been submitted in any previous application for any degree.

I was admitted as a research student at the University of St Andrews in September 2014.

I received funding from an organisation or institution and have acknowledged the funder(s) in the full text of my thesis.

Date   Signature of candidate

Supervisor's declaration

I hereby certify that the candidate has fulfilled the conditions of the Resolution and Regulations appropriate for the degree of PhD in the University of St Andrews and that the candidate is qualified to submit this thesis in application for that degree.

Date   Signature of supervisor

Permission for publication

In submitting this thesis to the University of St Andrews we understand that we are giving permission for it to be made available for use in accordance with the regulations of the University Library for the time being in force, subject to any copyright vested in the work not being affected thereby. We also understand, unless exempt by an award of an embargo as requested below, that the title and the abstract will be published, and that a copy of the work may be made and supplied to any bona fide library or research worker, that this thesis will be electronically accessible for personal or research use and that the library has the right to migrate this thesis into new electronic forms as required to ensure continued access to the thesis.

I, Brianna Vandrey, confirm that my thesis does not contain any third-party material that requires copyright clearance.

The following is an agreed request by candidate and supervisor regarding the publication of this thesis:

Printed copy

Embargo on all of print copy for a period of 5 years on the following ground(s):

- Publication would be commercially damaging to the researcher, or to the supervisor, or the University
- Publication would preclude future publication

Supporting statement for printed embargo request

Thesis contains data which is pending publication.

Electronic copy

Embargo on all of electronic copy for a period of 5 years on the following ground(s):

- Publication would be commercially damaging to the researcher, or to the supervisor, or the University
- Publication would preclude future publication

Supporting statement for electronic embargo request

Thesis contains data which is pending publication.

Title and Abstract

- I require an embargo on the abstract only.

Date   Signature of candidate

Date   Signature of supervisor

Underpinning Research Data or Digital Outputs

Candidate's declaration

I, Brianna Vandrey, understand that by declaring that I have original research data or digital outputs, I should make every effort in meeting the University's and research funders' requirements on the deposit and sharing of research data or research digital outputs.

Date   Signature of candidate

Permission for publication of underpinning research data or digital outputs

We understand that for any original research data or digital outputs which are deposited, we are giving permission for them to be made available for use in accordance with the requirements of the University and research funders, for the time being in force.

We also understand that the title and the description will be published, and that the underpinning research data or digital outputs will be electronically accessible for use in accordance with the license specified at the point of deposit, unless exempt by award of an embargo as requested below.

The following is an agreed request by candidate and supervisor regarding the publication of underpinning research data or digital outputs:

Embargo on all of electronic files for a period of 5 years on the following ground(s):

- Publication would be commercially damaging to the researcher, or to the supervisor, or the University (e.g. Intellectual Property Rights)
- Publication would preclude future publication

Supporting statement for embargo request

Thesis contains data which is pending publication.

Title and Description

- I require an embargo on the description only

Date   Signature of candidate

Date   Signature of supervisor

Acknowledgements

Funding Acknowledgement

Abstract

Episodic memory relies on the hippocampus and its surrounding cortical network. The superficial layers of the entorhinal cortex provide substantial input to the hippocampus within this network. Recent evidence suggests that the lateral entorhinal cortex (LEC) is critical for binding together features of an episode, and single neurons in the LEC encode spatial information about local cues in the environment. However, the relationship between entorhinal-hippocampal circuit components and cognition is unclear. Therefore, the experiments presented in this thesis investigated the functional contributions of projections to the hippocampus from the superficial LEC (layers 2/3; L2/3) to associative memory processes. First, I examined whether input from entorhinal cortex influences the activity of place cells in the CA1 region of the hippocampus. In an environment which contained objects, place cells which receive direct input from LEC L3 demonstrated a higher degree of spatial tuning than place cells which receive input from MEC L3, and exhibited firing patterns which were precisely tied to current and previous object locations. However, further elucidation of this finding was precluded by the lack of a tool which permits the selective manipulation the superficial LEC layers. Therefore, a second set of experiments investigated the arrangement of projecting neurons in LEC L2 and identified a molecular tool, the Sim1:Cre mouse, which permits the precise manipulation of excitatory neurons in LEC L2 which are positive for the protein reelin and project to the dentate gyrus. A final experiment selectively suppressed the output from these neurons in a cohort of Sim1:Cre mice and examined performance on a series of object-based recognition memory tasks. Indeed, inactivation of this pathway resulted in profound impairment on an episodic memory task and mildly impaired novel object recognition. Overall, these data suggest that projections from the superficial LEC to the hippocampus make critical contributions to associative memory processes.

Table of Contents

0.362, $P = 0.730$), which indicates that both groups recognised the novel configurations.

Further, there was no significant difference across groups in the amount of time spent

exploring the objects in standard ($F_{(1, 6)} = 1.594$, $P = 0.162$) or object manipulation trials

Table of Figures

List of Tables

Chapter 1: General Introduction

1.1 Introduction to Episodic Memory and the Brain

Episodic memory is classically defined as memory which 'receives and stores information about temporally dated episodes or events and temporo-spatial relations between them' (Tulving, 1983). In operational terms, an episodic memory is an integrated representation of 'what', 'where', and on 'which occasion' an event occurred, where 'which occasion' is defined as any attribute of an experience, contextual or temporal, which permits experiences to be discriminated from one another (Eacott & Norman, 2004; Eacott & Easton, 2010). Soon after its conception, the definition of episodic memory was expanded to include autonoetic consciousness, a temporal characteristic which permits one to mentally project themselves backwards in time to experience an event from the past (Tulving, 1985). This additional constraint was accompanied by the argument that episodic memory is uniquely human, and may have evolved to support the flexible use of past experiences to approach novel situations and anticipate future needs (Tulving, 1985; Clayton, Busby, Emerson, & Dickinson, 2003; Suddendorf & Busby, 2003; Suddendorf & Corballis, 2007). However, behavioural paradigms have been developed to demonstrate 'episodic-like' memory in animals which meet the original criteria dictated by Tulving, yet do not necessitate autonoetic consciousness (Clayton & Dickinson,1998; Eacott & Norman, 2004; Babb & Crystal, 2005; Dere, Huston, De Souza Silva, 2005; Kart-Teke, De Souza Silva, Huston, & Dere, 2006). These paradigms have been invaluable for studying the neural substrates of episodic memory.

It is well established that episodic memory is dependent on the integrity of the hippocampus, a sub-cortical structure which is seated in the medial temporal lobe of the brain (Scoville & Milner, 1957; Vargha-Khadem et al. 1997; Langston & Wood, 2010). Within the anatomical framework of the medial temporal lobe, the entorhinal cortex is the primary source of cortical input into the hippocampus (Witter & Amaral, 2004; Witter, 2007; Van Strien, Cappaert, & Witter, 2009). Based on the arrangement of entorhinal cortex projections, it has

been suggested that information about an experience converges on the hippocampus via two anatomically segregated pathways; spatial information is relayed via the medial entorhinal cortex (MEC) and non-spatial information is relayed via the lateral entorhinal cortex (LEC), respectively (Naber, Caballero-Bleda, Jorritsma-Byham, & Witter, 1997; Witter et al. 2000; Knierim, Lee & Hargreaves, 2006; Eichenbaum, Sauvage, Fortin, Komorowski, & Lipton, 2012). In this 'parallel processing' model, the entorhinal cortex functions as an interface between the neocortex and the hippocampus, where the two information streams are integrated to form a unified representation of an experience.

Although the parallel processing model has provided a useful framework for experimental work, recent findings indicate that it is reductive. There is mounting evidence that spatial and non-spatial components of an experience are integrated upstream of the hippocampus within the entorhinal cortex (Deshmukh & Knierim, 2011; Van Cauter et al., 2012; Hunsaker, Chen, Tran & Kesner, 2013; Wilson et al. 2013a; Wilson, Watanabe, Milner & Ainge, 2013b). Further, neurons in the LEC exhibit robust spatial tuning under certain experimental conditions, which is inconsistent with the predictions of the parallel processing model (Deshmukh & Knierim, 2011; Deshmukh, Johnson, & Knierim, 2012; Tsao, Moser & Moser, 2013; Keene et al. 2016).

Although the entorhinal cortex has been extensively studied in the past decade, the LEC has received considerably less attention than its medial counterpart. Strikingly, LEC deterioration is an early marker of Alzheimer's disease (see Stranahan & Mattson, 2010; Khan et al. 2014), and selective damage to this structure results in profound memory impairment in rodents (Wilson et al. 2013a; 2013b). These findings compel further research which addresses the role of the LEC in episodic memory. To date, the field has largely examined the LEC in its entirety, rather than considering the role of discrete projection pathways between the entorhinal cortex and the hippocampus. Experiments which tease apart the contributions of entorhinal-

hippocampal circuit components to memory will be critical for extending the understanding of functional connectivity in the medial temporal lobe.

To this end, this introduction reviews the current body of research which has addressed the role of the hippocampus and LEC in episodic memory and other forms of associative recognition. Firstly, the anatomical organisation of the medial temporal lobe is reviewed for reference, with a focus on the connectivity of the entorhinal cortex. Secondly, information processing in the hippocampus and the entorhinal cortex are discussed in turn, with the overarching aim of examining how the LEC and hippocampus interact to encode information about experiences, specifically within the lateral perforant pathway. This review forms the theoretical framework for the experiments presented in this thesis.

1.2 Anatomy of the Medial Temporal Lobe

Panel A of Fig. 1.1 contains a diagram of the medial temporal lobe structures in the rat brain. The medial temporal lobe consists of the hippocampus and parahippocampal cortex. The hippocampus includes the dentate gyrus (DG), regions CA1-CA3, and the subiculum. The parahippocampal cortex includes the entorhinal cortex (MEC and LEC), perirhinal cortex (PER), postrhinal cortex (POR), pre-subiculum and para-subiculum. This section reviews the extrinsic and intrinsic connectivity of the entorhinal cortex (Section 1.2.1) and the known sub-populations of cells within each layer of this structure, with a focus on the LEC (Sections 1.2.2-3). The latter sections concentrate on layers 2, 3, and 5 of the entorhinal cortex, given that layers 1 and 4 are largely devoid of principal cells, and there is little information available regarding the organisation of layer 6.

1.2.1 Extrinsic and Intrinsic Connectivity of the Entorhinal Cortex

The subregions of the entorhinal cortex receive input from two anatomically segregated pathways within the parahippocampal cortex. The MEC is connected to a network of structures which are associated with spatial processing, including the POR, restrosplenial cortex, presubiculum, and parasubiculum. In contrast, the LEC is connected to a network of structures associated with object perception and attention, including the perirhinal, olfactory, insular, and oribito-frontal cortices (Caballero-Bleda & Witter, 2003; Burwell et al. 2000; Kerr, Agster, Furtak, & Burwell, 2007; Van Strien et al. 2009). However, as reviewed here, anatomical work has determined that there is significant overlap between these two networks.

Briefly, the LEC receives substantial input from the PER, which receives dense unimodal input from sensory cortices (Burwell et al. 2000). The MEC receives dense input from the POR, which receives input from parieto-occipital regions. However, the PER and POR are heavily interconnected, and both entorhinal subdivisions receive some input from both structures (Van Strien et al. 2009). The connectivity between the PER-LEC is stronger than the connectivity between the PER-MEC, but the MEC receives equal input from PER and POR (Burwell, 2000; Van Strien et al. 2009). Further, the PER and POR both send sparse projections to CA1 and the subiculum, indicating that output from these structures can exert influence in the hippocampus without passing through the entorhinal cortex (Witter et al. 2000a).

In addition, the para-subiculum projects to the MEC and LEC, whereas connectivity with the pre-subiculum is largely restricted to the MEC (Caballero-Bleda & Witter, 1993), though there may be pre-subiculum projections to the deep LEC (Van Strien et al. 2009). The pre-subiculum and para-subiculum also send sparse projections to all subregions of the hippocampus (Van Strien et al. 2009). Importantly, all connections between parahippocampal
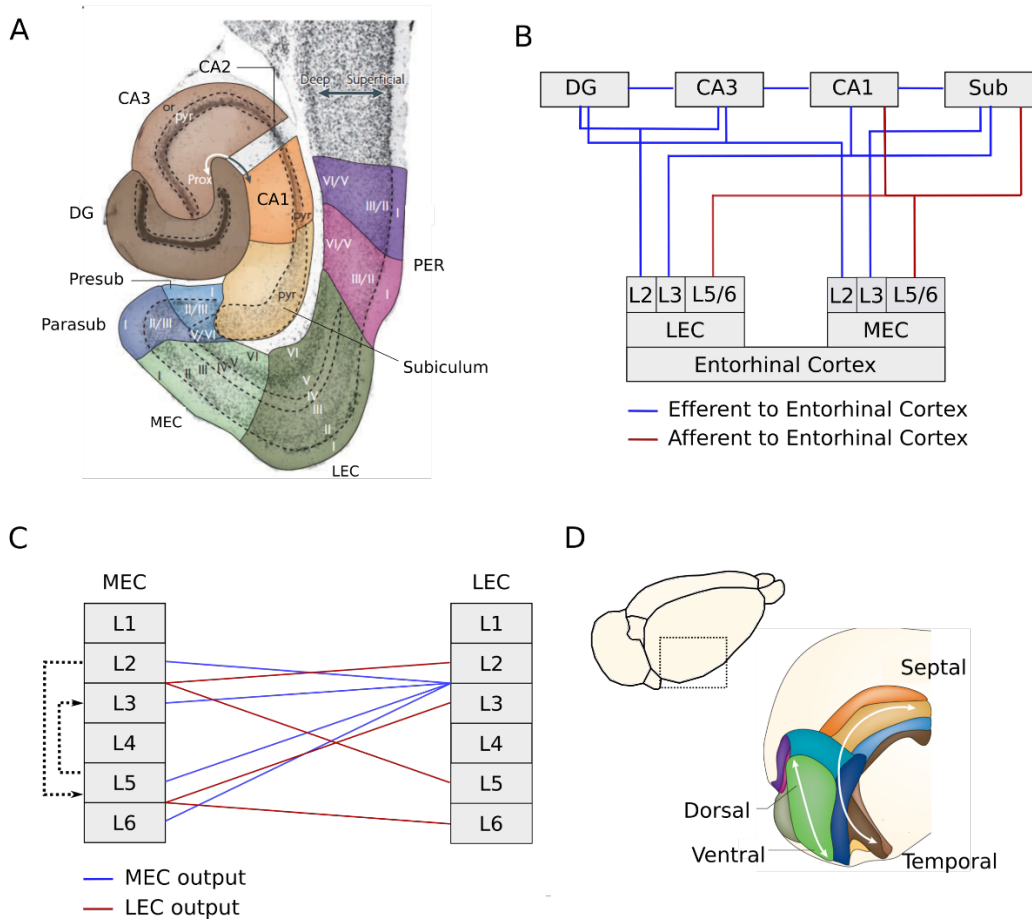
Figure 1.1: Anatomical organisation and connectivity of the entorhinal cortex and hippocampus. A) Horizontal section of rat brain overlaid with colours corresponding to different medial temporal lobe structures. B) Diagram depicting main projections between the entorhinal cortex and the hippocampus. Input pathways are indicated in blue, output pathways are indicated in red. C) Diagram depicting intrinsic connections between the medial and lateral entorhinal cortex. Projections from medial entorhinal cortex (blue) terminate in L2/L3 of lateral entorhinal cortex, and projections from lateral entorhinal cortex (red) terminate in L2/L3 and L5/L6. Black dotted lines indicate microcircuitry of the medial entorhinal cortex. D) Diagram depicting the approximate location and organisation of entorhinal cortex in relation to other medial temporal lobe structures. Colours correspond with structures as depicted in Panel A. Panels A, B & D are adapted from Van Strien et al. 2009. Abbreviations: Presub, pre-subiculum; Parasub, para-subiculum; MEC, medial entorhinal cortex; LEC, lateral entorhinal cortex; PER, perirhinal cortex; DG, dentate gyrus; Sub, subiculum.

structures and the entorhinal cortex are reciprocal; projections from PER, POR, pre-subiculum and para-subiculum terminate in the superficial entorhinal cortex, and feedback is relayed to these structures via the deep entorhinal cortex.

The MEC and LEC are further distinguished by the laminar and topographical organisation of their projections to the hippocampus. Like other cortical structures, the entorhinal cortex is arranged in layers, which differ in their cytoarchitecture and connectivity (Witter & Amaral, 2004; Canto et al. 2008; Canto & Witter, 2012a, 2012b; Van Strien et al. 2009; Witter, Doan, Jacobsen, Nilssen, & Ohara, 2017). Panel B of Figure 1.1 contains a diagram of the extrinsic organisation of projections between the entorhinal cortex and the hippocampus. Entorhinal cortex layer 2 (L2) projects to the DG and CA3 of the hippocampus, and entorhinal cortex layer 3 (L3) projects to the CA1 and subiculum (Seward, 1976; Kohler, 1986; Kohler, 1988; Dolorfo & Amaral, 1998; Naber, Lopes da Silva, & Witter, 2001; Kerr et al. 2007; Van Strien et al. 2009). These projections from the superficial entorhinal cortex form the perforant pathway.

However, the pattern of input to the hippocampus from each layer is not consistent across the LEC and MEC. While L2 projections from MEC and LEC converge on the same populations of cells in the DG and CA3, they project to slightly different regions; MEC L2 projects to the middle molecular layer of the DG and the deep region of CA3, and LEC L2 projects to the outer molecular layer of the DG and the superficial region of CA3 (see Van Strien et al. 2009). In contrast, L3 projections from entorhinal cortex are divergent; the MEC innervates the proximal CA1 and distal subiculum, and the LEC innervates the distal CA1 and proximal subiculum (see Van Strien et al. 2009). In addition, there is recent evidence that the projections from entorhinal cortex further diverge across the layers of CA1, with projections from LEC and MEC innervating neurons in the superficial and deep layers of CA1, respectively

(Masurkar et al. 2017). Notably, CA3 projections to CA1 diverge in a similar manner (Kerr et al. 2007; Van Strien et al. 2009).

In return, projections from the CA1 and subiculum terminate in L5 and L6 of the entorhinal cortex, which then feedback to the superficial entorhinal cortex and other cortical structures (Kosel, Van Hoesen, & West, 1981; Cappaert, Van Strien, & Witter, 2014). There are also sparse projections from CA1 and subiculum to entorhinal cortex L2 and L3 (Van Strien et al. 2009). Importantly, projections from CA1 and subiculum maintain a divergent organisation in their feedback to the entorhinal cortex, with distal CA1 and proximal subiculum projecting to the LEC and proximal CA1 and distal subiculum projecting to the MEC (Tamamaki & Nojyo, 1995; Naber et al. 2001; Kloosterman et al. 2003). In combination with divergent projections to the CA1 from entorhinal cortex and CA3, this suggests that the segregation of information processed by the MEC and LEC is largely maintained throughout the entorhinal-hippocampal circuit.

The MEC and LEC are further distinguished by the topographical arrangement of projections to the hippocampus along the septotemporal axis (see Panel D of Fig. 1.1). Based on these projections, the entorhinal cortex separates into three distinct bands: dorsolateral, intermediate, and ventromedial. Each band contains a portion of the MEC and LEC: the septal hippocampus receives input from the lateral LEC and dorsal MEC, the intermediate hippocampus receives input from the intermediate LEC and MEC, and the temporal hippocampus receives input from the medial LEC and ventral MEC (Dolorfo & Amaral, 1998a; Witter & Amaral, 2004; Kerr et al. 2007; Van Strien et al. 2009). These bands differ in their connectivity with cortical structures, which might suggest functional segregation along this axis.

Lastly, the MEC and LEC are heavily interconnected. Panel C of Fig. 1.1 contains a diagram of known connections between the subregions of the entorhinal cortex. Briefly, MEC

L2, L3, L5 and L6 project to the L2 and L3 of the LEC (Kohler, 1986; Dolorfo & Amaral, 1998b). In return, LEC L2 and L5 project to L2 and L3 of the MEC, and L3 and L6 project to the L5 and L6 of the MEC (Kohler, 1986; Kohler, 1988; Dolorfo & Amaral, 1998b; Burwell & Amaral, 1998). The connectivity between the two regions of entorhinal cortex might support the integration of different types of information independently from the hippocampus.

1.2.2 Intrinsic Properties of the Superficial Entorhinal Cortex

MEC and LEC L2 contain at least four types of excitatory principal cell. In MEC L2, the largest subgroup are stellate cells, named for the star-like arrangement of dendrites around the soma. The second largest subgroup of principal cells are pyramidal cells, named for their pyramidal-shaped soma and the arrangement of dendrites towards the superficial and deep layers of MEC. Further, there are smaller groups of intermediate stellate and pyramidal cells which do not strictly adhere to the morphological properties of either group (Canto & Witter, 2012b). The neuronal sub-types of MEC L2 have distinct electrophysiological profiles (for a review, see Witter et al. 2017).

Figure 1.2 contains example images of the two largest subgroups of excitatory principal cells in LEC L2. The largest subgroup of excitatory principal cells are stellate-like 'fan cells', named for the branching arrangement of dendrites horizontally through L2 and vertically towards the pia. As in the MEC, the second largest subgroup of principal cells are pyramidal cells. Finally, LEC L2 contains a subgroup of 'multi-form' cells, which do not have a consistent morphology (Tahlvidari & Alonso, 2005; Canto & Witter, 2012a, & Leitner et al. 2016).
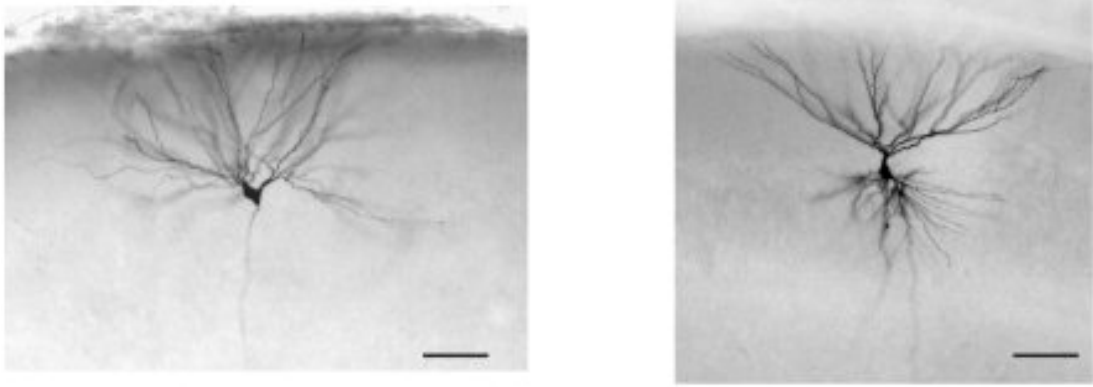
Figure 1.2: Morphology of principal cells in lateral entorhinal cortex L2. Left: Example of a fan cell, with a characteristic polygonal soma and dendrites branching horizontally within L2 and vertically towards the pia. Right: Example of a pyramidal cell, with a characteristic polygonal some and dendrites branching towards superficial and deep lateral entorhinal cortex. Scale bars represent 100 μm. Extracted from Tahlvidari & Alonso, 2005.

Recent experiments have examined the distribution of different proteins across L2 of the entorhinal cortex, and have found that the different cell types described in L2 are further discriminated by the proteins they contain. In MEC L2, stellate cells are positive for the glycoprotein reelin, and pyramidal cells are positive for the calcium-binding protein calbindin D-28k (calbindin; Kitamura et al. 2014). Similarly, LEC L2 fan cells are positive for reelin and L2 pyramidal cells are positive for calbindin (Leitner et al. 2016). Interestingly, these types of cells are arranged across two sub-layers within LEC L2, with the most superficial layer containing reelin-positive fan cells and the deeper layer containing calbindin-positive pyramidal cells (Fujimara & Kosaka, 1996; Leitner et al. 2016). Intermediate cell types in both layers have been observed to express reelin and calbindin (see Witter et al. 2017). In both entorhinal subregions, reelin-positive cells project to the DG and CA3, and calbindin-positive cells project to CA1 or other cortical structures (Kitamura et al. 2014; Surmeli et al. 2015; Leitner et al. 2016). Therefore, the arrangement of projections from entorhinal cortex L2 to the

hippocampus are better defined by protein expression than anatomical location. Further, MEC and LEC L2 differ in the expression of interneuron markers, most notably parvalbumin (PV); there is a high degree of PV-expressing interneurons in MEC L2, with only sparse PV expression in LEC L2 (Wouterlood, Hartig, Bruckner, & Witter, 1995; Fujimaru & Kosaka, 1996; Leitner et al. 2016). The microcircuitry of interneurons in the entorhinal cortex is outside of the scope of this thesis, but for a review see Witter et al. (2017).

There is currently less data available regarding the organisation of neuronal sub-types in entorhinal cortex L3. In both subregions of entorhinal cortex, L3 is largely comprised of excitatory pyramidal cells, which communicate with the hippocampus and the contralateral entorhinal cortex (Tahvildari & Alonso, 2005; Canto & Witter, 2012a; 2012b; Tang et al. 2015), and in the MEC, a smaller population of multipolar neurons have also been described (Germroth, Schwerdtfeger, & Buhl, 1989). Although there are reports that the interneurons in MEC L3 express a wide array of markers (see Witter et al. 2017), the chemical characterisation of LEC L3 is understudied. Further, MEC L3 receives the majority of intrinsic projections from MEC L5, but this circuitry remains poorly understood in the LEC (Kloosterman, van Haeften, Witter & Lopes da Silva, 2003; van Haeften et al. 2003).

1.2.3 Intrinsic Properties of the Deep Entorhinal Cortex

MEC and LEC L5 both contain large populations of pyramidal neurons, which are divisible into further sub-types (Canto & Witter et al. 2012a; 2012b). Entorhinal cortex L5 bifurcates into two distinct layers (L5a and L5b), and in the MEC, these sub-layers are distinguished by the expression of transcription factors Etv1 and Ctip2, respectively (Ramsden et al. 2015; Surmeli et al. 2015). This may also be true of LEC L5 (see Witter et al. 2017). These sub-layers are further discriminated by the morphology of the neurons they contain; the most superficial layer of entorhinal cortex L5 (L5a) contains pyramidal neurons, whereas the

deeper layer (L5b) contains a mix of multipolar and pyramidal neurons (Hamam et al. 2000; Witter et al. 2012a; 2012b). Interestingly, L5a of the MEC and LEC feedback to cortical and sub-cortical structures, whereas L5b receives the majority of feedback from the hippocampus. In the MEC, L5b neurons also receive input from MEC L2 stellate cells, which suggests that L5b is critical for integrating information from the hippocampus and superficial MEC within the circuit (Surmeli et al. 2015). MEC L5b also provides the main feedback projection to MEC L3 (Kloosterman et al. 2003; van Haeften et al. 2003). At present, it is unknown whether the circuit is similarly organised in LEC.

1.3 Methodologies for Examining Circuit Components

The organisation of connectivity between the entorhinal cortex and the hippocampus might suggest functional specialisation within the different projection pathways to the hippocampus or neuronal sub-populations which contribute to the network. To address this possibility, the experiments presented in this thesis use a combination of electrophysiological (Section 1.3.1) and molecular (Section 1.3.2) tools. For reference, this section provides a brief introduction to the relevant methodologies.

1.3.1 Electrophysiological Methodologies

As a reference for the electrophysiological measures reported in Chapters 2 and 3, this section briefly reviews in-vivo and in-vitro methods for measuring the electrical signal from single neurons in the brain. Panel A of Fig. 1.3 depicts an action potential of a typical neuron. Briefly, an action potential is the electrical impulse generated by a neuron which communicates information to connected cells. These impulses are largely driven by the movement sodium (Na^+) and potassium (K^+) ions across the cell membrane. At rest, there are more Na^+ ions in the extracellular space and more K+ ions in the intracellular space, which results in the intracellular

voltage being approximately 70mV less than the outside (Panel B, Fig 1.3; resting membrane potential). When stimulated with positive current, experimentally or biologically, the intracellular voltage becomes more positive, encouraging voltage-gated Na^+ channels to open (depolarisation). If depolarisation reaches a critical threshold, the neuron fires an action potential. This is characterised by a rapid influx of Na^+ neurons into the neuron, followed by an efflux of K^+ neurons, which reverses the depolarisation (repolarisation). During repolarisation, Na^+ channels begin to close, limiting the influx of Na^+ ions. Further, there is usually an 'overshoot', where the membrane potential is more negative than -70 mV before returning to resting membrane potential (hyperpolarisation).
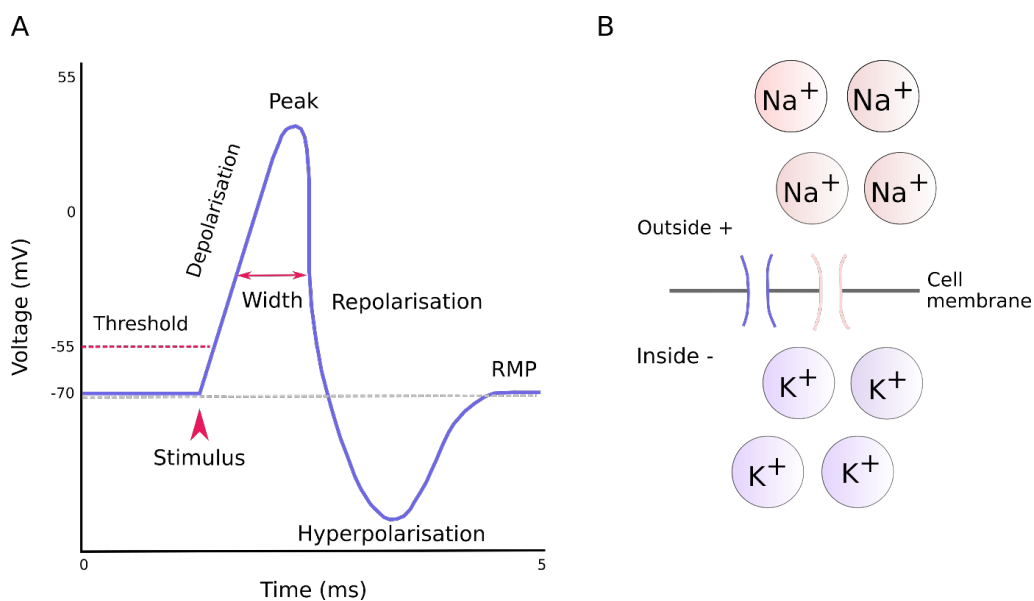
Figure 1.3: Anatomy of an action potential. A) Annotated action potential waveform. Characteristics are based on a typical neuron. Stimulus indicates injection of depolarising current. B) Schematic of the membrane of a neuron in a resting state. When sodium channels are closed, there is a high gradient of sodium outside of the cell. Abbreviations: RMP, resting membrane potential.

Table 1.2 summarises the key intrinsic properties of neurons. Action potentials vary in width, amplitude, and frequency, depending on the type of neuron. Intrinsic membrane properties of a neuron are determined by examining the electrophysiological response to injections of depolarising or hyperpolarising current in-vitro. These properties might include input resistance, time constant, time-dependent inward rectification (Sag), rheobase and resonance frequency.

Table 1.2

Key intrinsic properties of neurons

Property	Description
Input resistance (mΩ)	Value reflects the extent to which ion channels are open. Low values indicate open channels, high values indicate closed channels. In neurons with high input resistance, smaller current injections can result in larger membrane responses.
Time Constant/τ (ms)	Value describes the speed at which a neurons voltage level returns to resting potential after injection of current. The value is exponential, and indicates the amount of time between action potential emission and decay to a level 37% above previous resting state.
Sag	Value indicates self-rectification towards resting membrane potential after initial decrease in voltage in response to injection of hyperpolarising current.
Rheobase (pA)	Value indicates the minimum amplitude of depolarising current which induces an action potential response.
Resonance Frequency (Hz)	Value indicates the input frequency which a neuron responds to the most powerfully.

Panel A of Fig. 1.4 contains a schematic of in-vitro whole-cell patch clamp recordings. Sections of brain tissue are immersed in a heated bath which contains an electrolyte solution that mimics cerebrospinal fluid. The bath contains a reference electrode and a recording electrode. An electrical circuit is formed between these electrodes when the recording electrode contacts the membrane of neuron. The recording electrode is encased in a glass micropipette which contains a second solution designed to mimic intracellular fluid. To record from a neuron, the micropipette is guided under a microscope to press against the cell membrane. Upon contact, suction is applied to draw a portion, or 'patch', of the cell membrane into the pipette. If successful, this results in a high resistance seal ('gigaseal'), permitting precise measurement of currents across the attached portion of the cell membrane. At this stage, the resting membrane potential is kept at a constant voltage determined by the experimenter (voltage-clamp technique). To perform whole-cell recordings, further suction is applied to displace the patch of cell membrane and provide access to the inside of the cell. Once whole-cell access is gained, the current is clamped rather than the voltage, which permits the membrane potential to fluctuate. Any voltage generated by the neuron in response to injection of current is amplified and recorded, and can be examined to reveal intrinsic properties of the cell.

Panel B of Fig. 1.4 contains a schematic of in-vivo electrophysiological recording. In behaving animals, the activity of single cells can be recorded by implanting electrodes into the brain which detect action potentials from the extracellular space. Electrodes are constructed of wire tetrodes, each containing multiple channels. By comparing the electrical activity across the channels of a tetrode, putative action potentials are isolated and assigned to individual neurons on the basis of principle components, such as width of waveform and time to peak. This technique reveals information about the shape of action potentials generated by a single cell, but doesn't measure the intrinsic membrane properties. In the hippocampus, the
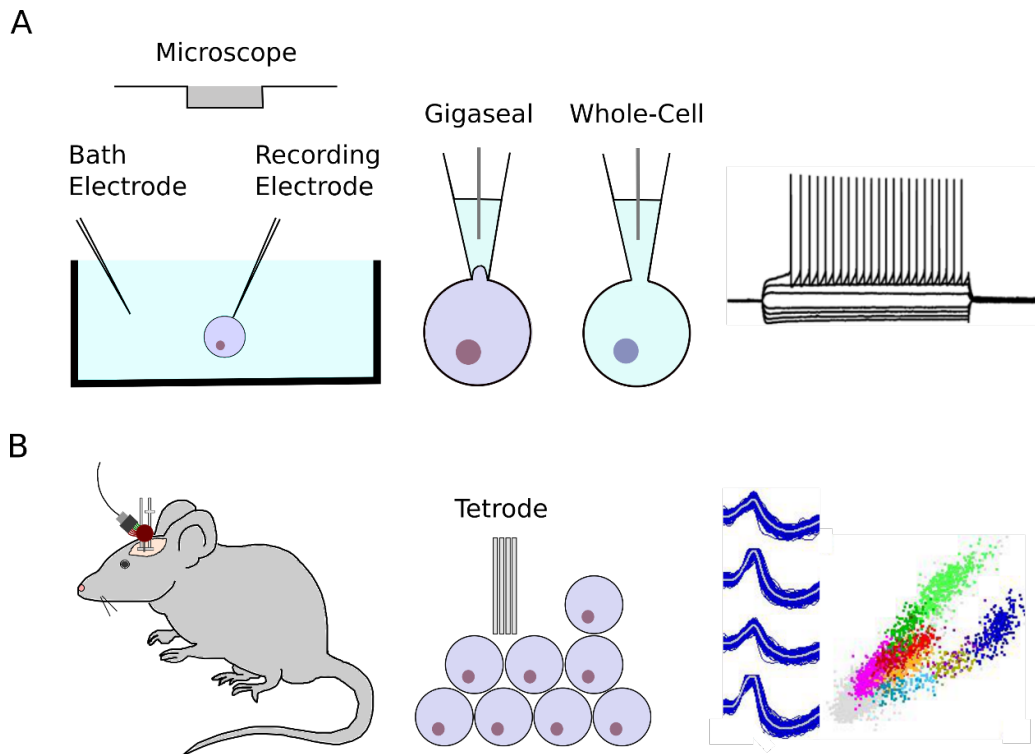
Figure 1.4: Electrophysiological methods used in rodent tissue. A) Schematic of whole-cell patch clamping. Left: The recording rig contains two electrodes, one which detects changes in voltage from the cell and one which functions as a reference electrode. Middle: Two types of seal which are formed with a recorded cell using the recording electrode. Whole-cell technique punctures the membrane to access intracellular space. Right: Example of action potentials emitted in response to the injection of positive current from a neuron in the superficial lateral entorhinal cortex (see Chapter 3). B) Schematic of in-vivo tetrode recordings. Left: Cartoon of a rodent with a micro-drive implant. Middle: Schematic of electrode placement in the extra- cellular space of a cell layer. Right: Example of a recorded cell in the CA1 of the hippocampus (see Chapter 2). Waveforms indicate signal detected on each channel of a tetrode for a single cell (blue). Principle components are examined to isolate this neuron from other cells and noise.

action potentials of a single cell frequently correspond to unique locations in an environment and a specific point in time. Therefore, this technique is useful for measuring the response of single cells in the hippocampus to environmental stimuli, such as objects.

1.3.2 Molecular Methodologies

As a reference for the molecular methodologies used in Chapters 3 and 4, this section briefly overviews the use of Cre transgenic mouse lines and adeno-associated virus in behavioural neuroscience. One strategy for investigating the contribution of circuit components to behaviour is the use of molecular tools which permit precise manipulation of neuronal sub-populations based on their chemical composition or connectivity. This can be achieved by the use of adeno-associated virus (AAV) and the generation of mice which express the enzyme Cre recombinase (Cre) under the control of the promoter of a gene which is expressed in a single cell population. Figure 1.5 contains a schematic of the use of AAV in neuroscience research. AAV can be engineered to encode a range of proteins depending on the experimental question. Further, AAV can be engineered to express proteins conditionally on the presence of Cre, so when it is injected into the brains of transgenic Cre-expressing mice (Panel A, Fig. 1.5), the desired protein is expressed exclusively in cells which are positive for Cre (Panels B and C, Fig 1.5). AAV is usually manufactured to encode a fluorescent reporter (eg. green fluorescent protein; GFP) in conjunction with an operational protein, such as channelrhodopsin-2 or tetanus toxin light chain.

These techniques have been useful for dissecting MEC L2 circuit components which contribute to memory (eg. Kitamura et al. 2014; Tennant et al. 2018). For example, channelrhodopsin-2 renders neurons sensitive to light, which permits optogenetic manipulation with light stimulation. When Cre-dependent AAV encoding inhibitory channelrhodopsin-2 was injected into the entorhinal cortex of a mouse which expresses Cre
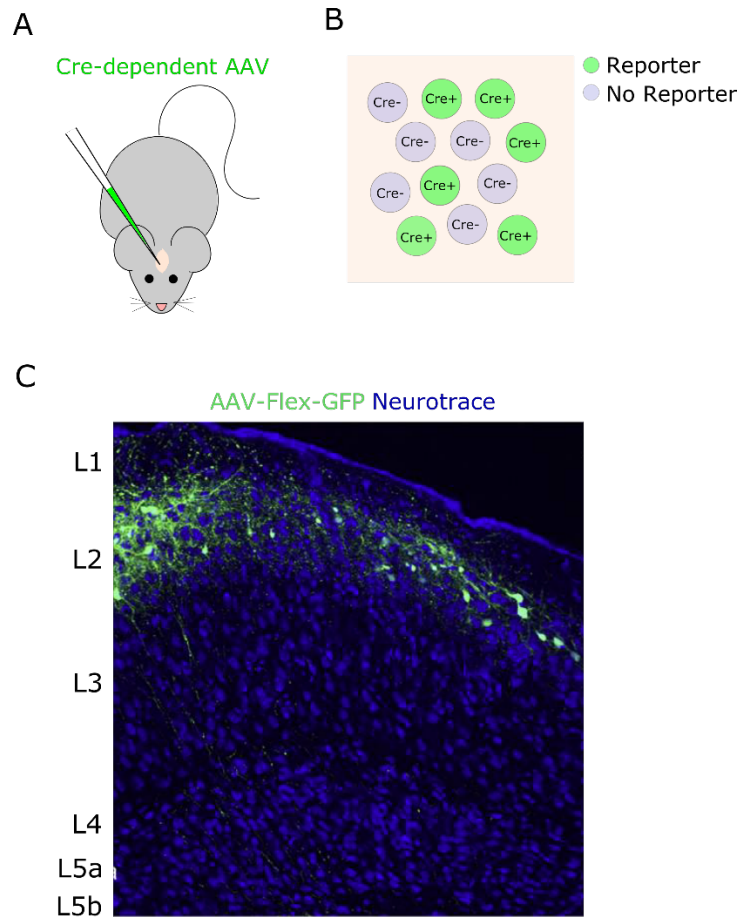
Figure 1.5: Cre-dependent adeno-associated virus injection in a transgenic mouse. A) Cartoon of an injection of AAV into the brain of a mouse. B) Cre-dependent AAV is only expressed in Cre-positive neurons (green), not Cre-negative neurons (violet). C) Example of Cre-dependent AAV expression (AAV-Flex-GFP) in a subset of MEC L2 neurons in a Cre-expressing transgenic mouse (Wfs1:CreEr). Infected neurons express a fluorescent reporter (GFP, green). All neurons are counterstained with Neurotrace (blue). Extracted from Surmeli et al. 2015.

in MEC L2 pyramidal cells, it was found that optogenetic inhibition of these cells impaired the ability to associate an aversive stimulus with a specific context (Kitamura et al. 2014). In contrast, tetanus toxin light chain suppresses the firing of neurons by preventing neurotransmitter release. When Cre-dependent AAV encoding tetanus toxin light chain was injected into the entorhinal cortex of a transgenic mouse which expresses Cre in MEC L2 stellate cells, mice were impaired at estimating distance in a virtual navigation task (Tennant et al. 2018). These tools offer a sophisticated approach to studying the relationship between circuit components and cognition.

1.4 Episodic Memory and the Hippocampus

1.4.1 Lesion Evidence

It is well-established that episodic memory relies on the medial temporal lobe. In a landmark case study, Henry Molaison (HM) suffered from profound memory impairment following the surgical removal of tissue from his medial temporal lobe to treat intractable epilepsy (Scoville & Milner, 1957). The extensive study of HM resulted in memory function being attributed to the hippocampus, which was severely damaged in his surgery, as were the parahippocampal cortices and amygdala (Corkin et al. 1997; Annese et al. 2014). Since HM, many studies have investigated the functional role of the hippocampus and its surrounding cortical network. However, systematic study of memory impairment after damage to medial temporal lobe structures is difficult in human subjects, given that damage is usually non-specific to a single structure and the extent and location of tissue loss varies across individuals.

To circumvent these limitations, paradigms have been developed for rodents which model different types of associative memory by requiring the animal to integrate spatial and non-spatial information about stimuli in an environment (Day, Langston & Morris, 2003; Eacott & Norman, 2004; Fortin, Wright, & Eichenbaum, 2004; Dere et al. 2005; Kart-teke et

al. 2009; Veyrak et al. 2015). The use of object-based paradigms has been a particularly popular strategy for determining the neural substrates of episodic memory, yet some paradigms do not incorporate objects but use other salient stimuli such as odour or reward (eg. Day et al. 2003; Fortin et al. 2004; Veyrak et al. 2015). However, given that the experiments presented in this thesis use an object-based approach, the present review focuses on object-based paradigms.

These paradigms largely stem from the spontaneous novel object recognition (NOR) task developed by Ennaceur & Delacour (1988). In this task, an animal is presented with two copies of an object, one of which is replaced by a completely novel object at test (Panel A, Fig 1.6). Due to an innate preference for novelty, the animal spends more time exploring the novel object if it remembers the previous experience with the familiar object. The NOR task can be extended to include spatial, contextual and/or temporal components to model episodic memory or other forms of associative recognition memory, such as object-place and object-context (Eacott & Norman, 2004; Dere et al. 2005, Kart-Teke et al. 2009). In the extended versions of the NOR task, different contexts are generated by modifying local visual or tactile cues, such as colour or texture of the test environment (see Panel B, Fig. 1.6).

These tasks have been combined with selective lesions to the hippocampus and surrounding cortical structures to determine which parts of the medial temporal lobe network are required for different types of memory. There is extensive evidence that PER lesions impair novel object recognition (Ennaceur, Neave & Aggleton, 1996; Winters, Forwood, Cowell, Saksida & Bussey, 2004; Winters & Bussey, 2005), yet hippocampal lesions do not generally result in a deficit on this task (Winters et al. 2004; Ainge et al. 2006). Further, hippocampal lesions impair performance on some object-place recognition tasks (Save, Poucet, Foreman, & Buhot, 1992; Bussey, Duck, Muir, & Aggleton, 2000; Mumby, Glenn, Nesbitt, & Kyriazis, 2002; Lee, Hunsaker & Kesner, 2005; Good, Barnes, Staal, & Honey, 2007; Devito & Eichenbaum, 2010; Langston & Wood, 2010; Barker & Warburton, 2011), but not others

(Eacott & Norman, 2004; Langston & Wood, 2010), a disparity which might be due to differential reliance on allocentric versus egocentric cues (Langston & Wood, 2010). Further, lesions of the hippocampus do not impair memory for configurations of object and context, in contrast with a severe impairment in object-context memory elicited by damage to the POR or LEC (Norman & Eacott, 2005; Langston & Wood, 2010; Wilson et al. 2013a; 2013b).
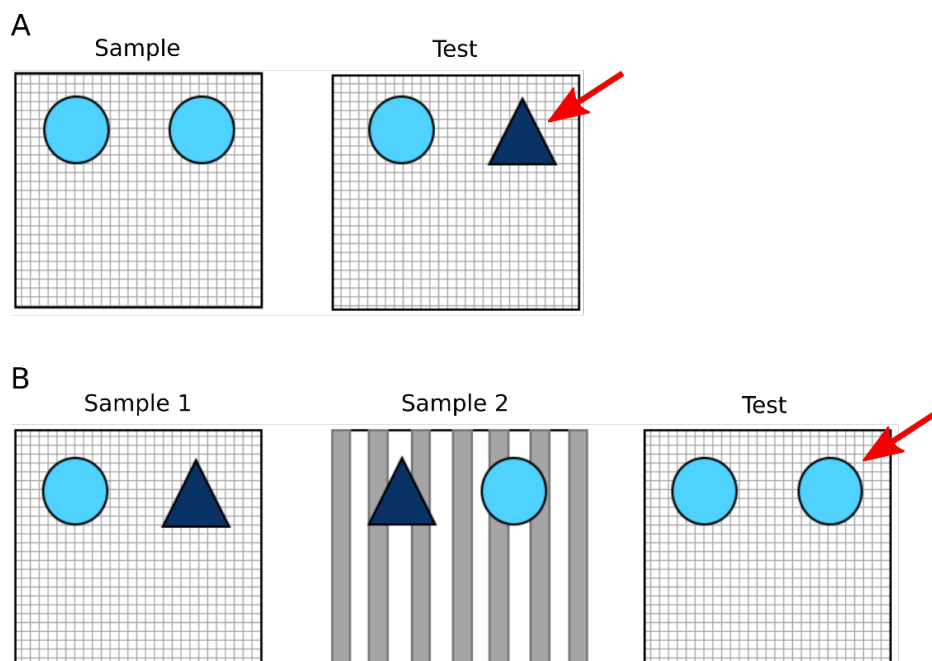
Figure 1.6: Example of object recognition memory tasks used with rodents. Novel object or configuration is indicated by the red arrow. A) Schematic of the novel object recognition (NOR) task. At test, the animal is presented with a novel and familiar object. B) Schematic of the object-place-context (OPC) task, which models episodic memory. The animal is presented with two different objects in two different locations across two contexts, as defined by local tactile and visual cues (mesh floor versus striped walls). At test, one object is in a novel configuration of object, place, and context.

In contrast, hippocampus lesions impair performance on an episodic memory task where the animal is required to integrate object, place, and context information (Panel B, Fig 1.6; Eacott & Norman, 2004; Langston & Wood, 2010). Further, hippocampus lesions impair performance on different object-based episodic memory task which requires the integration of object, location and temporal context (Good et al. 2007; DeVito & Eichenbaum, 2010; Fellini & Morellini, 2013). These findings are consistent with the episodic memory impairment observed after damage to the human hippocampus (Scoville & Milner, 1957; Vargha-Khadem et al. 1997; Spiers, Maguire & Burgess, 2001; Spiers et al. 2001; Spiers, Burgess, Hartley, Vargha-Khadem, & O'Keefe, 2001).

1.4.2 Hippocampal Place Cells and Remapping

According to the parallel processing model, episodic memory impairment after hippocampal damage stems from the inability to integrate spatial and non-spatial information in the hippocampus. However, how the hippocampus integrates this information remains unclear. One possibility is that the hippocampus maintains a 'cognitive map' of the environment, to which information about an episode is bound (Tolman, 1948). This notion is supported by the existence of 'place cells' in the hippocampus, which might provide the spatial framework for this map (O'Keefe & Dostrovsky, 1971; O'Keefe, 1976; O'Keefe & Conway, 1978; O'Keefe & Nadel, 1978). Place cells are neurons which develop discrete 'place fields' at specific locations in an environment, firing exclusively when an animal traverses these locations (see Fig 1.7). The combination of active place cells and the locations of their place fields is unique to each environment experienced (Muller & Kubie, 1978; Leutgeb et al. 2004). The phenomenon by which place cells form a distinct map of each environment is referred to as remapping (Leutgeb et al. 2005a), and may represent a mechanism for encoding different experiences (see Colgin et al. 2008; Yassa & Stark, 2011).

It is well established that place cells are sensitive to global spatial changes. For example, if an animal explores the same environment in two different locations (eg. different rooms), the hippocampus can form distinct neural representations of the environment in each location; there is little overlap in active cell populations or the location of place fields (Muller & Kubie, 1978; Leutgeb et al. 2005a). Remapping can also be induced by local spatial changes, such as changes to the size or shape of an environment (Muller & Kubie, 1978; Leutgeb et al. 2005a). However, if an animal explores two different environments in the same location, place cells sometimes encode this change by modifying their firing rate ('rate remapping', Leutgeb et al. 2005b). Rate remapping indicates that place cells have the capacity to flexibly integrate new information into pre-existing neural representations of an environment, which may facilitate memory.
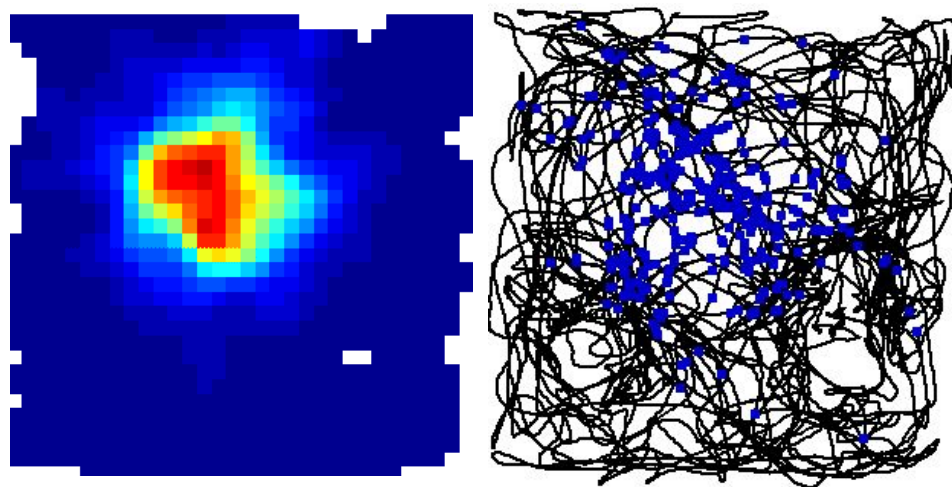
Figure 1.7: Place cell from a rat hippocampus. Left: Rate map shows the place field of the place cell in a square environment. Warm colours indicate high firing rates, cool colours indicate low firing rates / no activity. Right: Exploration of the animal within the square environment. The black line indicates the path of the animal through the environment, and each blue dot represents a single spike from the neuron.

The ability to discriminate between different experiences on the basis of context is a main feature of episodic memory, and remapping in response to contextual cues might represent a neural mechanism for this capacity. Consistent with this notion, it has been demonstrated that place cells manifest a robust remapping response to non-physical environmental features which define the context of an experience. Place cells exhibit different firing patterns across experiences in the same environment depending on behavioural context, including the location of reward and intended destination (Frank, Brown & Wilson, 2000; Wood, Dudchenko, Robitesk, & Eichenbaum, 2000; Ainge, Tamosiunaite, Woergoetter, & Dudchenko, 2007; Johnson & Redish, 2007) and emotionally salient attributes, such as aversive stimuli (Moita, Rosis, Zhou, LeDoux & Blair, 2004). Further, place cells have been observed to have distinct firing patterns within the same environment depending on the temporal context or task demands dictated by temporal cues (Smith & Mizumori, 2006; Manns, Howard & Eichenbaum, 2009; MacDonald, Lepage, Eden & Eichenbaum, 2011, see Eichenbaum, 2014). Considered together, these findings suggest that place cells encode the contextual features of an experience.

1.4.3 Place Cells Encode Object-Place Information

Place cells also encode non-spatial perceptual features of the environment, such as objects or odours (O'Keefe, 1976; Muller & Kubie, 1978; Wood et al. 1999; Lenck-Santini et al. 2005; Manns & Eichenbaum, 2009; Komorowski et al. 2009; Deshmukh & Knierim, 2013). Early arguments posited that place cell firing is modulated by distal extra-maze cues, when available, but not local cues (O'Keefe, 1976; Olton, Branch, & Best, 1978). However, it has been demonstrated that the orientation and location of place fields is heavily influenced by intra-maze cues, such as cue cards, under experimental conditions which control for distal cues (O'Keefe & Conway, 1978; Kubie & Ranck, 1983). Transcending purely visual cues, further

experiments have explicitly linked place cell activity to object location, demonstrating that the unexpected presence or absence of objects in specific locations within an environment can induce remapping (O'Keefe,1976; Muller & Kubie, 1987; Lenck-Santini et al. 2005; Manns & Eichenbaum, 2009; Deshmukh & Knierim, 2013).

Episodic memory often requires binding specific items to a spatial context, therefore it is interesting to consider how place cells encode information about objects in space. Understanding the place cell response to objects has further benefits, given that objects might shape spatial representations of an environment in memory by functioning as landmarks, and interaction with objects is integral to some memory tasks developed for rodents (eg. Eacott & Norman, 2004). Indeed, place cells encode object location by developing place fields at, or at discrete distances away from objects in the environment, and can be highly modulated by object displacement (O'Keefe, 1976, Lenck-Santini et al. 2005; Manns & Eichenbaum, 2009; Deshmukh & Knierim, 2013). For example, when a familiar configuration of two objects is rotated in an environment, place fields which are near objects rotate with the displaced object, disappear, or completely remap (O'Keefe, 1976, Lenck-Santini et al. 2005; Manns & Eichenbaum, 2009). Further, a sub-population of place cells have been observed which fire at empty locations where objects were previously located, which might indicate a neural mechanism which supports object-place memory (O'Keefe, 1976; Deshmukh & Knierim, 2013).

Conversely, place cell activity is relatively unaffected by the presentation of a novel object in a location which previously housed a different object (Lenck-Santini et al. 2005; Deshmukh & Knierim, 2013). This suggests that place cells encode the location, but not perceptual attributes, of objects in the environment. Consistent with this viewpoint, it was reported that place cells primarily encode information about object location, not identity, as a rat continuously forages on a circular track which contains displaced familiar objects and novel

objects (Manns & Eichenbaum, 2009). This is consistent with reports that hippocampus lesions do not impair novel object recognition (Brown & Aggleton, 2001; Winters et al. 2004; Ainge et al. 2006). However, Larkin et al. (2014) reported increased activity of CA1 place cells when an animal foraged in a familiar environment which contained a displaced familiar object or a novel object. Interestingly, activity increase was not spatially restricted to regions of the environment where the novel stimulus was presented. This indicates that CA1 broadcasts a general novelty signal, yet does not precisely encode the location of a novel stimulus at the level of a single cell.

While it is clear that the hippocampus encodes information about objects in space, it is unclear whether the spatial firing of place cells reflects explicit object-place or object-context associations, as is required for episodic memory. A recent experiment reported that place cells develop discrete responses to individual stimuli based on locations where they have behavioural significance (Komorowski et al. 2009). In their task, an object was defined as a pot of sand which contained a distinct odour. Rats were presented with two different objects across two different contexts, and were required to learn that digging would only elicit a reward when that object was encountered in a specific context. Place cells expressed place fields across the environment in the early stages of learning the task, however conjunctive representations of object and locations only emerged in later stages of the experiment. Importantly, these conjunctive representations were defined by rate remapping; place cells displayed enhanced activity conditionally on which object was present, but did not shift the location of their place fields within the environment. This finding suggests that rate remapping may represent a neural mechanism for explicit associations between objects and their spatial context.

1.4.4 Influences of Entorhinal Input on Place Cell Firing

As reviewed, there is clear evidence that place cells generate representations of spatial and contextual information, and maintain an integrated representation of some components of episodic memory. As previously discussed, hippocampus lesions result in impaired episodic memory, but do not impair associative recognition memory for object-place or object-context configurations (Section 1.4.1; Langston & Wood, 2010, but see Mumby et al. 2002). Therefore, these representations might be generated elsewhere within the network, such as the entorhinal cortex. Notably, place cell characteristics and patterns of remapping are not uniform across the hippocampus (see Colgin, Moser, & Moser, 2008 or Yassa & Stark, 2011). Given that the entorhinal cortex is the main source of cortical input into the hippocampus, it is possible that the organisation of entorhinal input drives differences in place cell activity.

Indeed, the size of place fields increases systematically along the dorsoventral axis of the hippocampus (Jung, Wiener, & McNaughton, 1994; Kjelstrup et al. 2008), a pattern which is also observed in spatially-modulated cells in the MEC (See Section 1.5.1; Hafting, Fyhn, Molden, Moser & Moser, 2005; Brun et al. 2008). Given that entorhinal cortex input to the hippocampus is topographically organised (see Section 1.2.1), it is possible that the scale at which space is represented in the hippocampus is driven by the spatial signal generated by the MEC (McNaughton, Battaglia, Jensen, Moser & Moser, 2006; Mallory, Hardcastle, Bant & Giacomo, 2018). Secondly, there are clear quantitative differences between place cells in CA3 and CA1, which receive input from entorhinal cortex L2 and L3, respectively. Place cells in CA1 tend to be more active (Leutgeb et al. 2004) and have more firing fields than place cells in CA3 (Fenton et al. 2008; Park et al. 2011). Further, it has been suggested that place cells in CA1 are more likely to be governed by local cues than place cells in CA3, which are more likely to be influenced by self-movement and spatial information (Skaggs & McNaughton, 1998; Leutgeb et al. 2004).

Further, there is evidence that input from the MEC and LEC differentially influence place cell activity in CA1, where input from the entorhinal cortex is segregated along the proximodistal axis (See Section 1.2.1). Interestingly, neurons in distal CA1, which receive input from LEC L3, display differential firing between experimental conditions where an object is present or absent, have more place fields when objects are present, and consistently remap when objects are displaced (Burke et al. 2011). Further, place cells in distal CA1 remap more frequently in response to non-spatial changes in task demands than place cells in proximal CA1 (Schmidt, Satvat, Agraves, Markus & Marrone, 2012). In contrast, place cells in proximal CA1 are more likely to remap to global spatial changes, consistent with input from spatially selective cells in MEC L3 (Hartzell et al. 2014). Electrophysiological differences across the proximodistal axis of CA1 are echoed by differences in active cell populations during a variety of behavioural tasks, as identified by early-gene imaging. Distal CA1 neurons are more active in response to novel objects, whereas proximal CA1 neurons are recruited in response to novel contexts (Ito & Schuman, 2012; Hartzell et al. 2014; Nakazawa, Peyzner, Tanaka, & Wiltgen, 2016). These findings suggest that different inputs from entorhinal cortex can influence the response of single cells in the hippocampus to spatial and contextual changes in an environment.

If entorhinal cortex input modulates place cell activity, the loss of entorhinal input should have measureable consequences. Indeed, bilateral entorhinal cortex lesions do not eliminate the spatial firing of place cells, but do result in place fields which are larger, less stable, and less spatially selective (Brun et al. 2008; Van Cauter, Poucet, & Save, 2008; Hales et al. 2014). Further, place fields remain stable in the CA1 when this region is isolated from CA3 input, which suggests that input from the entorhinal cortex L3 or other cortical structures is sufficient to maintain selective spatial signal in the hippocampus (Brun et al. 2002).

A few studies have explicitly examined place cell activity after inactivation or targeted lesions of the LEC. Lu et al. (2013) lesioned the LEC and recorded the activity of CA3 place cells as the shape and colour of a test environment was manipulated. Disruption of LEC input did not change the basic firing properties of CA3 place cells, but did attenuate rate remapping in response to the local changes. However, recording from the LEC during the same task revealed no rate remapping in LEC cells, which indicates that rate remapping in the hippocampus is not directly inherited from LEC input. More recently, Scaplen et al. (2017) recorded from CA1 place cells in rats as they foraged in an environment with two-dimensional object or landmark stimuli projected onto the floor. In the first and last trials, these stimuli were in a consistent configuration, with an intermittent trial where the stimuli were rotated 90°. Interestingly, inactivation of the ipsilateral LEC increased the likelihood of place cell remapping to the rotation of landmarks, but not objects, and increased the spatial tuning of place cells in response to the presence of objects, but not landmarks. These data suggest that input from LEC L2 input modulates how the place cells in the hippocampus attend to local cues in the environment.

Considered together, these findings indicate that input from the entorhinal cortex contributes to the generation of spatial signalling in the hippocampus, and input from the LEC may be particularly important for processing spatial information about local environmental cues. If the cognitive map generated by the hippocampus is influenced by entorhinal input, then examining the nature of this input is key to understanding how episodic memories are encoded within this network. Therefore, the subsequent section reviews information processing in the entorhinal cortex, with a focus on the LEC.

1.5 Episodic Memory and the Entorhinal Cortex

1.5.1 Information Processing in the MEC

Information processing in the MEC is only briefly addressed for the purpose of this review (but see Moser et al. 2008; Derdikman & Moser, 2014 or Save & Sargolini, 2017). The MEC plays a critical role in representing space; this structure contains several cell-types which encode spatial aspects of the environment and movement related information, including grid cells (Hafting et al. 2005), border cells (Savelli, Yoganarasimha & Knierim, 2008; Solstad, Boccara, Kropff, Moser, & Moser, 2008), head-direction cells (Taube, 1998), and speed cells (Kropff, Carmichael, Moser, & Moser, 2015). Grid cells are neurons which periodically fire as an animal navigates through space to form a triangular lattice which spans the entire environment (Hafting et al. 2005). It has been hypothesised that grid cells support spatial navigation by encoding the current location of an animal, and how far it has moved ('path integration'; Moser et al., 2008; McNaughton et al. 2006). Consistent with this, MEC damage consistently impairs performance on navigation-based spatial memory tasks (Steffenach, Witter, Moser & Moser, 2005; Van Cauter et al. 2013; Hales et al. 2014). Further, Tennant et al. (2018) recently reported that selective inactivation of MEC L2 stellate cells, which are theorised to correspond to grid cells in the superficial MEC, results in an impaired ability to use path integration to estimate distance in a virtual environment.

Given the high degree of spatial tuning in the MEC, it has been suggested that the MEC influences the spatial selectivity of place cells. Indeed, lesions to the MEC influence the stability of place cells in the hippocampus, but do not abolish spatial signaling (Solstad et al. 2006; Brun et al. 2008; Hales et al. 2014; Mallory, Hardcastle, Bant, & Giacomo, 2018), which indicates that other components of the network contribute to the spatial metric of the hippocampus. Further, there is little evidence that MEC cells attend to local cues (Neunuebel et al. 2013; for a review, see Knierim et al. 2014), although animals with MEC lesions are

impaired at detecting the movement of a familiar object to a novel location in an environment (Van Cauter et al. 2013). Therefore, it is likely that the spatial signal reaching the hippocampus from the MEC contains information about space and self-motion cues rather than spatial information about local objects (Knierim et al. 2013).

1.5.2 Information Processing in the LEC

In the parallel processing model, the LEC exclusively processes non-spatial information about an experience. There is some support for this notion. Firstly, LEC neurons are activated in response to non-spatial cues in the environment, including objects (Zhu et al. 1995; Wan, Aggleton, & Brown, 1999; Xiang & Brown, 1999) and odours (Young, Otto, Fox, & Eichenbaum, 1997; Xu & Wilson, 2012; Leitner et al. 2016; Ku et al. 2017). Secondly, selective lesions of the PER, which provides substantial input to the LEC, result in severely impaired recognition memory for objects or object configurations (Aggleton & Brown, 1999; Norman & Eacott, 2005; Murray, Bussey, & Saksida, 2007; see Brown & Aggleton, 2001). Finally, in stark contrast with the MEC, LEC cells display minimal spatial tuning in test environments which contain no local cues (Hargreaves, Yogaranasimha, & Knierim, 2005; Yogaranarasimha, Rao, & Knierim, 2011).

However, recent reports suggest that some LEC neurons are spatially tuned under experimental conditions where an object is present (Deshmukh & Knierim, 2011; Deshmukh et al. 2012; Tsao et al. 2013). When an animal foraged in an environment which contains a configuration of objects, a significant proportion of LEC neurons were object-responsive, either developing a place field at locations which contain objects, or firing at stable distances away from objects (Deshmukh & Knierim, 2011). Further, the firing of LEC neurons was modulated by the displacement of objects, and a sub-population of neurons dubbed 'object-trace' cells fired exclusively at locations where an object was previously located, yet remained

silent when the object was physically present (see Fig. 1.8; Deshmukh & Knierim, 2011; Deshmukh et al. 2012, Tsao et al. 2013). These firing patterns may represent a neural mechanism for encoding information about object and location in memory.
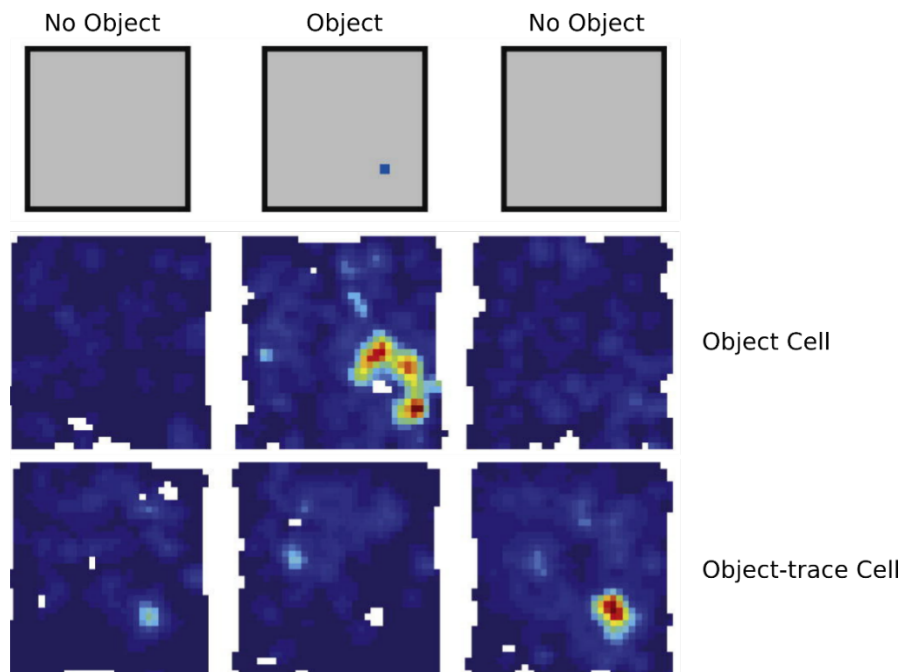
Figure 1.8: Object-modulation in lateral entorhinal cortex. Warm colours indicate high firing rates, whereas cool colours indicate low firing rates / no firing. Top row: Schematic of trials; No object was present in the first and last trials, and rats were presented with an object in the bottom right quadrant in the second trial. Middle: Example of a cell which fires at an object. This cell does not have a field when the environment is empty. Bottom: Example of an object-trace cell. This cell does not fire when the object is in the environment, but fires at the empty location in the subsequent trial. All panels adapted from Tsao et al. 2013.

This research was extended by recent work which suggests that the LEC processes contextual information about environmental stimuli. Keene et al. (2016) examined the activity of LEC neurons to rewarded configurations of odor and context. In this task, the animal was

trained to associate an odor with reward in a context-dependent manner. When the animal foraged in two different contexts, they were presented with two objects (scented pots of sand), each of which was only associated with a reward in one of the contexts. The authors reported that single neurons in the LEC demonstrated spatially selective firing for objects and locations in the environment, yet also encoded conjunctive representations of object and context. Interestingly, similar characteristics were observed upstream of the LEC in the PER, indicating that conjunctive representations of object and context exist within this pathway.

Complementing this finding, it was recently reported that LEC neurons encode conjunctive information about stimulus and context, both during and after an experience (Pilkiw et al. 2017). In this study, rats experienced two different environments, each of which was associated with a stimulus (a combination of light, tone, or eyelid stimulation). Some LEC neurons encoded integrated environment and stimulus information during behavioural trials, and nearly all recorded cells encoded information about the previous trial during a rest interval. Considered in combination with the discovery of object-trace cells in the LEC (Deshmukh & Knierim, 2011; Deshmukh et al. 2012; Tsao et al. 2013), this finding strongly suggests that the LEC is explicitly involved in memory for location and context of environmental stimuli. This is consistent with severe associative recognition memory impairments after LEC lesions, including memory for object-place or object-context configurations, and episodic memory (Wilson et al., 2013a; 2013b). Further, LEC lesions impair the ability to associate stimuli with aversive or appetitive stimuli, which may rely on an overlapping network (Ferry, Ferreira, Traissard, & Majchrzak 2006; Tanninen, Morissey, & Takehara-Nishiuchi, 2013; Ferry, Herbeaux, Javelot & Majchrzak, 2015).

1.5.3 Dissociating the LEC + MEC

As reviewed, the current body of research indicates that spatial and contextual information about an object or stimulus is integrated within the LEC. The evidence weakens the argument that the LEC and MEC are dissociated by the types of information they process, and has driven experiments which systematically study behavior after selective lesions to each entorhinal subregion.

To investigate whether the MEC and LEC differentially process spatial and non-spatial information, Van Cauter et al. (2013) compared the effects of MEC and LEC lesions on performance in two object-recognition tasks, which could be solved using spatial and non-spatial information, respectively, and two spatial navigation tasks. LEC lesions resulted in impaired performance on both object-recognition tasks, but not the spatial navigation tasks. MEC lesions did not result in impaired object recognition memory, but did impair performance on both spatial navigation tasks. Interestingly, this study and further work have observed that LEC lesions do not impair performance on the standard NOR task, but do impair performance on complex versions of the task with >2 objects (Van Cauter et al. 2013; Kuruvilla & Ainge, 2017; Rodo et al. 2017). Together, these findings suggest that while the LEC is not required for spatial navigation, it does contribute to processing spatial information about local cues in the environment, particularly when the demands of the task are complex.

Given evidence that the POR is involved in processing contextual information, it is possible that the entorhinal subregions differentially encode information about environmental context. To investigate this, Hunsaker et al. (2013) compared the effects of MEC and LEC lesions on the ability of a rat to recognise a novel object or context. LEC lesions impaired object-novelty detection, whereas MEC lesions impaired contextual-novelty detection. However, both lesions produced an unexpected mild impairment in the other task, which indicates that information about objects and context are not processed wholly independently

prior to the hippocampus. These results echoed a previous study from the same research group which failed to distinguish between item and context processing in the lateral and medial pathways to the hippocampus using pharmacological intervention (Hunsaker et al. 2007). Building on this work, Yoo & Lee (2017) inactivated the MEC or LEC with muscimol in a cohort of rats trained to choose a spatial or non-spatial behavioural response depending on context, as defined by patterns projected onto the wall of an environment. Interestingly, MEC inactivation impaired the capacity to correctly make a context-based spatial response, whereas LEC inactivation resulted in high variability in the capacity to choose the correct non-spatial response.

Considered together, these findings suggest that both entorhinal subregions encode some information about environmental context, and the involvement of either subregion may depend on the spatial or non-spatial content of an experience. Overall, the current body of evidence indicates partial segregation of information streams prior to the hippocampus, as predicted by the parallel processing model, yet also suggests a degree of interaction between spatial and non-spatial information within the entorhinal cortex, particularly in relation to local cues.

1.5.4 Alternative Models of Entorhinal Cortex Function

Given the inadequacy of the parallel processing model, it is necessary to consider alternative models of entorhinal function. Given that the entorhinal cortex is a primary source of input to the hippocampus, and place cell activity in the hippocampus can be driven by local and global changes to an environment, it was suggested that it might be useful to dissociate the two entorhinal regions by their respective roles in processing local and global cues (Knierim & Hamilton, 2011). This hypothesis was operationalized in an experiment which utilized a double rotation protocol; local and global cues were rotated in opposite directions in a circular

environment while the activity of single cells were recorded in the entorhinal cortex (Neunuebel et al. 2013). Consistent with the local-global hypothesis, the authors reported that cells in the LEC and MEC were predominantly driven by the movement of local and global cues, respectively. However, the proportion of cells modulated by local cues was equal between the two areas, and the majority of LEC cells were unclassified. Arguably, a more justified interpretation would be a difference in the neural response to global information, which was substantial in the MEC, and negligible in the LEC. Similarly, Kuruvilla & Ainge (2017) trained rats to forage for a reward in relation to global or local set of environmental cues, and then lesioned the LEC or MEC. Interestingly, LEC lesions impaired the ability to use a local, but not global framework, to perform the task, whereas MEC lesions did not impair performance on either version of the task. These findings suggest that the recruitment of MEC and LEC in attending to local and global cues is not absolute, and the engagement of each subregion depends on the demands of each task (see Save & Sargolini, 2017).

A more flexible model which encompasses these findings, proposed by Deshmukh & Knierim (2011), suggests that the MEC and LEC are functionally distinguished by 'internally based, path integration mechanisms' and 'external sensory information processing', respectively. In this model, the LEC attends to the non-spatial attributes of an experience, but also creates spatial representations on the basis of local landmarks. This is consistent with reports of spatial tuning in LEC neurons in relation to local objects (Deshmukh et al. 2012; Tsao et al. 2013), but not global cues (Yogaranasimha et al., 2010; Neunuebel et al. 2013), and explains the pattern of impairment reported in lesion studies (Van Cauter et al. 2013; Hunsaker et al. 2013).

Another interesting model of entorhinal function is the 'contextual gating' hypothesis (Hayman & Jeffrey, 2008). This model posits that the LEC provides input about non-spatial, contextual information, which is combined with spatial input from the MEC to modulate the

firing of place cells across different environments. In their model, these inputs originate from L2 of the entorhinal cortex, where projections from MEC and LEC innervate the DG. The contextual gating hypothesis predicts the attenuated place cell remapping reported after lesions which encompass the LEC (Van Cauter et al. 2008; Lu et al. 2013) and the place cell response to non-spatial aspects of the environment, such as behavioural context (Frank et al. 2001; Ainge et al. 2007; Griffen et al. 2007) and salient local cues (O'Keefe, 1976, Muller & Kubie, 1978; Wood et al. 1999; Lenck-Santini et al. 2005; Manns & Eichenbaum, 2009; Komoroswki et al. 2009; Deshmukh & Knierim, 2013). By progressing from the strict dichotomy offered by the parallel processing model, these models of entorhinal function may provide a useful scaffold for future experimental work.

1.5.5 Information Processing in LEC Circuit Components

The experiments reviewed here reveal a great deal about information processing in the LEC, yet there is limited information available regarding the underlying circuit components which might contribute to an episodic memory network. There are no reported differences between the firing patterns of recorded neurons across the superficial and deep layers of the LEC (Keene et al. 2016; Pilkiw et al. 2017), yet not all studies discriminated between superficial and deep electrode locations (Deshmukh & Knierim, 2012; Tsao et al. 2013). Given the organisation of entorhinal projections to the hippocampus, some inferences can be made by examining the firing patterns of neurons in different hippocampal subregions. Reduced rate remapping in CA3 and altered object modulation of CA1 place cells after selective LEC lesions may provide insight into the roles of entorhinal output from L2 and L3, respectively (Lu et al. 2013; Scaplen et al. 2017). Indeed, the perforant path shows early pathology in animal models of Alzheimer's Disease and human patients (Gomez-Isla et al. 1996; Stranahan & Mattson, 2010; Khan et al. 2014), and altered signalling from LEC L2 has been explicitly associated

with age-related cognitive decline in rats (Stranahan, Haberman, & Gallagher, 2013). However, there is also evidence that the deep LEC is recruited in memory processes. Yoo & Lee (2017) observed that the variability in performance on their non-spatial task was driven by muscimol inactivation of deep, but not superficial LEC. Further, when rats were trained to perform on a delayed non-match to sample (DNMS) task with odours as stimuli, the deep, but not superficial, LEC was engaged in a complex version of the task where the animal had to identify the novel odour from a set of 10 odours (Ku et al. 2017).

Clearly, teasing apart the function of the different layers of the LEC is a complex task, as most types of memory are likely to recruit multiple parts of the circuit. Indeed, recent evidence from high-resolution imaging of human brains indicated that the superficial entorhinal cortex was recruited in processing novel information, whereas activity in the deep entorhinal cortex corresponded with recall of information (Maass et al. 2014). Future experiments which systematically elucidate the roles of these circuit components will be key to advancing the field.

1.6 Conclusion and Thesis Overview

This introduction has discussed the anatomical and functional organisation of the hippocampus and LEC, with the overarching aim of reviewing current knowledge regarding the role of the lateral perforant pathway in episodic memory processes. First, the anatomical connectivity of the medial temporal lobe was reviewed, with a focus on the intrinsic and extrinsic networks of the entorhinal cortex. Notably, the main cortical projections from entorhinal cortex to the hippocampus arise from L2 and L3, and in L2 these projections are known to be driven by molecularly distinct populations of neurons. Secondly, the role of the hippocampus in episodic memory was discussed, with a focus on how place cells might support episodic memory by encoding various aspects of the environment. Indeed, there is clear

evidence that place cells encode information about objects in their spatial, perceptual, and even temporal context, although the relationship between place cell activity and input from the entorhinal cortex remains unclear. Thirdly, research addressing the role of the LEC in various types of memory was reviewed. Given profound associative recognition memory impairment after LEC damage, and the existence of spatially modulated cells in the LEC, it is possible that spatial and non-spatial content of an episode is integrated within this structure. If true, the input to the hippocampus via the lateral perforant pathway might be a critical component of the episodic memory circuit.

The experiments presented in this thesis examined this possibility and investigated the contributions of components of the lateral perforant pathway to different episodic memory processes. This was addressed separately for LEC L2 and L3 projections using a combination of electrophysiological, behavioural and molecular methods. Firstly, an experiment is presented which capitalised on the divergent projections from entorhinal cortex L3 into the CA1 region of the hippocampus (Chapter 2). In this experiment, place cell activity was compared across the proximodistal axis of CA1 as rats explored an environment which contained objects that underwent a series of spatial manipulations. However, results from this study were limited by being correlational, highlighting the need for a technique for specific manipulation of circuit components to determine how important they contribute to cognition. To this end, a series of experiments were conducted which characterised the arrangement of projecting neurons in LEC L2 and identified a novel molecular tool (Sim1:Cre mouse) which permits precise manipulation of neurons which project to the hippocampus from this layer (Chapter 3). Lastly, to examine the contribution of projections from LEC L2 to the hippocampus to episodic memory, LEC L2 output to the dentate gyrus of the hippocampus was genetically supressed in a cohort of Sim1:Cre mice and performance on a series of object recognition tasks was measured (Chapter 4). The experiments in this thesis begin to tease apart

the components of the entorhinal-hippocampal network which supports episodic memory processes.

Chapter 2: Input from Layer 3 of the Entorhinal Cortex Influences Object

Representation in CA1

2.1 Introduction

The ability to associate items in an environment with their spatial context is a critical component of episodic memory, and it has been suggested that these representations are generated in the hippocampus (see Section 1.4.1 of the General Introduction; Knierim et al. 2006; Eichenbaum et al. 2012). Indeed, there is substantial evidence that place cells in the hippocampus encode non-spatial attributes of an experience, such as objects in the environment (O'Keefe,1976; Muller & Kubie, 1987; Lenck-Santini et al. 2005; Komorowski et al. 2009; Manns & Eichenbaum, 2009; Deshmukh & Knierim, 2013). Place cells may develop place fields near objects in the environment, and remap in response to object displacement by developing a place field at the novel object location or expressing additional or fewer place fields (Muller & Kubie, 1978; Lenck-Santini et al. 2005; Manns & Eichenbaum, 2009; Deshmukh & Knerim, 2011; Deshmukh & Knierim, 2013). Further, when an object is introduced into a pre-existing place field, the field may be suppressed or remap to a new location (O'Keefe, 1976; Muller & Kubie, 1978; Lenck-Santini et al. 2005). Interestingly, a sub-population of place cells express place fields at empty locations where an object was previously located, which may represent a neural mechanism for object-place memory (O'Keefe, 1976; Deshmukh & Knierim, 2013). In addition, there is evidence that altering the identity, spatial configuration, or behavioural saliency of objects is encoded in changes in firing rate, both at the level of a single cell (Komoroswki et al. 2009; Manns & Eichenbaum, 2009) and the whole population (Larkin et al. 2014).

However, spatial tuning in relation to objects is not unique to place cells in the hippocampus. Cells which exhibit similar patterns of object-modulation have been described in LEC and PER (see Section 1.5.2 of the General Introduction; Deshmukh & Knierim, 2011; Deshmukh et al. 2012). In addition, the LEC contains a sub-population of cells which demonstrate 'trace' firing at empty locations where an object was previously located (Tsao et

al. 2013), and as in the hippocampus, there is evidence that single cells in the LEC encode conjunctive representations of object and location or object and context within their firing rate (Keene et al. 2016). In contrast, the spatial firing of single cells in the MEC is not controlled by local cues (Hafting et al. 2005; Neuneubel et al. 2013). The parallels between object modulation in the hippocampus and LEC, but not MEC, suggests that input from the lateral perforant pathway might drive the spatial representation of objects in the hippocampus. As described in Section 1.2.1 of the General Introduction, input from entorhinal cortex L3 diverges along the proximodistal axis of CA1, with LEC L3 projecting to cells in distal CA1, and MEC L3 projecting to cells in proximal CA1 (see Van Strien et al. 2009). Therefore, this axis provides a valuable platform for examining how LEC and MEC input differentially influence place cell activity.

Experiments using early-gene imaging to examine neuronal activation across the proximodistal axis of CA1 during object-based memory tasks revealed that distal CA1, which receives projections from LEC L3, is preferentially recruited to process information about objects, and proximal CA1, which receives projections from MEC L3, is preferentially recruited to process information about context (see Section 1.4.4 of the General Introduction; Ito & Schuman, 2012; Nakamura et al. 2013; Hartzell et al. 2013; Nakazawa et al. 2016). Specifically, when animals are presented with a novel object in an open field, more neurons express the immediate early-genes *c-fos* or *Arc* in distal CA1 than in proximal CA1 (Ito & Schuman, 2012; Nakamura et al. 2016). However, there are mixed results in experiments which address the recruitment of proximal CA1 in processing information about context. Ito & Schuman (2012) reported that when an animal is placed in a new cage, which contained different flooring and a displaced local cue (food bin on the roof), neurons were similarly recruited across the proximodistal axis. In contrast, Hartzell et al. (2014) reported that when an animal is placed in a new environment which contains a familiar array of objects, but is located

in a different room, *Arc* expression was higher in proximal CA1. Although both studies manipulate context by introducing a novel environment, stable local landmarks were only available in the environment used by Hartzell et al. (2014). These landmarks may have functioned as non-spatial contextual cues for distal CA1 cells which receive input from LEC, resulting in decreased influence of the change in spatial context on activity in this region. Further, Nakazawa et al. (2016) observed that neurons in proximal CA1 were recruited preferentially in retrieval of memory for context in a contextual fear conditioning task, yet did not observe differences in recruitment across the proximodistal axis of CA1 during encoding. As with Ito & Schuman (2012), the lack of local landmarks may have precluded differential activation during encoding in this paradigm. Considered together, these findings suggest that both distal and proximal CA1 are engaged in processing contextual information, yet the extent of recruitment along this axis may be modulated by the presence of local cues.

These findings are further elucidated by examining place cell characteristics in CA1 in relation to the presence or absence of local cues. Burke et al. (2011) recorded the activity of CA1 place cells in the distal CA1 as rats traversed a circular track which contained no objects, or 6-8 novel or familiar objects in different spatial configurations. The presence of objects induced an increase in the number of expressed place fields, but a decrease in their size. However, Burke et al. did not report whether the new place fields were expressed near object locations, therefore whether object-modulation was explicitly driven by object location is unknown. More recently, Scaplen et al. (2017) demonstrated that inactivation of the ipsilateral LEC increased the spatial information content of CA1 place cells in response to the presentation of two-dimensional objects, and increased the likelihood of remapping in response to the rotation of two-dimensional landmark stimuli. The finding of increased spatial information content in response to objects after LEC inactivation is surprising, given that previous work would predict higher spatial tuning in relation to objects with intact LEC input.

Nonetheless, both studies suggest that input from LEC L3 modulates spatial tuning and place field expression in CA1 in the presence of local landmarks, yet restriction of recordings to distal CA1 precludes a comparison of characteristics across the proximodistal axis.

However, distinct differences in the spatial tuning of place cells along this axis has been reported in empty environments. Henriksen et al. (2010) recorded the activity of place cells in proximal, intermediate, and distal CA1 as rats explored a small or large cylindrical environment which contained no objects. Under these conditions, spatial tuning was graded along the proximodistal axis, where place cells in proximal CA1 contained more spatial information, expressed more coherent place fields, and maintained more stable representations of the environment across trials. Further, place cells in proximal CA1 expressed fewer place fields, being significantly more likely than place cells in distal CA1 to express only one field in each environment. However, there was no difference in the size of place fields expressed in either region. Further, place cells in proximal CA1 were more sensitive to changes in spatial context, and demonstrated stronger rate remapping in response to a change in the size of the environment. The arrangement of these properties along the proximodistal axis suggests that direct input from MEC L3 to proximal CA1 drives increased spatial modulation of place cells in empty environments where a global spatial metric is critical for navigation. However, given evidence that LEC input modulates the firing of distal CA1 place cells in environments with rich local cues (Burke et al. 2011; Lu et al. 2013; Scaplen et al. 2017), it is possible that a different pattern of spatial tuning may emerge across CA1 under conditions where objects are present.

To this end, the current experiment examined place cell activity in distal and proximal CA1 as an animal explored an environment which contained objects that underwent two spatial manipulations. In the first object manipulation, one object was moved to a novel location in the environment (displacement), and in the second object manipulation, one object was

presented in a novel object-place configuration. This experiment had two distinct aims. The primary aim of this experiment was to compare place cell characteristics across the proximodistal axis of CA1 in an environment which contained objects. Based on previous work, it was hypothesised that the presence of objects would reveal a different gradient of spatial modulation across place cells in distal and proximal CA1 than those described in an empty environment (Henriksen et al. 2010), particularly in relation to the spatial information content, and the size and number of expressed place fields (Burke et al. 2011; Scaplen et al. 2017). A secondary aim of this experiment was to examine object representation across the proximodistal axis of CA1. Given similarities in spatial tuning in relation to objects in LEC and hippocampus, it was hypothesised that place cells in distal CA1 would demonstrate a higher degree of object modulation than place cells in proximal CA1. This hypothesis was three-fold; it was predicted that place cells in distal CA1 would be more likely to express place fields at object locations, more likely to remap to object displacement, and more likely to rate remap in response to either spatial manipulation. Given that input into CA1 originates from entorhinal cortex L3, an overarching aim of the current experiment was to provide insight regarding the contribution of LEC L3 input to the episodic memory network.

2.2 Methods

2.2.1 Animals

Male Lister-hooded rats (n=14) were used in this experiment. Animals weighed 330-450g at the time of surgery. Prior to surgery, animals were housed in groups of 2-4 in diurnal light conditions (12-hr light/dark cycle). After surgery, animals were housed individually. All habituation and testing occurred during the light phase. Animals had *ad libitum* access to water throughout the study. To encourage exploration during the behavioural task, animals were food deprived to no less than 90% of their free-feeding weight. All experiments and surgery were

conducted under a project license (70/8306) and personal license (180825F26) acquired from the UK home office and in accordance with national (Animal [Scientific Procedures] Act, 1986) and international (European Communities Council Directive of 24 November 1986 (86/609/EEC) legislation governing the maintenance of laboratory animals and their use in scientific research.

2.2.2 Apparatus

The electrophysiology suite included a screening location (a pot lined with a towel) and a test environment. The suite was fitted with an overhead pulley system designed to support the weight of recording cables and allow the animal to move freely during screening and behaviour. The test environment was a square wooden box (60cm x 60cm x 90cm), with a white floor and black and white vertically striped walls. To secure objects in place within the test environment, square sections of fastening tape (Dual Lock, 3M) were attached to the middle of each quadrant of the box floor. A local cue (coloured cardboard) was attached to the wall of the upper right quadrant, and stable global cues in the room (eg. lamps) were visible to the animal throughout testing.

2.2.3 Objects

This experiment used an array of junk objects which were approximately the same size as a rat and varied in colour, shape, and texture. Any object used in habituation was not recycled during testing. During behavioural sessions, identical copies of each object were presented across trials. The same copy of each object was used across standard trials. Objects were cleaned thoroughly with veterinary disinfectant before each trial.

2.2.4 Habituation

Prior to habituation and surgery, animals were handled daily in their holding room for 1-2 weeks to familiarise them to human contact. Animals were habituated to the electrophysiology suite over five consecutive days. On each day of habituation, each animal was placed in the screening location individually for 10 minutes before exposure to the test environment. On day 1, each animal explored the test environment with their cagemates for 10 minutes. On days 2-5, each animal explored the test environment individually for 10 minutes. On day 5, two identical objects were introduced in the test environment at the locations occupied by objects in the standard trials of the behavioural task. For all trials, the animal was placed in the test environment facing away from the objects.

2.2.5 Electrodes

Each microdrive (Axona Ltd., U.K.) contained 4 tetrodes, each comprised of 4 channels. Tetrodes were constructed by twisting together 17 micrometre platinum-iridium wire (California Fine Wire, Grover City, CA). Tetrodes were threaded through a 20-gauge steel cannula, which was secured to the microdrive with dental cement. Each microdrive was fitted with a built-in groundwire and a screw mechanism which could be turned to lower the electrodes vertically into the brain. Before implantation, tetrodes were plated with gold to lower the impedance of the electrode tip to 200-300 kΩ.

2.2.6 Surgery

Rats were anaesthetised with Isoflurane in an induction chamber, before being transferred to a stereotaxic frame. The rats were administered analgesic (Carprofen) subcutaneously prior to incision. The skull was exposed, and the rats were implanted with microdrives aimed at distal or proximal CA1. Where implants were bilateral, one microdrive

was aimed each region of CA1. Coordinates for distal CA1 were 5.0 posterior to bregma and 3.2 lateral to midline. Coordinates for proximal CA1 were 3.6mm posterior to bregma and 3.8mm lateral to midline. For each implant, a craniotomy was made at these coordinates, dura was cut, and the electrode was lowered vertically 1.8mm from the surface of the brain. Implants were secured to the skull using a combination of jewelers screws and dental cement. The groundwire of each microdrive was secured to a screw near the front of the skull. Animals were administered oral analgesic (Metacam) in their diet for three days post-surgery.

2.2.7 Screening and Recording

Screening for units commenced within one week after surgery. A recording cable was connected to the microdrive as the animal rested at the screening location. The cable relayed unfiltered electrical signals from each tetrode to a digital acquisition system (DaqUSB, Axona Ltd., UK). Within the acquisition system, signals were amplified with a unity-gain operational amplifier, and passed through a pre-amplifier. The signal was bandpass filtered (600-6000 Hz) and amplified (5000-20000 times). The filtered electrical signal for each tetrode was visualised in real-time via an oscilloscope on a computer screen. To screen for units, the oscilloscope was examined for spiking events. Further, population-level EEG signal was examined for frequency characteristics of the hippocampus (theta; 8-12 Hz) to infer the position of each electrode in the brain. If no units were detected, electrodes were lowered vertically into the brain at small increments (≥ 50 μm). If putative units were detected, the triggering thresholds and gains were adjusted for each channel to minimise noise and maximise detection of action potential for recording. Each channel was referenced to a channel with low noise on which no putative units were detected.

2.2.8 Behavioural Task

A behavioural session comprised of the following trials (Fig 2.1):

a) Standard trials (S1-S3): The animal encountered two different objects in the bottom left and right quadrants of the test environment

b) Object Displacement (O1): The animal encountered a copy of each of the objects from the standard trials, but one was moved to a novel location in the upper left or right quadrant of the environment.

c) Novel Object-Place Recognition (O2): The animal encountered two copies of one object from the standard trial in the bottom right and left quadrants of the test environment. One copy was in a novel configuration of object and location, and one copy was in a familiar configuration.
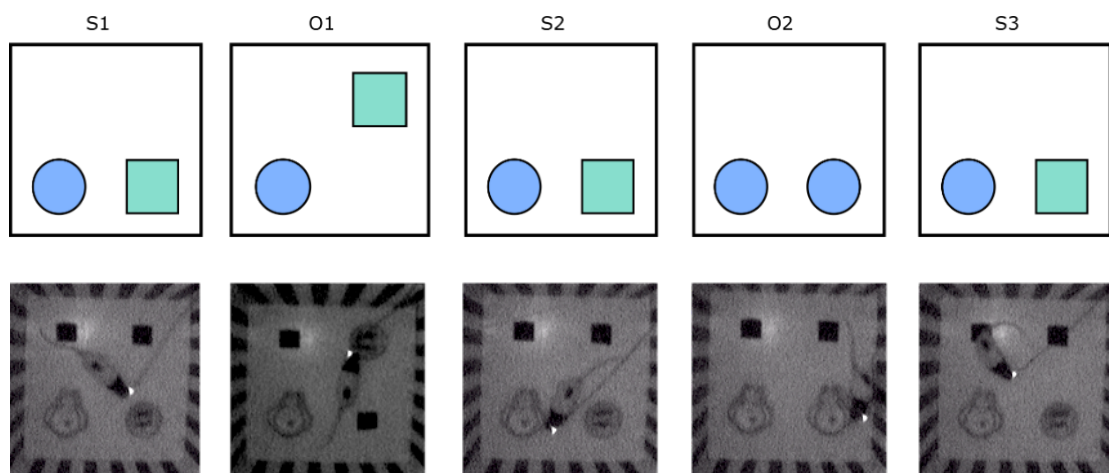
Figure 2.1: Schematic of trials in a recording session. Top row contains a schematic of the trials in a recording sessions, and the bottom row contains screenshots extracted from the video footage of a recording session. The object on the right is moved to the upper right quadrant in the first object manipulation trial (O1, object displacement), and replaced by a copy of the object on the left in the second object manipulation trial (O2, novel object-place recognition).

Each trial lasted eight minutes. The animal rested in the screening location for five minutes between trials. The environment was cleaned with veterinary disinfectant between trials to remove waste and neutralise olfactory cues. The standard trial was presented three times within each behavioural session; at the beginning (S1), between the object manipulation trials (S2), and at the end of the session (S3). Across testing days, the side on which the object manipulation occurred (left or right) was counter-balanced to be pseudo-random. Video footage of the first three minutes of exploration was recorded by a camera positioned above the environment. After three minutes elapsed, food pellets (Dustless Precision Pellets, 45 mg, BioServ) were scattered randomly throughout the box to encourage exploration of the entire environment.

2.2.9 Histology

Animals were administered a lethal dose of sodium pentobarbitol and transcardially perfused with phosphate-buffered saline (PBS), followed by a minimum of 300 ml paraformaldehyde (PFA, 4%). To encourage the brain tissue to shrink away from the electrode and increase visibility of the electrode tract, the brain was stored within the skull for a minimum of 24 hours at 4°C. Brains were then extracted and stored in a 20% sucrose solution prepared in PBS for a minimum of 24 hours at 4°C. The brain was sectioned coronally at 50μm on a freezing microtome. 1:4 sections were mounted on slides, and fixed for a minimum of one hour in a paraformaldehyde bath. To counterstain cell bodies, sections were de-fatted with xylene, and re-hydrated by briefly immersing the slides in a series of ethanol solutions: 100% ethanol, 50% ethanol solution prepared in dH_2O, then dH_2O. Slides were then immersed in a cresyl violet solution for two minutes, and washed in running tap water for five minutes. Sections were de-hydrated by briefly immersing the slides in the ethanol solutions in reverse order: dH2O, 50% ethanol in dH_2O, and then 100% ethanol. Sections were then coverslipped with

DPX. To confirm the location of the electrode tracts, slides were examined at a 4x magnification using a light microscope (Leitz Diaplan).

2.2.10 Behavioural Analysis

Behavioural footage was scored offline by the experimenter. The amount of time spent exploring each object was measured in seconds for all trials. To determine whether the animal preferentially explored the object in a novel configuration, a discrimination ratio was calculated for each object manipulation using the following formula (Ennaceur & Delacour, 1988):

$$Discrimination\ Ratio = \frac{(Exploration\ Novel\ (s) - Exploration\ Familiar\ (s))}{Total\ Exploration\ Time\ (s)}$$

The discrimination ratio is calculated by subtracting the amount of time spent exploring the object in the familiar configuration from the amount of time spent exploring the object in the novel configuration, and then dividing this value by the total exploration time. A positive discrimination ratio indicates an exploratory preference for the object in a novel configuration. For each animal, average discrimination ratios were calculated for each object manipulation. Population means and standard errors of the mean were calculated from these averages.

2.2.11 Place Cell Identification

Single units were isolated from the raw data using TINT (Axona). First, spike clusters were generated using an automated clustering software KlustaKwik, which clusters spikes using principle components. Clusters which did not resemble neuronal spikes were removed. The remaining clusters were manually refined by comparing peak amplitude, trough, and time-to-peak and trough on each channel. Only units with a minimum of one place field in any trial

of a session, a spatial information score of ≥ 0.5 in all trials where the unit expressed a place field, an average firing rate between 0.1 Hz and 2.5 Hz, and a mean spike duration of ≥ 250 ms were accepted for analysis. To detect place fields for each cell, the position data was sorted into 2 x 2 cm bins. Place fields were defined as contiguous regions of ≥ 6 bins where the firing rate was ≥ 20 % of the peak firing rate for that cell during the trial. To further quantify the quality of each cluster, the isolation distance was calculated as described previously (Schmitzer-Torbet, Jackson, Henze, Harris, & Redish, 2005). For each cluster c with n spikes, isolation distance is defined as the squared Mahalanobis distance of the nth closest non-c spike to the centre of the cluster. The squared Mahalanobis distance was calculated as:

$$D^2_{i,C} = (x_i - \mu_c)^T \sum_c^{-1} (x_i - \mu_c)$$

Where x_i is a vector containing feature for spike i, and μ_c is the main feature vector for cluster c. High isolation distances indicate better isolation. Place cells with an isolation distance ≥20 were classified as highly isolated, place cells with an isolation distance ≥10 but <20 were classified as intermediately isolated, and place cells with an isolation distance <10 were classified as poorly isolated. The calculation of isolation distances required a good connection on all channels of a tetrode. Where a channel was grounded due to noise the cluster quality was manually categorised as high, intermediate, or poor by visual comparison against clusters for which an isolation distance value could be determined. Where the same unit was recorded across multiple consecutive days, the recording with the highest average spatial information score was included in the analysis, and other recordings were excluded from the analysis. Repeat recordings were determined by examining the shape of the waveform, the tetrodes on which it was recorded, and location of the place field(s).

2.2.12 Analysis of Place Cell Characteristics

Isolated units were processed offline using customised MATLAB scripts. Rate maps were generated by dividing the area of the box into pixels corresponding to 2 x 2 cm bins of the environment. The firing rate in each pixel was determined by dividing the number of spikes by the dwell-time of the animal in that bin. Firing rate maps depict the firing rate of each bin in colour, where blue represents the lowest firing rate and red represents the highest firing rate. The firing rate maps were analysed to extract the following characteristics: spatial information content, sparseness, selectivity, spatial coherence, average firing rate, peak firing rate, place field frequency, and place field size.

The spatial information score, presented as a ratio of bits/spike, indicates the amount of information about the location of an animal which is encoded in each spike. This was calculated using the following formula (Skaggs, McNaughton, Gothard, & Markus, 1993):

$$Spatial\ Information\ Content\ = \sum_i P_i \frac{\lambda_i}{\lambda} \log_2 \frac{\lambda_i}{\lambda}$$

Where λ_i is the average firing rate of a unit in the i-th bin, λ is the overall average firing rate, and p_i is the probability of the animal being in the i-th bin (dwell time in the i-th bin / total recording time). The average firing rate was calculated by dividing the total number of spikes in a trial by the trial duration, and the peak firing rate was the maximum firing rate within the firing field(s) of the cell. Sparseness is an estimate of how confined the place field of a place cell is in relation to the area of the test environment, and was calculated using the following formula (Jung, Wiener, & McNaughton, 1994):

$$Sparsity = \frac{(\lambda)^2}{(\lambda^2)} = \frac{(\sum p_i \lambda_i)^2}{(\sum p_i \lambda_i^2)'}$$

Where λ_i, λ, and p_i correspond to the same values as described for the calculation of spatial information content. Selectivity is a measure of how specific the spikes from the cell are to the place field(s) in an environment, and was calculated by dividing the maximum firing rate by the average firing rate. Spatial coherence estimates how coherent a firing field is by determining the extent to which firing rates within a pixel are matched with firing rates in adjacent pixels. This measure is calculated by correlating firing rates within each pixel with the firing rates in eight adjacent pixels, and returning the z-transform of this correlation (Muller & Kubie, 1989). To determine the stability of rate maps across trials, each pixel of the rate map from one trial was correlated with the corresponding pixel from a rate map from a second trial, generating a Pearson's correlation coefficient. Pixels corresponding to locations in the environment which the animal did not visit in one or both of the trials were discarded.

To visualise the location of place fields in the environment, two-dimensional and three-dimensional frequency plots were generated by dividing the area of the test environment into 8 x 8 bins and plotting the coordinates assigned to the centroid of each place field across these bins. The centroid of a place field was defined as the average position of the pixels of a place field along the X and Y axis, weighted by the firing rate of those pixels. Using this division of the environment, each quadrant of the environment constituted an array of 16 bins, where the four inner bins (15 x 15 cm) corresponded to the location of the object in each quadrant and the outer 12 bins corresponded to locations within 7.5 cm of the object. Frequencies of place fields in individual quadrants, and at previous and current object locations were extracted using these criteria.

2.2.13 Analysis of Place Cell Remapping

Population changes in spatial coding were quantified by examining the correlation of rate maps across trials. Remapping of individual cells in response to object displacement was quantified by examining the location of place field centroids and correlation of rate maps across S1, O1 and S2. Any cell which expressed no field in S1 and O1 or had a correlation coefficient between S1 and O1 which was greater than or equal to the average correlation coefficient between S1 and S2 for that region (distal or proximal) was categorised as non-remapping. The place fields of the remaining cells were examined for patterns corresponding to remapping behaviours that have been described previously (Muller & Kubie, 1978; Lenck-Santini et al. 2005; Manns & Eichenbaum, 2009; Deshmukh & Knerim, 2011). Remapping of place field locations was not examined for the novel object-place recognition trial given that the literature does not predict remapping to this type of manipulation (Lenck-Santini et al. 2005; Manns & Eichenbaum, 2009; Deshmukh & Knierim, 2013). However, rate remapping was examined across both spatial manipulations. To quantify rate remapping, overlap values were calculated for the average firing rates for each cell between the first standard trial and subsequent trials. These values were calculated by dividing the firing rate from the trial where the cell was the least active by the firing rate from the trial where the cell was the most active (see Leutgeb et al. 2004). Higher ratios indicate similarity in firing rates across trials, which corresponds with low rate remapping.

56

Table 2.1

Types of remapping in response to object displacement.

Type	Schematic	Critical Feature of Remapping Type
	S1 O1	
Novel Location		• Field develops near the displaced object.
Disrupted		• Field is disrupted by the displaced object.
New Field or Field Shift		• New field develops away from the displaced object.
Lost Field		• Field disappears.
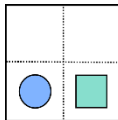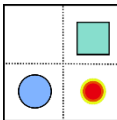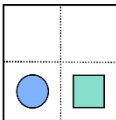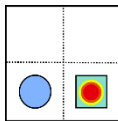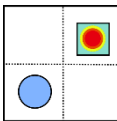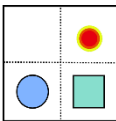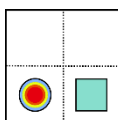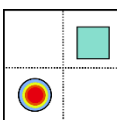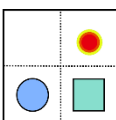
Note: Schematic contains idealised representations of place cells which demonstrate remapping responses. Red circles indicate location of place field centroid. Blue and green shapes indicate object locations. Right hand column summarises the key feature of each type of remapping.

Table 2.1 summarises the patterns of place field expression used to identify each type of remapping. Place cells were categorised as remapping to the novel object location if they expressed a place field in the quadrant which contained the displaced object in O1, but not S1. Place cells were categorised as disrupted by object displacement if a place field was expressed in the quadrant which contained the manipulated object in S1, and the peak firing rate was

57

reduced by ≥ 25% in O1 or the place field shifted ≥ 7.5 cm. 7.5 cm was chosen as cut-off value

given that this distance corresponds with the widths of the bins used to generate the plots of

centroid locations (see Section 2.2.12). Place cells were also categorised as remapping if the

pre-existing existing field shifted ≥ 7.5 cm or a new place field appeared at any location in the

box, or the number of place fields expressed reduced between S1 and O1.

Table 2.2

Types of trace firing observed in hippocampal place cells.

Type	Schematic			Critical Feature of Trace Firing Type
	S1	**O1**	**S2**	
Misplace				• Field develops in the 'old' object quadrant when an object is displaced.
Remap & Trace				• Field develops near the displaced object and persists firing there in subsequent trials.
No Remap & Trace				• Field develops in the 'new' object quadrant *after* the object is returned to its original location.

Note: Schematic contains idealised representations of place cells which demonstrate different patterns of trace

firing. Red circles indicate location of place field centroid. Blue and green shapes indicate object locations. Right

hand column summarises the key feature of each type of trace firing.

Table 2.2 summarises criteria used to identify trace firing. Trace firing was quantified by examining the location of place field centroids across S1, O1, and S2. Place cells were categorised as 'misplace' cells if they expressed a place field in the empty quadrant which previously contained the displaced object in O1, but not S1 (O'Keefe, 1976). Place cells were categorised as remapping 'trace' cells if they expressed a place field in the quadrant which contained the displaced object in O1, but not S1, and a place field persisted in this quadrant in S2. Place cells were categorised as non-remapping 'trace' cells if they did not express a place field in the quadrant which contained the displaced object in S1 or O1, but did express a place field in this quadrant in S2.

2.2.14 Statistical Analyses

All statistics were calculated in SPSS (IBM, version 24). Prior to analysis, normality of data was tested using the Shapiro-Wilk statistic. Where data was found to be non-normally distributed, an appropriate non-parametric alternative was used. To determine whether there was a significant difference across groups for behaviour and place cell characteristics, univariate ANOVAs or Kruskal-Wallis H-tests (non-parametric equivalent) were conducted with electrode location (distal versus proximal) as a between-subjects factor. For place cell characteristics, this analysis was conducted using average values collapsed across standard sessions alone, object manipulation sessions alone, and all trials collapsed for each cell. Where post-hoc multiple comparisons were conducted using t-tests or Mann-Whitney U tests, a Bonferroni correction was used to reduce the probability of Type I error. In these cases, the significance threshold was adapted by dividing the P-value of 0.05 by n comparisons. To determine whether patterns of remapping or trace firing were observed at similar proportions across groups, observed frequencies were compared across proximal and distal CA1 using a Chi-Square test of independence. Where there were < 5 observations in a category, Fisher's exact test of independence was used. To determine whether firing rates changed over the course

of a behavioural session, a repeated measures ANOVA or Friedman's repeated measures ANOVA (non-parametric equivalent) was conducted with electrode location (distal versus proximal) as a between-subjects factor. To determine whether there was a correlation between behaviour and place cell characteristics, Spearman's rank correlation coefficients were calculated with discrimination ratio for each object manipulation trial as a variable against the value (eg. spatial information score) for each unit recorded during that trial. To determine whether there was a correlation between behaviour and remapping, Spearman's rank correlation coefficients were calculated with discrimination ratio for each object manipulation trial as a variable against the correlation between rate maps in S1 and O1 (for object displacement), the correlation between rate maps in S1 and O2 (for novel object-place recognition), and the overlap between firing rates (for both object manipulation trials).

2.3 Results

2.3.1 Histology

Place cells were recorded from 7/14 of the implanted animals. Figure 2.2 contains images of electrode tract locations for all animals (Panel A and B). Visual inspection of the electrode tracts confirmed that all electrodes were positioned in CA1. The borders of CA1 were determined by referencing an atlas of the rat brain (Paxino & Watson, 2007). Electrode placement was confirmed to be in proximal CA1 for three of the seven animals, and distal CA1 for five of the seven animals. One animal (15049) had bilateral implants, with recordings in both proximal and distal CA1.
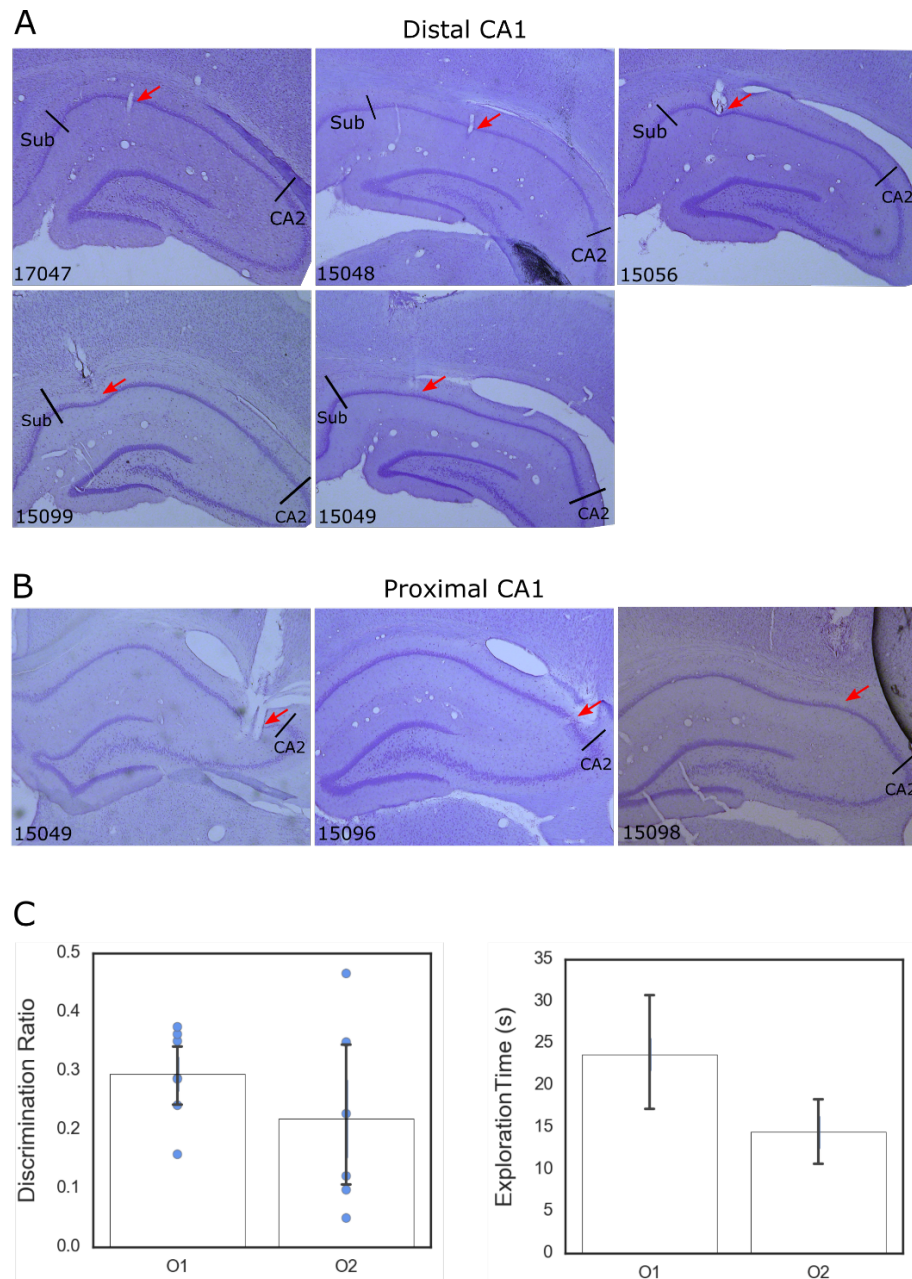
Figure 2.2: Electrode tract locations and behaviour. Electrodes were in distal (A) and proximal CA1 (B). Red arrows indicate electrode tract. Black lines indicate CA1 borders. Animal ID is noted in the bottom left corner of each image. (C) Average discrimination ratios (left) and exploration times (right) for all animals in object manipulation trials. Each dot indicates performance of a single animal. Error bars represent SEM. Abbreviations: Sub, subiculum; O1, object displacement; O2; novel object-place recognition.

2.3.2 Analysis of Behaviour

Panel C of Figure 2.2 shows discrimination ratios and exploration times for all animals from the object manipulation trials. Animals explored the displaced object more than predicted by chance in the object displacement trials (t (6) = 10.081, P < 0.001) and novel object-place recognition trials (t (6) = 3.305, P = 0.021). Importantly, there was no significant difference in performance between animals with electrodes in distal and proximal CA1 for object displacement ($F_{(1, 6)}$ = -0.309, P = 0.768), or novel object-place recognition, ($F_{(1, 6)}$ = -0.362, P = 0.730), which indicates that both groups recognised the novel configurations. Further, there was no significant difference across groups in the amount of time spent exploring the objects in standard ($F_{(1, 6)}$ = 1.594, P = 0.162) or object manipulation trials ($F_{(1, 6)}$ = 0.775, P = 0.468) which indicates that animals in both groups attended to the objects equally.

2.3.3 Cell Sample

A total of 395 place cells were recorded across 73 recording sessions from seven animals. After exclusion of repeat recordings, 285 place cells were accepted for analysis as determined by the criteria described in Section 2.2.11. A total of 1585 place fields were detected across all trials in all sessions (n distal = 1288, n proximal = 297). Of the accepted cells, 233 were recorded from distal CA1, and 52 were recorded from proximal CA1. Table 2.3 details the number of place cells recorded for each animal. Some cells were not recorded from the second object manipulation trial (n proximal = 3 cells, n distal = 11 cells) or in the final standard trial (n proximal = 7 cells, n distal = 11 cells). These cells were excluded from the analysis of place cell characteristics for these trials.

Table 2.3

Number of place cells recorded in distal and proximal CA1 across animals.

Animal ID	Electrode Location	# Cells	# Sessions	# Tetrodes
15049	Proximal CA1	22	7	3
15096	Proximal CA1	28	12	4
15098	Proximal CA1	2	1	2
15099	Distal CA1	3	1	2
15056	Distal CA1	46	7	4
15049	Distal CA1	106	23	4
15048	Distal CA1	75	20	4
17047	Distal CA1	3	2	2

Figure 2.3 contains representative units from the cell sample with high, intermediate and low isolation distances. Isolation distances were not different between place cells in distal and proximal CA1 (distal: $\bar{x} = 27.8 \pm 1.9$, $M = 19.8$; proximal: $\bar{x} = 25.2 \pm 2.9$, $M = 18.6$; $H(1) = 0.002$, $P = 0.840$) nor were the proportions of high, intermediate and poor quality clusters different between the two regions (High isolation, distal: 110/233 cells, 47.2%; proximal: 22/52 cells, 42.3%; $\chi^2 (1) = 0.411$, $P = 0.522$; intermediate isolation, distal: 100/233 cells, 42.9%; proximal: 23/52 cells, 44.23%; $\chi^2 (1) = 0.030$, $P = 0.862$; poor isolation, distal = 23/233 cells, 9.9%; proximal: 7/52 cells, 13.5%; $\chi^2 (1) = 0.582$, $P = 0.446$). This indicates that any differences reported between the two regions are not driven by poorly isolated units.

High Isolation   Intermediate Isolation   Poor Isolation

Calculated

Manual
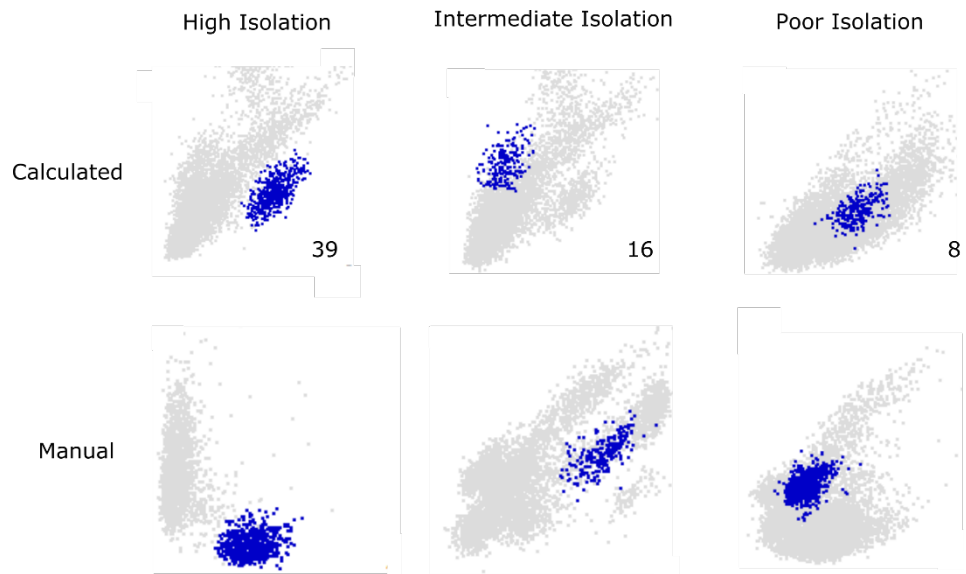
Figure 2.3: Representative examples of cluster quality. Each image shows all spikes for a trial plotted against principle components. Blue indicates spikes which belong to the isolated cluster. Top row shows representative units for which cluster quality was determined using the squared Mahalanobis distance, denoted by the value in the bottom right corner of each image. Bottom row shows representative units for which cluster quality was determined manually.

2.3.4 Increased Spatial Information and Selectivity in Distal CA1

The primary aim of this experiment was to determine whether place cell characteristics differed across the proximodistal axis of CA1 in an environment which contains objects. First, measures of spatial tuning were compared across place cells in distal and proximal CA1. The spatial information content of place cells was higher in distal CA1 in all trials (Fig. 2.4, Panel A). Place cells in distal CA1 contained significantly more spatial information in standard trials ($H(1) = 4.36$, $P = 0.037$), but not object manipulation trials ($H(1) = 1.974$, $P = 0.160$). Post-hoc pairwise comparisons revealed that distal CA1 cells had significantly higher spatial information content in the last standard trial, $U = 3305.5$, P = 0.009, adjusted significance threshold = 0.01), but not any other trial.

The higher spatial information content of place cells in distal CA1 was matched with higher spatial selectivity in all trials compared to proximal CA1 (Fig 2.6, Panel A). The firing of place cells in distal CA1 was significantly more selective in standard trials (H (1) = 4.888, P = 0.029), but not object manipulation trials (H (1) = 0.768, P = 0.381). Post-hoc pairwise comparisons revealed no significant difference in spatial selectivity for any individual trial (adjusted significance threshold = 0.01).

In contrast, there was no significant difference in the sparsity or spatial coherence of place cells in distal and proximal CA1 (Figure 2.6, Panel B and C). Although the firing of place cells in proximal CA1 was sparser than the firing of place cells in distal CA1 in all trials, this difference did not reach significance for standard (H (1) = 3.678, P = 0.055), or object manipulation trials (H (1) = 1.923, P = 0.166). The spatial coherence of place fields was similar across distal and proximal CA1 in standard (H (1) = 0.461, P = 0.497), or object manipulation trials (H (1) = 0.054, P = 0.816). These findings are at odds with reports of lower spatial information and coherence in distal CA1 (Henriksen et al. 2010), and suggest that the presence of objects in the environment drives increased spatial tuning in this region.

Given variability in the number of place cells recorded across animals, it is possible that the results reported here are driven by data from animals in which a large number of place cells were recorded (eg. 15049. See Table 2.3). To examine this possibility, plots were generated which compared place cell characteristics across all animals which yielded >5 place cells (Fig. 2.5 & Fig. 2.7). Importantly, for both spatial information (Fig 2.5) and selectivity (Fig 2.7), the mean values for animals with electrodes in distal CA1 were higher than those for animals with electrodes in proximal CA1 as collapsed across standard trials in all cases. This suggests that the observation of significantly higher spatial information and selectivity in distal CA1 place cells in standard trials is not driven by recordings from a single animal.
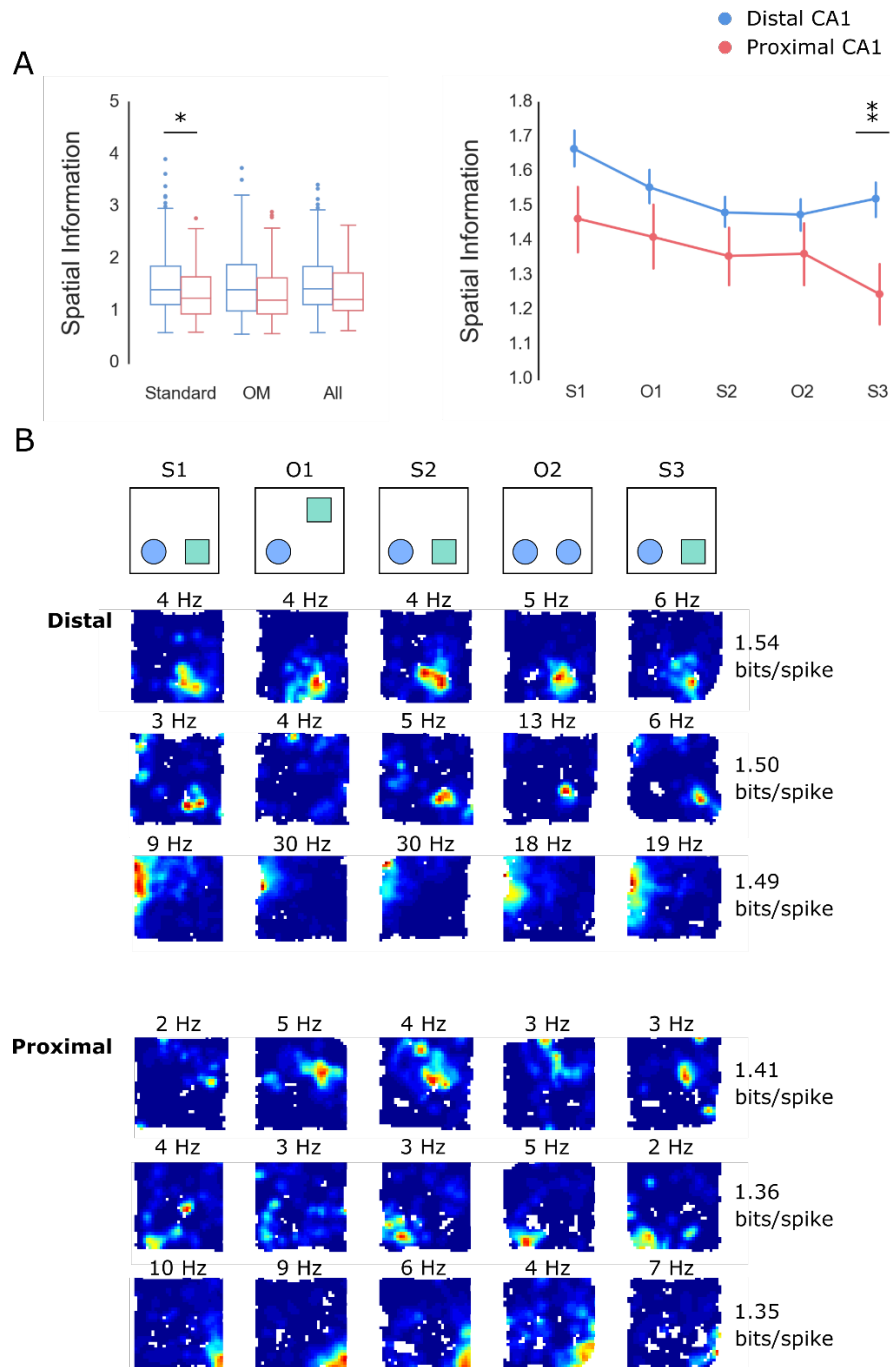
Figure 2.4: Spatial information content along the proximodistal axis of CA1. A) Plots compare values across distal (blue) and proximal (red) cells. Boxplots (left) represent values collapsed across standard, object manipulation (OM), and all trials for each region. Line plots (right) show mean values for each trial. Error bars represent SEM. Asterisks indicate *P*-values <0.05 (*) or <0.01 (**). B) Examples of place cells in distal (top) and proximal (bottom) CA1 with spatial information scores within one standard error of the mean for that region. (Top) Schematic of trials in a session. Rows contain rate maps and peak firing rate of a single cell for each trial.
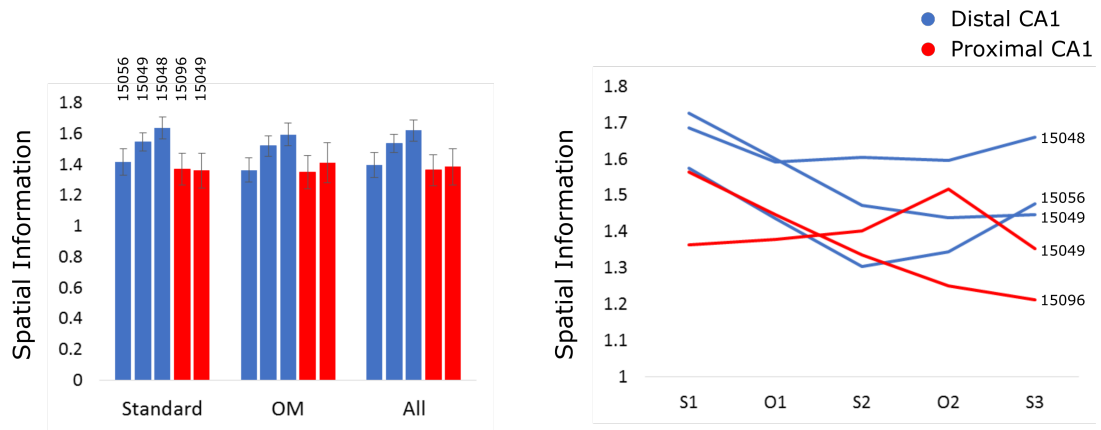
Figure 2.5: Spatial information along the proximodistal axis of CA1 by individual animal. Data is shown for all animals where >5 place cells were recorded (n = 4). Data from electrodes implanted in distal CA1 are represented in blue, and data from electrodes implanted in proximal CA1 are represented in red. Bar chart (left) shows average spatial information scores across all place cells recorded in each region for each animal. Data is collapsed across standard, object manipulation (OM), and all trials. Corresponding animal identification numbers are denoted above bars for standard trial data. Error bars represent SEM. Line plot (right) shows mean values for each trial. Each line represents values for an individual animal. Corresponding animal identification numbers are denoted to the right of the line plot.
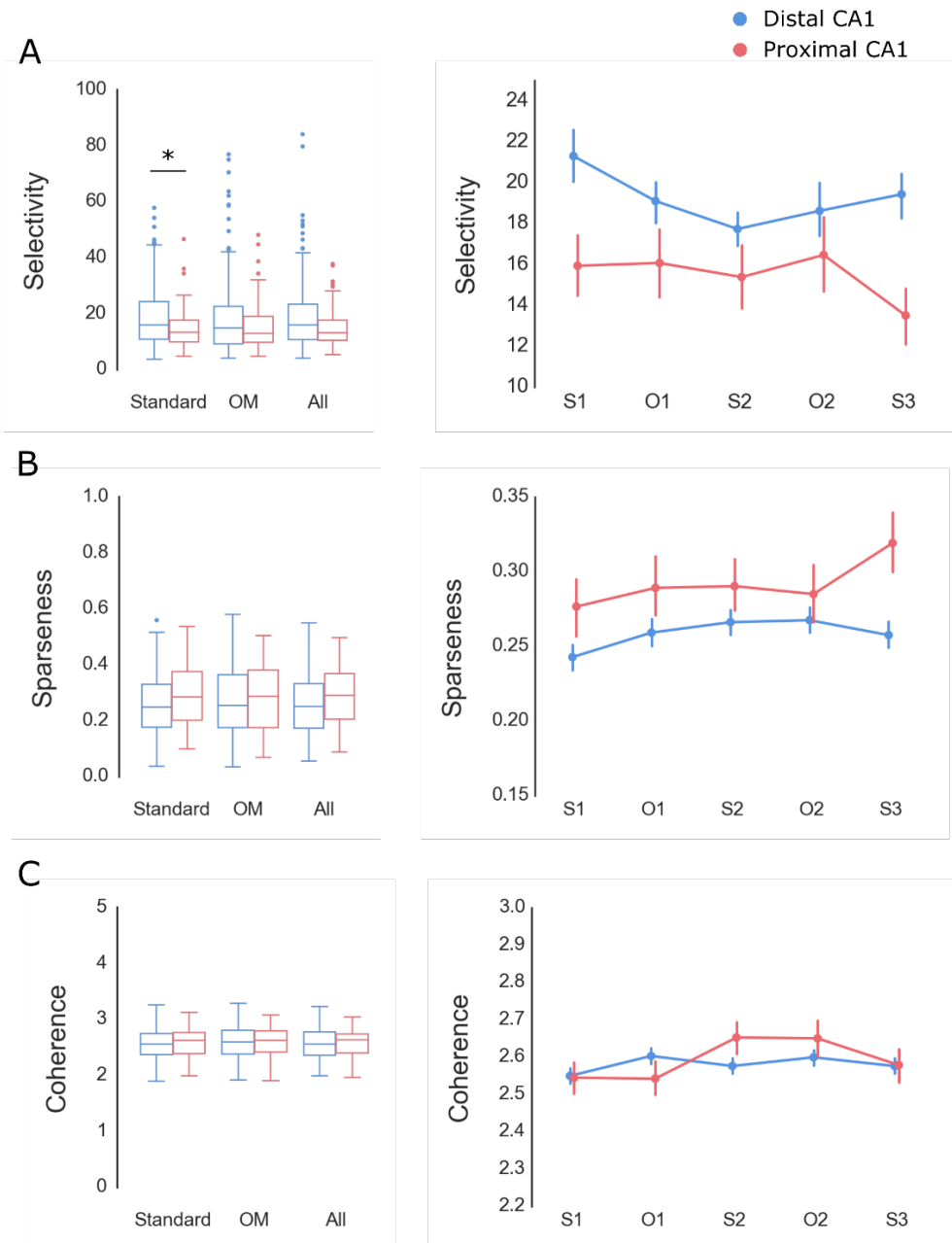
Figure 2.6: Spatial tuning along the proximodistal axis of CA1. Plots compare values for selectivity (A), sparseness (B), and spatial coherence (C) across distal (blue) and proximal (red) cells. Boxplots (left) represent data collapsed across standard, object manipulation (OM), and all trials. Dots indicate outlier values. Line plots (right) show mean values for each trial. Error bars represent SEM. Asterisks indicate *P*-value <0.05 (*).
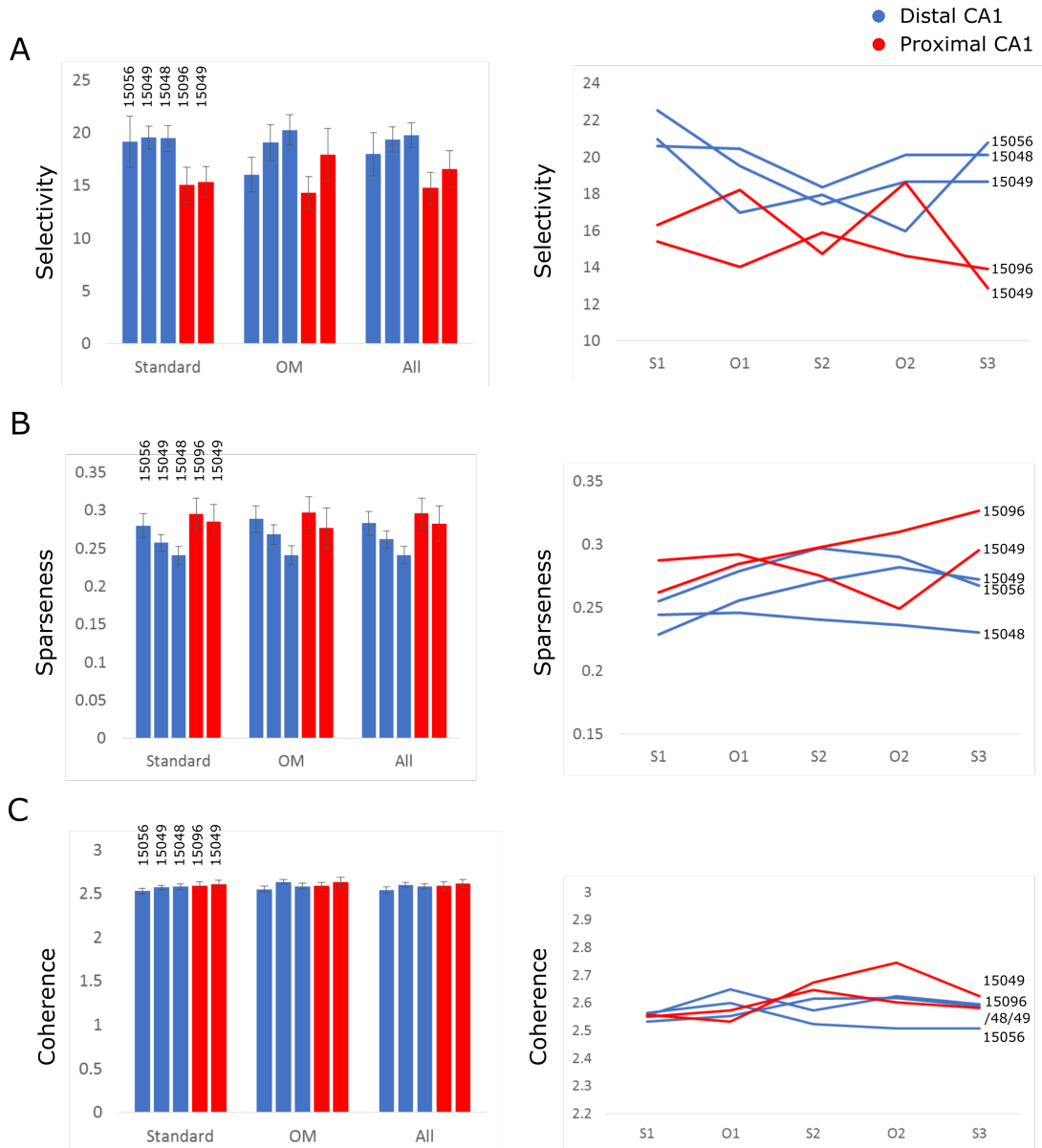
Figure 2.7: Spatial tuning along the proximodistal axis of CA1 by individual animal. Data is shown for all animals where >5 place cells were recorded (n = 4). Data from electrodes implanted in distal CA1 are represented in blue, and data from electrodes implanted in proximal CA1 are represented in red. Bar charts (left) show average values across all place cells recorded for each region for each animal. Data is collapsed across standard, object manipulation (OM), and all trials. Corresponding animal identification numbers are denoted above bars for standard trial data. Error bars represent SEM. Line plot (right) shows mean values for each trial. Each line represents values for an individual animal. Corresponding animal identification numbers are denoted to the right of the line plot.

2.3.5 Increased Stability in Distal CA1

To determine whether there was a difference in the amount of remapping across the distal and proximal CA1, the stability of place cells across trials was examined in each region. Stability was measured as the correlation of rate maps for each cell between the first standard trial and all subsequent trials. Higher spatial information content and selectivity in distal CA1 was matched by increased stability across standard and object manipulation trials (Fig. 2.8, Panel A). However, though the correlation between the first standard trial and subsequent standard trials were higher in distal CA1, this was not significant as compared across the first and second standard trial (H (1) = 1.815, P = 0.178), or first and last standard trial (H (1) = 2.601, P = 0.107). However, distal place cells were significantly more stable across the first standard trial and object displacement (H (1) = 6.344, P = 0.012), but not novel object-place recognition (H (1) = 1.376, P = 0.241). This suggests that distal CA1 cells maintain more stable representations of an environment which contains objects than cells in proximal CA1, particularly when the location of objects changes.

It is possible that the finding of higher stability across the first standard trial and object displacement is driven by data from animals in which a large number of place cells were recorded. However, all animals in the distal group had higher average correlations across the first standard trial and object displacement in comparison to animals in the proximal group (Fig. 2.8, Panel B), which suggests that this finding was not driven by data from a single animal.
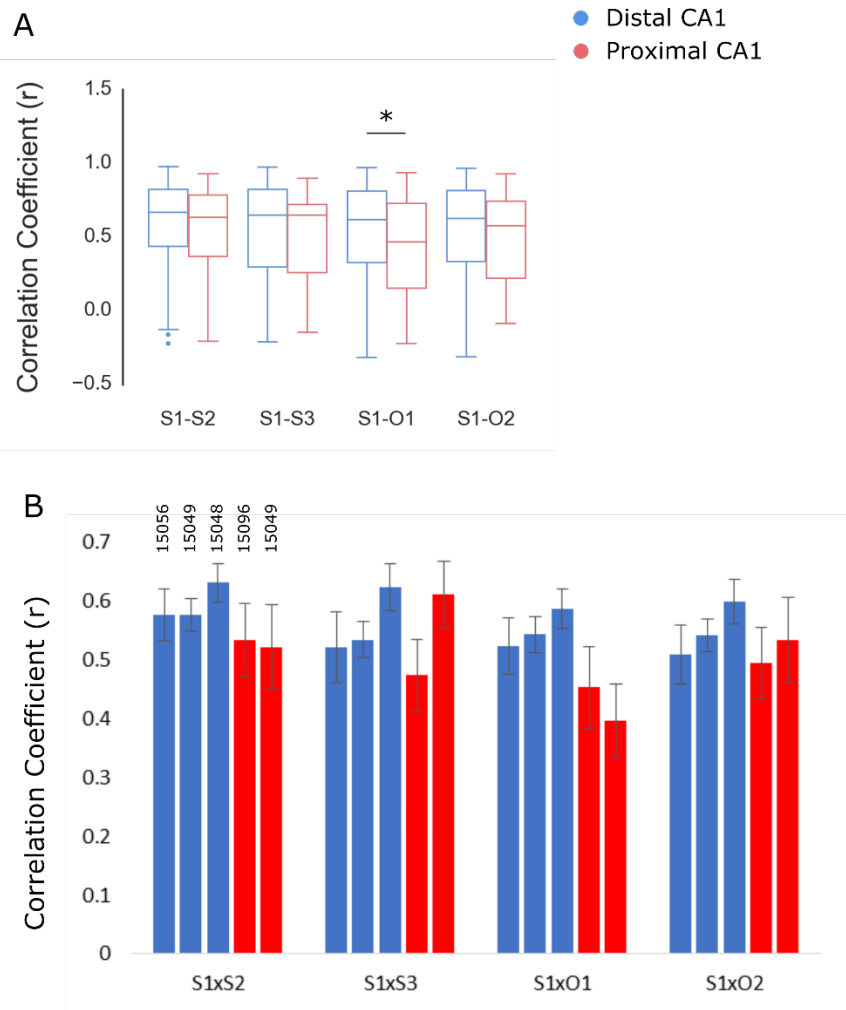
Figure 2.8: Stability across the proximodistal axis of CA1 (A) Boxplots show correlation values between the first standard trial (S1) and the last standard trial (S3), object displacement (O1), and novel object-place recognition (O2) for distal (blue) and proximal (red) cells. Dots indicate outlier values. Asterisks indicate P-values > 0.05 (*). (B) Bar charts show average correlation values between S1 and S3, O1 and O2 for place cells from each animal where >5 place cells were recorded (n=4). Data from electrodes implanted in distal CA1 are represented in blue, and data from electrodes implanted in proximal CA1 are represented in red. Data is collapsed across standard, object manipulation (OM), and all trials. Corresponding animal identification numbers are denoted above bars for standard trial data. Error bars represent SEM.

2.3.6 Place Field Size and Frequency Along the Proximodistal Axis of CA1

Given evidence that the presence of objects modulates the size and number of place fields expressed in distal CA1 (Burke et al. 2011), the frequency and size of place fields along the proximodistal axis of CA1 was examined. Although place fields were smaller in proximal CA1 than distal CA1 in all trials, this difference did not reach significance for standard (Fig. 2.9, Panel A; $H(1) = 3.534$, $P = 0.053$) or object manipulation trials ($H(1) = 0.121$, $P = 0.830$). Further, the average number of place fields exhibited by place cells in each region was similar in standard (Fig. 2.7, Panel B; $H(1) = 1.116$, $P = 0.291$) and object manipulation trials ($H(1) = 0.079$, $P = 0.778$).

Next, the frequency distribution of place fields across each trial for place cells in distal and proximal CA1 was examined (Fig. 2.9, Panel C). Similar proportions of cells in each region expressed only one field in standard trials (distal: 117/233 cells, 50.2%; proximal: 25/52 cells; 48.1%, $\chi^2(1) = 0.077$, $P = 0.780$) and both object manipulation trials (O1, distal: 158/233 cells, 67.8 %; proximal: 33/52 cells, 63.5 %, $\chi^2(1) = 0.364$, $P = 0.546$; O2, distal: 138/222 cells, 62.2 %; proximal: 32/49 cells, 65.3 %; $\chi^2(1) = 0.168$, $P = 0.680$). Further, although a higher percentage of proximal cells had more than one field in at least one session, this difference was not significant (distal: 135/233 cells, 57.9%; proximal: 36/52 cells, 69.2%; $\chi^2(1) = 2.258$, $P = 0.133$). These findings are inconsistent with previous reports that place cells in distal CA1 express more place fields than place cells in proximal CA1 (Henriksen et al. 2010; Burke et al. 2011), and suggest that distal and proximal CA1 place cells express similar numbers of place fields during recognition memory trials.

2.3.7 Distribution of Place Fields Across the Proximodistal Axis of CA1

A secondary aim of this experiment was to examine the object-modulation of place cells across the proximodistal axis of CA1. First, it was assessed whether place fields in either region of CA1 were more likely to be expressed at or near the locations of objects in the environment. Figure 2.10 shows frequency plots of place field locations in the box for each trial for distal (Panel A) and proximal CA1 (Panel B). Interestingly, place cells in proximal CA1 expressed a significantly higher proportion of place fields in a quadrant which contained an object in standard trials (distal: 364/776 fields, 46.9 %; proximal: 102/184 fields, 55.4%, χ^2 (1) = 4.33, P = 0.037) and object manipulation trials (distal = 240/512 fields, 46.9 %; proximal = 66/113 fields, 58.4 %, χ^2 (1) = 4.93, P = 0.026) compared to distal CA1 (Fig. 2.10, Panel C).

To further elucidate this finding, analysis was restricted to place fields expressed in quadrants which contained an object. Interestingly, a significantly higher proportion of the place fields in distal CA1 which were expressed in object quadrants were located in bins corresponding to object locations in standard trials (Fig 2.10, Panel D; distal = 106/364 fields, 29.1%; proximal: 18/102 fields, 17.7%; χ^2 (1) = 5.371, P = 0.021), but not object manipulation trials (distal = 62/240 fields, 25.8 %; proximal = 14/66 fields, 21.2 %; χ^2 (1) = 0.017, P = 0.898). These findings indicate that within quadrants of the environment which contain objects, place cells in distal and proximal CA1 are equally selective for objects when they are in a novel spatial configuration, but place cells in distal CA1 are more selective for objects when the location of objects in the environment is stable.
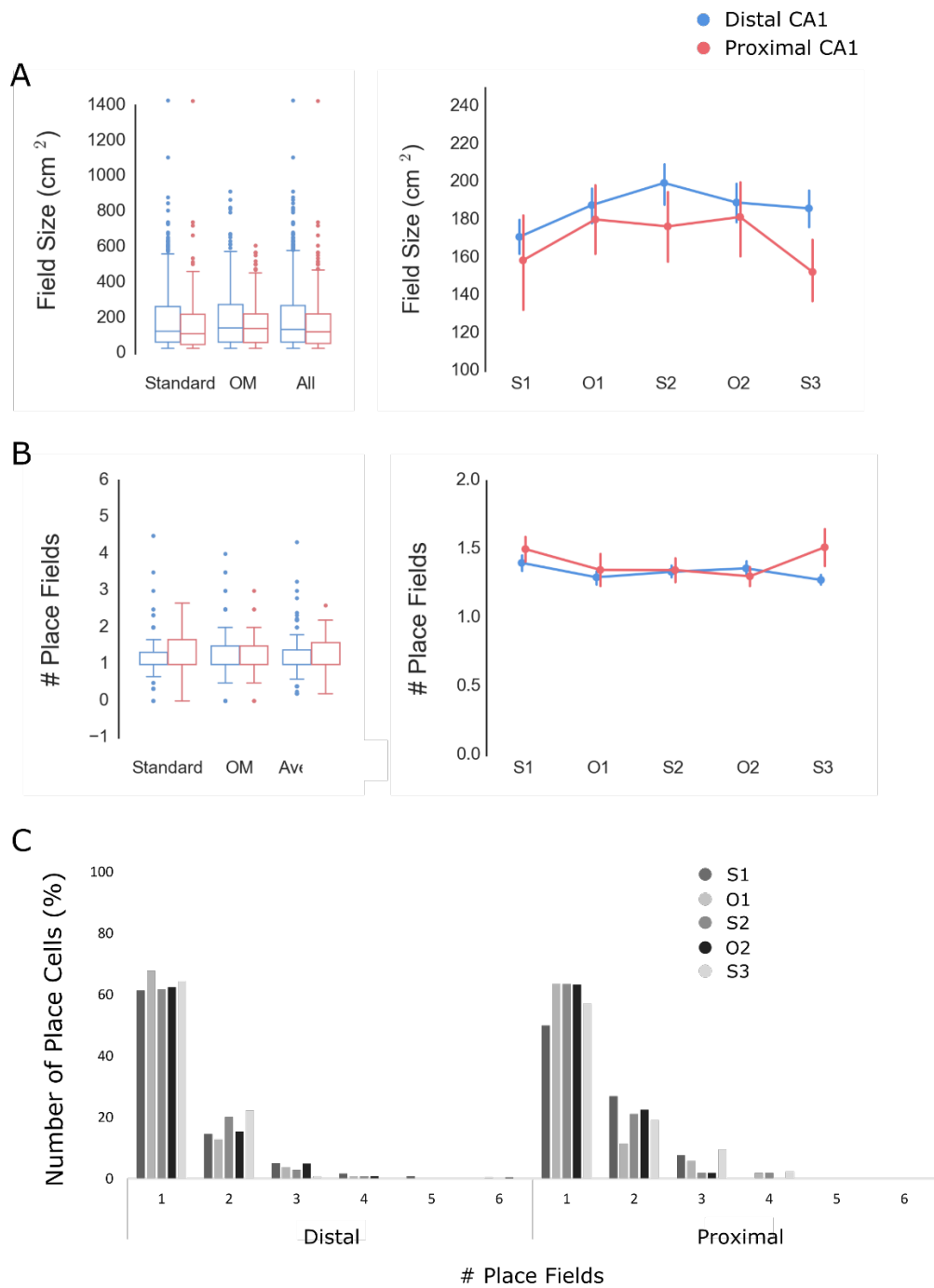
Figure 2.9: Place field size and frequency along the proximodistal axis of CA1. (A) Graphs show the size of place fields in distal (blue) and proximal (red) CA1. (B) Number of place fields expressed by cells in distal and proximal CA1. Boxplots (left) represent data collapsed across standard, object manipulation (OM), and all trials. Dots indicate outlier values. Line plots (right) show mean values for each trial. Error bars represent SEM. (C) Bar represent percentage of place cells which exhibit each number of fields in each trial for distal (left) and proximal CA1 (right). Grey shades indicate trial, and trials are presented in the order in which they occur in a recording session.
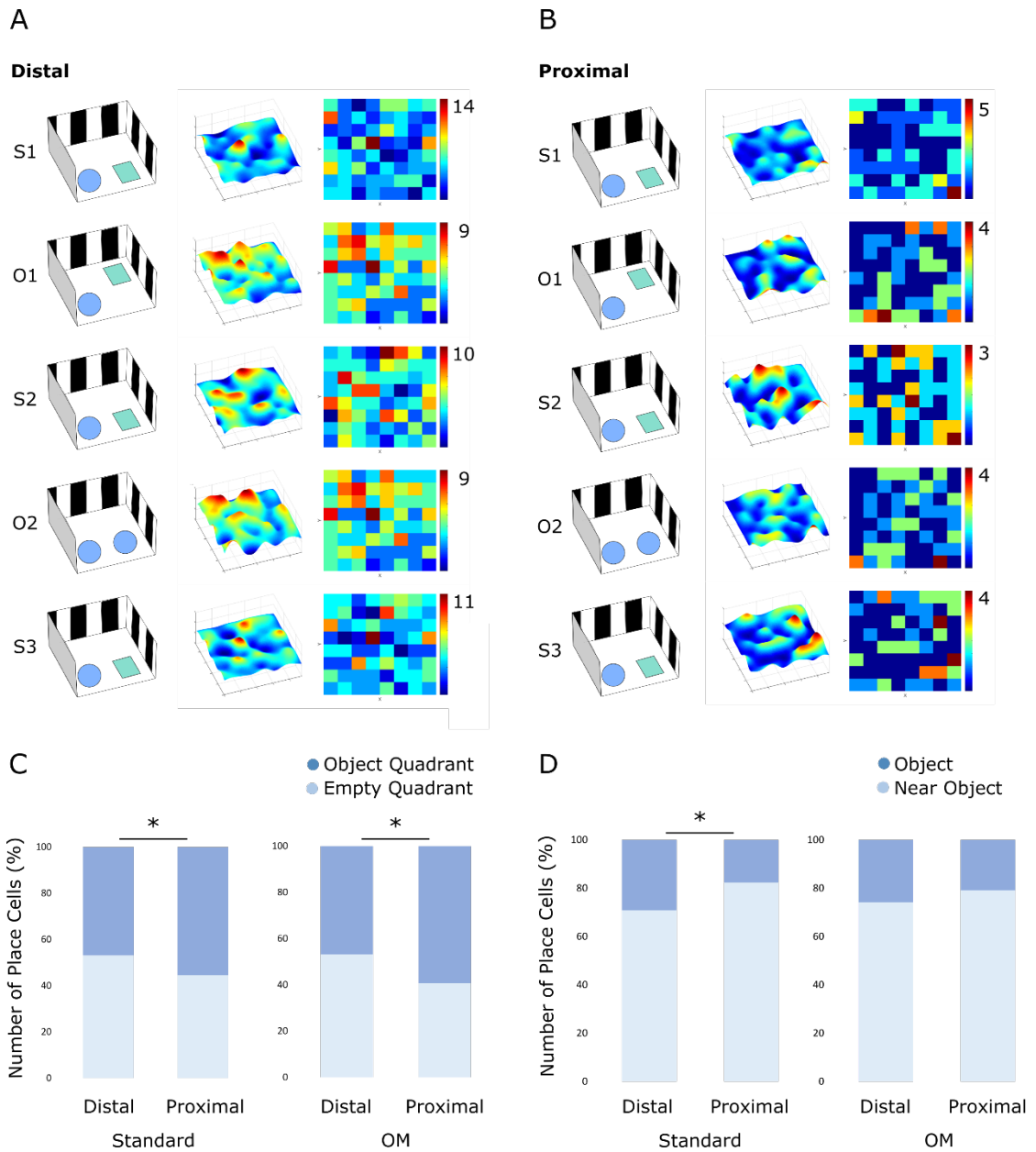
Figure 2.10: Place field locations across the proximodistal axis of CA1. Top panels contain three-dimensional (middle) and two-dimensional (right) representations of place field locations in the environment for distal (A) and proximal CA1 cells (B). High and low frequencies are indicated by warm and cool colours, respectively. Minimum frequency for all plots is 0, and maximum frequency is indicated by values to the right of the colour bar. (C) Bars show percentages of cells for each region with fields in the object quadrants (dark blue) or empty quadrants (light blue) for standard (left) and object manipulation trials (OM, right). (D) Bars show percentage of cells for each region with field at the object location (dark blue) or within the object quadrant (near the object, light blue) for standard (left) and object manipulation trials (OM, right). Asterisks indicate P-values <0.05.

2.3.8 Remapping to Object Displacement along the Proximodistal Axis of CA1

Next, remapping responses to object displacement were examined in distal and proximal CA1. Figure 2.11 contains representative examples of place cell activity across all trials of a session for both regions (Panel A). The proportion of place cells which remapped in response to object displacement was similar across distal and proximal CA1 (Fig. 2.11, Panel B; distal: 88/233 cells, 38.2%; proximal: 24/52 cells, 46.2%; χ^2 (1) = 1.125, P = 0.263). Proportions observed in individual animals were consistent with this finding (see Appendix A). To determine whether the strength of remapping differed between distal and proximal CA1, the correlation between the rate maps of remapping cells across the first standard trial and the object displacement trial was determined for each region. Rate maps for proximal CA1 were less similar across trials than in distal CA1, yet this difference did not reach significance (Fig 2.11, Panel C; distal: x̄ r = 0.25 ± 0.03, M r = 0.28; proximal: x̄ r = 0.15 ± 0.04, M r = 0.16; H (1) = 3.472, P = 0.052).

Within the population of remapping cells in each region, four types of remapping were observed, each consistent with previous observations (O'Keefe, 1976; Muller & Kubie, 1987; Lenck-Santini et al. 2005; Manns & Eichenbaum, 2009; Deshmukh & Knierim, 2013). The observed proportions of each type of remapping within the population of remapping cells are summarised in Table 2.4. Firstly, similar proportions of remapping cells in each region developed a place field in the quadrant which contained the displaced object (distal: 30/89 cells, 33.7%, proximal: 7/24 cells, 29.2%; χ^2 (1) = 0.207, P = 0.649). Within these cells, a higher proportion of cells in distal CA1 remapped to bins corresponding with the novel object location than cells in proximal CA1, yet this difference did not reach significance (distal: 15/30 cells, 50.0%, proximal 1/7 cells, P = 0.113, Fisher's exact test). Secondly, a subset of remapping cells in both regions suppressed their firing or remapped when the displaced object
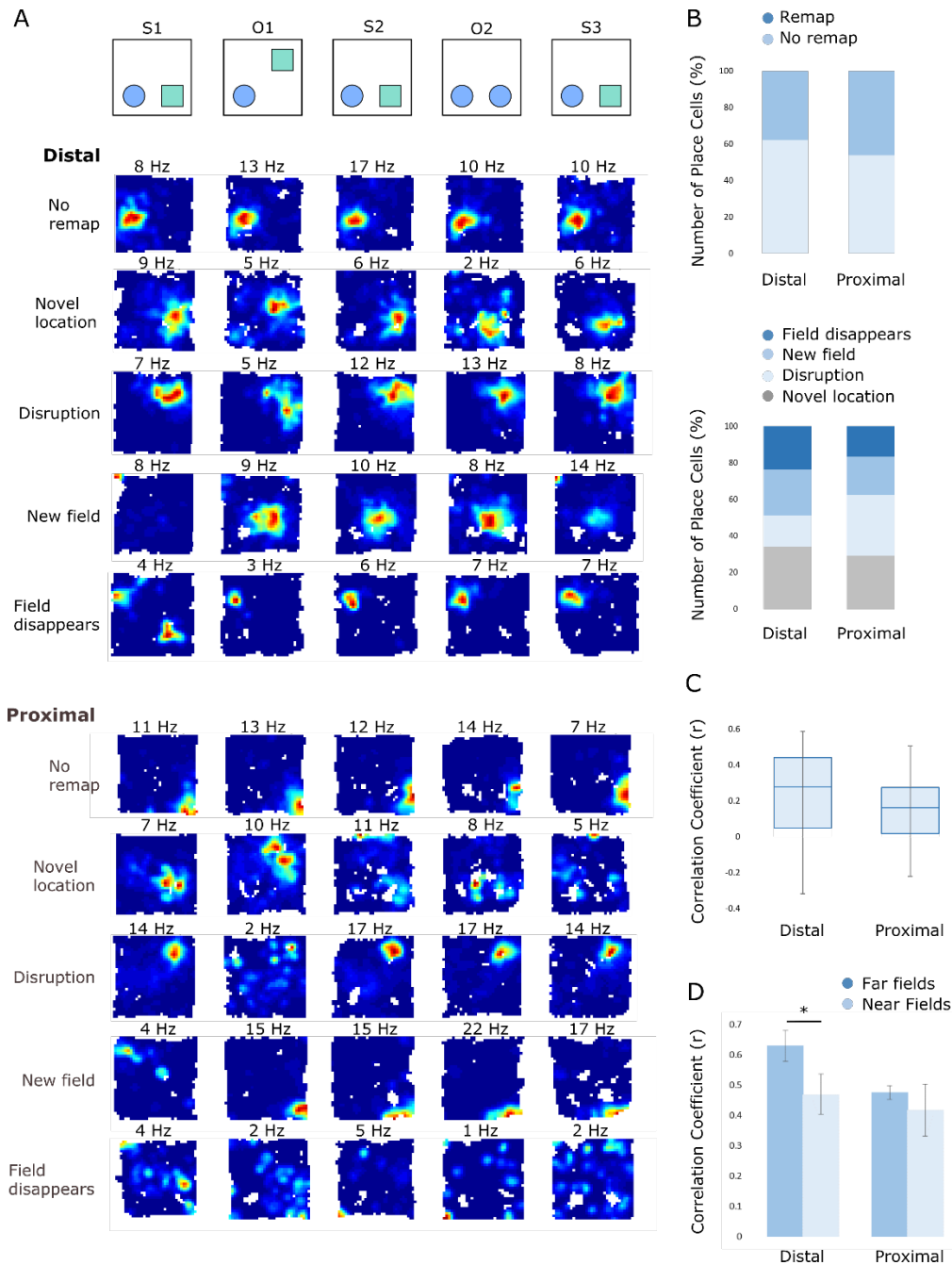
Figure 2.11: Remapping in distal and proximal CA1. (A) Representative examples of place cells in distal and proximal CA1. Top: Schematic of trials in a session. Rows contain rate maps and peak firing rate of a single cell for each trial. (B) Bars portray the observed proportion of remapping cells in each region (top) and of each type of remapping (bottom). (C) Boxplot portrays correlation between the first standard trial (S1) and object displacement (O1) for remapping cells in distal and proximal CA1. (D) Bars portray the correlations between rate maps of place cells expressing place fields near and far from the manipulated objects in S1 and O1. Error bars represent SEM. Asterisk indicates *P*-value <0.05.

entered a quadrant which contained a pre-existing place field (distal: 15/89 cells, 16.9%; proximal: 8/24 cells, 33.3%). Although proximal CA1 contained a higher proportion of cells which demonstrated this type of remapping, this difference did not reach significance ($\chi^2(1) = 3.066$, $P = 0.079$). Lastly, similar proportions of remapping cells in each region remapped to or developed a new place field at a novel location in the environment which was not in the quadrant containing the displaced object (distal: 21/88 cells, 24.7%, proximal: 5/24 cells, 20.8%; $\chi^2(1) = 0.097$, $P = 0.755$) or reduced the number of expressed place fields in response to object displacement (distal: 23/88 cells, 24.7%; proximal: 4/24 cells, 16.7%; $P = 0.426$, Fisher's exact test). Notably, proportions observed in the individual animal data were consistent with these findings (see Appendix B).

Further, to determine whether remapping was more likely in place cells which expressed place fields near objects, as described previously (Lenck-Santini et al. 2005), the proportion of remapping cells and correlation between firing rate maps across the first standard trial and object displacement were compared between 'near' and 'far' place cells for distal and proximal CA1. For these analyses, place cells which expressed place fields in the quadrant which contained the manipulated object in the first standard trial were categorised as 'near' the object, and place cells which expressed place fields elsewhere in the environment were categorised as 'far' from the object. Although the proportion of remapping cells was higher in 'near' place cells in both regions, this difference was significant for distal (53.4% of 'near' cells, 30.9% of 'far' cells, $\chi^2(1) = 7.418$, $P = 0.006$), but not proximal CA1 (56.3% of 'near' cells, 39.3% of 'far' cells, $\chi^2(1) = 1.181$, $P = 0.277$). Further, univariate ANOVAs with place field location (near vs far) as a between-group factor revealed that the correlation between rate maps for the first standard trial and object displacement was significantly lower for place cells with place fields near the objects in distal, but not proximal CA1 (Fig 2.11, Panel D, distal: $F_{(1, 195)} = 9.224$, $P = 0.003$, $\eta^2 = 0.045$; proximal: $F_{(1,42)} = 0.282$, $P = 0.626$). These data suggest

that place cells in distal and proximal CA1 are equally likely to remap in response to displacement, but this effect is modulated by proximity to object location in distal, but not proximal CA1.

Table 2.4

Proportions of remapping cells in distal and proximal CA1.

Type	Schematic	Distal Cells (%)	Proximal Cells (%)
Novel Location		33.7	29.2
Disrupted		16.9	33.3
New Field or Field Shift		24.7	20.8
Lost Field		24.7	16.7

Note: Schematic contains idealised representations of place cells which demonstrate remapping responses. The first box (left) represents the first standard trial (S1), and the second box (right) represents the object displacement trial (O1). Red circles indicate location of place field centroid. Blue and green shapes indicate object locations. Percentages represent a proportion of the remapping cells which demonstrate each response for each region.

2.3.9 Object-Place Memory along the Proximodistal Axis of CA1

A subset of 'trace' cells in both regions fired at empty locations in the environment where an object had previously been located, as described previously (O'Keefe, 1976; Deshmukh & Knierim, 2013). Figure 2.10 contains representative examples of these cells from each region of CA1 (Panel A). These cells were observed in similar proportions across distal and proximal CA1 (Fig 2.12, Panel B; distal: 42/233 cells, 18.0%; proximal: 11/52 cells, 21.2%; χ^2 (1) = 0.275, P = 0.600). Proportions observed in the individual animal data were consistent with this finding (see Appendix C & D).

Two types of trace firing were observed. Table 1.5 summarises the proportions of each type of trace firing observed within the population of trace cells. A subset of trace cells expressed place fields in the newly empty quadrant in the object displacement trial (distal = 17/42 cells, 40.5%; proximal = 6/11 cells, 54.6 %). The behaviour of these cells is consistent with the 'misplace' cells originally described by O'Keefe (1976). These cells were observed at similar frequencies across distal and proximal CA1 (Fig 2.12, Panel B; χ^2 (1) = 0.702, P = 0.402). A second subset of trace cells expressed a place field in the empty quadrant which housed the displaced object in subsequent trials after the object manipulation, consistent with the 'object-place memory' cells described by Deshmukh & Knierim (2013). These cells were also observed at similar frequencies across distal and proximal CA1 (distal: 27/42 cells, 64.3%, proximal: 5/11 cells, 45.5%; χ^2 (1) = 1.292, P = 0.256).

In our data set, these cells were further split into two categories. Some developed a place field in the novel quadrant in response to object displacement, and persisted firing there in subsequent trials after the object was returned to its original location ('remapping trace' cells), and were observed in similar frequencies across distal and proximal CA1 (distal: 15/42 cells, 35.7%; proximal: 4/11 cells, 36.4%; P = 1.00, Fisher's exact test). Similarly, some cells expressed a new place field in the empty novel quadrant, but only after the object was returned
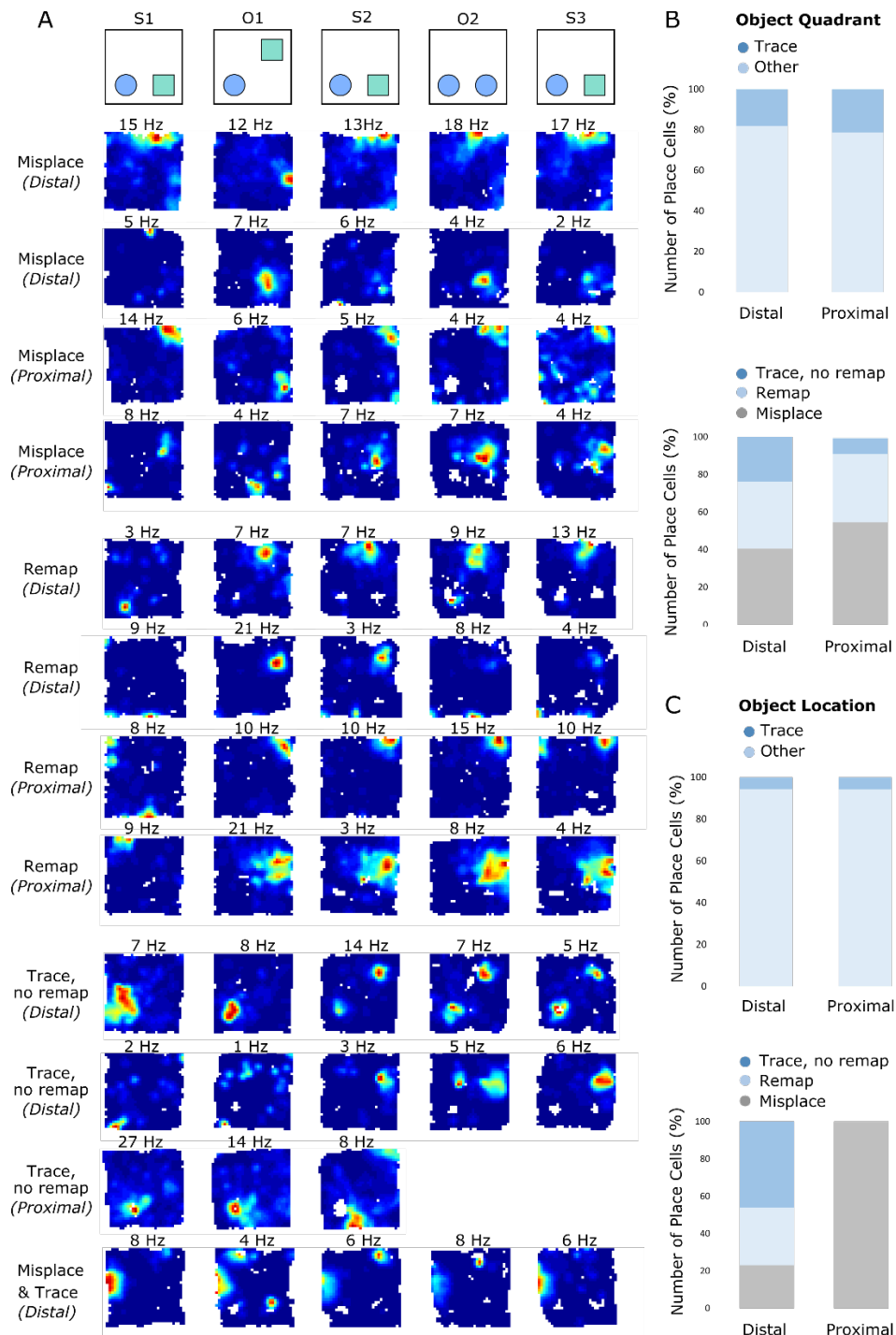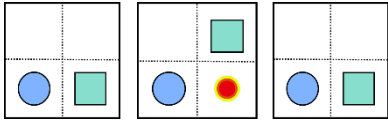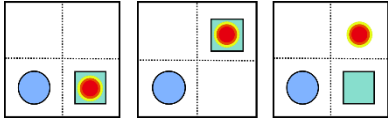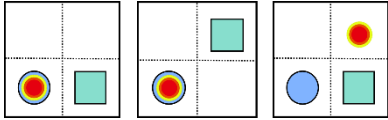
Figure 2.12: Trace cells in distal and proximal CA1. (A) Rows contain rate maps and peak firing rates of a single cell for each trial. Examples of remapping to the old location of a displaced object (top), the novel object location which persists in subsequent trials (middle), and trace firing in subsequent trials without remapping (bottom). (B) Bar graphs portray the proportion of trace cells in each region (top) and frequency of subtypes (bottom). (C) Bar graphs portray the proportion of trace cells with fields corresponding to object locations in each region (top) and frequency of subtypes (bottom).

81

to its original location ('non-remapping trace' cells), and were also observed in similar frequencies across distal and proximal CA1 (distal = 12/42 cells, 28.6%; proximal = 1/11 cells, 9.1%; P = 0.257. Fisher's exact test). Notably, two cells recorded from distal CA1 demonstrated misplace and trace behaviour, so were included in the above analyses for both categories (See Fig 2.12, bottom of Panel A).

Table 2.5

Proportions of trace firing in distal and proximal CA1.

Type	Schematic			Distal Cells (%)	Proximal Cells (%)
	S1	**O1**	**S2**		
Misplace				40.5	54.5
Remap & Trace				35.7	36.4
No Remap & Trace				28.6	9.1

Note: Schematic contains idealised representations of place cells which demonstrate different patterns of trace firing. The first box (left) represents the first standard trial (S1), the second box (middle) represents the object displacement trial (O1), and the third box represents the second standard trial (S2). Red circles indicate location of place field centroid. Blue and green shapes indicate object locations. Percentages represent a proportion of the trace cells which demonstrate each type of trace firing for each region.

Given our observation that distal CA1 place cells are more selective for object locations and more likely to be modulated by object displacement if they express place fields near an object, these analyses were repeated on cells which expressed place fields with centroids at coordinates corresponding to the previous object location. With these criteria, similar proportions of place cells in distal and proximal CA1 were classified as trace cells (Fig. 2.10, Panel C; distal: 13/233 cells, 5.6%; proximal: 3/52 cells, 5.8%; $P = 1.00$, Fisher's exact test). Although all proximal trace cells were classified as misplace cells, this proportional difference did not reach significance (distal: 4/13 cells, 23.1%; proximal: 3/3 cells, 100.0%; $P = 0.063$, Fisher's exact test). However, all cells which developed a field at the novel object location were recorded from distal CA1, a distribution which was statistically significant (distal: 10/13 cells, 76.9%, 4/13 remapping trace and 6/13 non-remapping trace; proximal: 0/3 cells, 0.0%; $P = 0.036$, Fisher's exact test). Notably, one cell recorded from distal CA1 demonstrated misplace and trace behaviour which was selective for object location. Considered together, these data suggest that trace cells are observed in similar proportions across the proximodistal axis of CA1, however only place cells in distal CA1 precisely encode recent new object locations within an environment.

2.3.10 Rate Remapping Along the Proximodistal Axis of CA1

Next, the firing rates of place cells in distal and proximal CA1 were examined. Place cells in proximal CA1 had higher average firing rates than place cells in distal CA1 in all trials, yet this difference was not significant for standard (Fig 2.13, Panel A; $H (1) = 1.470, P = 0.225$) or object manipulation trials ($H (1) = 0.429, P = 0.512$). Further, there was no difference in peak firing rates between place cells in distal and proximal CA1 for standard (Fig 2.13, Panel B; $H (1) = 0.551, P = 0.458$) or object manipulation trials ($H (1) = 0.129, P = 0.719$).
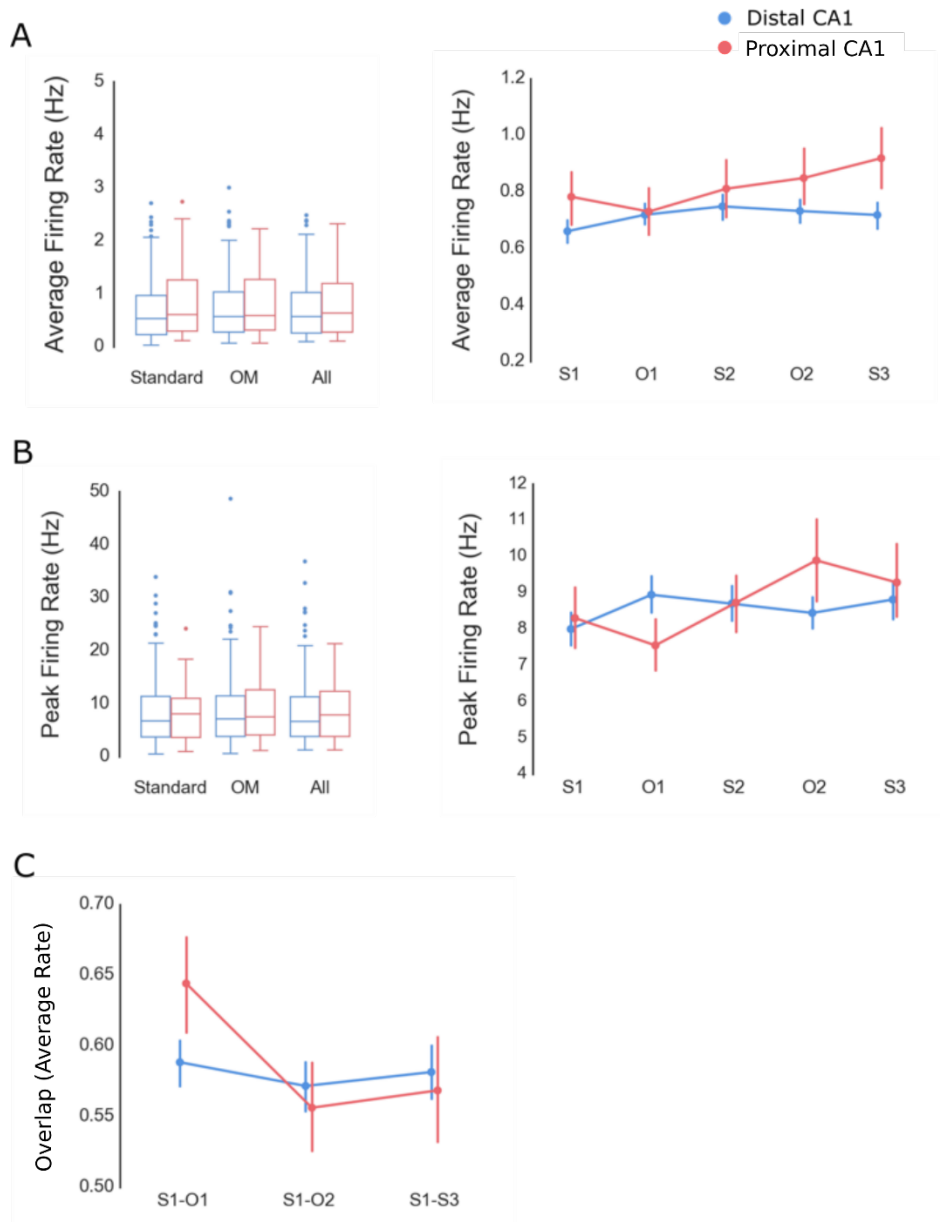
Figure 2.13: Firing rates across the proximodistal axis of CA1. Plots show average (A) and peak (B) firing rates for place cells in distal (blue) and proximal (red) CA1. Boxplots (left) represent data collapsed across standard, object manipulation (OM), and all trials. Dots indicate outlier values. Line plots (right) show mean values for each trial. Error bars represent SEM. (C) Overlap values for average firing rates between the first standard trial and object displacement (left), novel object-place (middle) and final standard trial (right).

Further, it was assessed whether rate remapping in response to either object manipulation was stronger in distal or proximal CA1. There were similar degrees of overlap between the average firing rates of place cells in distal and proximal CA1 across the first standard trial and object displacement (H (1) = 2.214, P = 0.137), novel object-place recognition (H (1) = 0.029, P = 0.866) and the last standard trial (H (1) = 0.135, P = 0.714). Interestingly, average firing rates did not change significantly as a function of trial distal, (χ^2 (4) = 6.771, P = 0.149), or proximal CA1 (χ^2 (4) = 8.743, P = 0.068). These data suggest that neither region demonstrated robust rate remapping to either object manipulation.

2.3.11 No Relationship Between Place Cell Characteristics and Behaviour

Finally, the relationship between place cell activity and behaviour was examined by determining whether there was a correlation between place cell characteristics and discrimination ratios for each object manipulation trial. There was no relationship between performance on the object displacement trial and spatial information (distal: r_s = 0.006, P = 0.927; proximal: r_s = -0.192, P = 0.192), selectivity (distal: r_s = -0.34, P = 0.618; proximal: r_s = -0.111, P = 0.453), sparseness (distal: r_s = -0.009, P = 0.894; proximal: r_s = 0.133, P = 0.368), spatial coherence (distal: r_s = 0.061, P = 0.365; proximal: r_s = -0.134, P = 0.365), place field frequency (distal: r_s = 0.024, P = 0.719; proximal: r_s = -0.218, P = 0.136) or place field size (distal: r_s = 0.018, P = 0.794; proximal: r_s = 0.162, P = 0.270) for place cells in distal or proximal CA1. Similarly, there was no relationship between performance on the novel object-place recognition trial and spatial information (distal: r_s = -0.039, P = 0.594; proximal: r_s = -0.103, P = 0.505), selectivity (distal: r_s = -0.080, P = 0.269; proximal: r_s = -0.021, P = 0.889), sparseness (distal: r_s = -0.076, P = 0.273; proximal: r_s = 0.090, P = 0.547), spatial coherence (distal: r_s = -0.009, P = 0.899; proximal: r_s = -0.028, P = 0.853), place field frequency (distal: r_s = 0.064, P = 0.366; proximal: r_s = -0.197, P = 0.185) or size (distal: r_s = 0.064, P = 0.366;

proximal: r_s = -0.105, P = 0.484) for place cells in distal or proximal CA1. Overall, these data indicate that performance on either object manipulation trial has no significant effect on spatial tuning or place field expression.

Similarly, there was no relationship between performance on the object displacement trial and stability across the first standard trial and object displacement (distal: r_s = -0.058, P = 0.389; proximal: r_s = -0.118, P = 0.426). There was also no relationship between performance on the novel object-place recognition trial and stability across the first standard trial and the novel object-place recognition trial (distal: r_s = -0.044, P = 0.533, proximal: r_s = -0.136, P = 0.361). Lastly, there was no relationship between performance and the overlap of average firing rates between the first standard trial and object displacement (distal: r_s = -0.073, P = 0.276, proximal: r_s = 0.079, P = 0.593) or novel object-place recognition (distal: r_s = -0.016, P = 0.823, proximal: r_s = -0.093, P = 0.532) for either region. Overall, these data indicate that performance on either object manipulation trial has no significant effect on remapping.

2.4 Discussion

The aim of this experiment was to examine whether differential input from entorhinal cortex L3 influences place cell activity in CA1 of the hippocampus. To this end, the activity of place cells in distal and proximal CA1 were recorded as rats explored an environment which contained objects that underwent two spatial manipulations. In the first object manipulation, an object was moved to a novel location in the environment which was previously empty. In the second object manipulation, one object was presented in a novel object-place configuration. It was hypothesised that input into distal CA1 from LEC L3 would drive differences in spatial tuning and object modulation between the two regions.

First, spatial tuning and place field expression was examined across distal and proximal CA1. Indeed, it was observed that the firing of place cells in distal CA1 was more stable, more

spatially selective and contained higher spatial information content than place cells in proximal CA1. This contradicts previous reports of higher spatial tuning in proximal CA1 in empty environments (Henriksen et al. 2010). However, these differences were not consistent across all trials of a behavioural session, but were driven by recordings from standard trials where the objects were in stable locations. This might suggest that both regions of CA1 are equally spatially modulated under experimental conditions where local cues are unstable. Further, there was no difference in the coherence, sparsity, size or number of place fields expressed by cells in distal and proximal CA1. This contrasts with the exhibition of fewer, more coherent place fields by place cells in proximal CA1 in empty environments (Henriksen et al. 2010), and suggests a degree of uniformity in place field expression under experimental conditions where objects are present. Considered together, these findings provide strong evidence that the presence of objects influences the basic characteristics of place cells in CA1.

The similarity in size and number of place fields is particularly interesting given previous reports of increased place field expression in distal CA1 in empty and cue-rich environments, and a decrease in place field size in distal CA1 upon presentation of objects (Henriksen et al. 2010; Burke et al. 2011). Conversely, in our dataset, place fields expressed by place cells in proximal CA1 were consistently larger than those expressed in distal CA1, and were more likely to express more than one place field in a session, although neither of these trends reached statistical significance. This disparity may be due in part to a difference in electrode location; Burke et al. (2011) recorded place cells in intermediate CA1, where the segregation of lateral and medial entorhinal input is more difficult to establish. Our test environment was also smaller than environments used by others, which may affect the size and number of place fields expressed by place cells in both regions. Further, it is possible that any object-modulation of place fields in distal CA1 is masked by the exclusion of a no-object trial in our experimental design. Future work might integrate object and no-object trials to determine

the flexibility of spatial tuning in these regions. If objects function as landmarks, their presence in the environment might result in less dependence on proprioceptive spatial signalling from the MEC, and result in an increased influence of LEC L3 input in CA1. Therefore, the characteristics of single cells in either region may fluctuate with the availability of local cues.

Given stark similarities in the patterns of object modulation described in the LEC and hippocampus, it was further hypothesised that place cells in distal CA1 would be more likely to express place fields at object locations, remap to object displacement, and rate remap to either object manipulation. Surprisingly, it was observed that place cells in proximal CA1 are more likely to develop place fields in quadrants of the environment which contain objects. However, within these quadrants, place cells in distal CA1 are more selective for object location, whereas place cells in proximal CA1 are more likely to fire at locations around the object. It is possible that place cells which fire near object locations bear resemblance to 'object-vector' cells described by Deshmukh & Knierim (2013), which fire at discrete distances away from objects in a large environment. In their experiment, object-vector cells were observed in both regions of CA1, yet a small sample size precluded an analysis of their distribution. Extending this, our data might suggest that these cells are more likely to occur in proximal CA1, whereas place cells which express place fields at object locations are more likely to occur in distal CA1. Repetition of our experiment in a larger environment where vectors could be calculated would address this possibility.

Further, though remapping in response to object displacement was observed in similar proportions of place cells in distal and proximal CA1, remapping was only modulated by place field proximity to the object in distal CA1. The high degree of object-modulation in proximal CA1 is unexpected, and is at odds with previous reports of increased recruitment of distal CA1 in object-based memory tasks (Ito & Schuman, 2012; Nakamura et al. 2013; Hartzell et al. 2013; Nakazawa et al. 2016). However, this finding is consistent with significantly lower

stability across the first standard trial and object displacement in proximal CA1. These data suggest that distal CA1 place cells maintain stable representations of an environment which is rich in local landmarks, and are less sensitive to changes to the spatial configuration of objects unless they encode space near an object location.

Relatedly, it was observed that both distal and proximal CA1 contain a small subset of neurons which fire at previous object locations. Interestingly, place cells in proximal CA1 are more likely to develop a new field at the old object location when an object is displaced, and place cells in distal CA1 are more likely to maintain a new field at the new object location after the object has been returned to its original location. Though these cells have been described previously (O'Keefe, 1976; Deshmukh & Knierim, 2013), this is the first examination of their distribution across the proximodistal axis. Interestingly, the trace behaviour described in distal CA1 bears clear similarities to trace cells in the LEC (Tsao et al. 2013), which suggests that this type of spatial signalling may be generated via input from the lateral perforant pathway. It would be interesting to examine whether these memory traces are robust over time, as has been described within the LEC.

Finally, no significant difference in firing rates was observed across regions, and neither region encoded the spatial changes to objects in their firing rate, as has been described previously (Komoroswki et al. 2009; Manns & Eichenbaum, 2009; Larkin et al. 2014). This finding is difficult to reconcile with previous literature, but may be driven in part by differences in saliency and abundance of objects used; Komorowski et al. (2009) utilised rewarded objects, Manns & Eichenbaum (2009) presented > 2 objects in their paradigm, and Larkin et al. (2014) presented a completely novel object during novel object-place recognition. It is possible that increasing the saliency of our stimuli would reveal a different pattern of rate remapping across the proximodistal axis.

Our analysis is limited by several factors. Firstly, our dataset contains substantially more recordings from distal CA1, which affects the statistical power of our findings. Supplemental recordings from proximal CA1 might strengthen the patterns described here and further elucidating proportional differences across the proximodistal axis of CA1 for different remapping and trace behaviours. A larger datsaset would also permit a more thorough examination of trace firing across this axis, given that this phenomenon is only observed in a small portion of the population. Secondly, as discussed, the exclusion of a no-object trial precludes an explicit comparison between measures of spatial tuning in the same population of place cells in an empty and cue-rich environment. Future work could integrate different types of trials, possibly comparing activity of place cell populations during manipulations of objects and/or spatial context, as well as no-object trials, to further elucidate how input from LEC and MEC L3 may contribute to the processing of objects and spatial context, respectively. Thirdly, this experiment uses a correlational method to measure the influence of LEC L3 input on place cell activity in CA1. These data are restricted by the lack of evidence that LEC L3 input is required for the effects described here. Future work could examine place cell activity across the proximodistal axis of CA1 after selective lesions to LEC and MEC to further elucidate the present finding. Further, molecular tools which isolate the output from entorhinal cortex L3, as have recently been developed for entorhinal cortex L2 (Surmeli et al. 2015), would be valuable for further discerning the contribution of entorhinal cortex L3 to the episodic memory circuit.

Overall, the data provide strong support for our primary hypothesis; in an environment which contains objects, place cells in distal CA1 demonstrate a higher degree of spatial tuning than place cells in proximal CA1. Given the object-modulated spatial tuning observed upstream in the PER and LEC, it is possible that this pattern is driven by perforant pathway input into distal CA1 via LEC L3. In contrast, there is mixed support for our secondary hypothesis; place cells in distal and proximal CA1 demonstrate similar levels of remapping to the spatial

manipulation of objects, and place cells in proximal CA1, which receive input from MEC L3, are more likely to develop place fields in quadrants which contain an object, but not at precise object locations. This suggests that encoding spatial changes to local landmarks is not differentially organised across regions of CA1 which receive input from LEC or MEC. However, remapping in distal CA1 appears to be closely tied to current and previous object locations in the environment, whereas proximal CA1 is more likely to remap to locations near a displaced object within the novel quadrant, or remap elsewhere in the environment. This might suggest that place cells in distal CA1 are more selective for object location, whereas place cells in proximal CA1 encode a more general representation of each novel spatial configuration. This could be driven by the types of input each region receives; input from the global spatial metric of the MEC drive remapping across the entire environment, whereas spatial signalling originating from object-responsive cells in the LEC might drive patterns of remapping which are more selective for landmarks in the environment. Considered together, these findings suggest that LEC L3 might contribute to the episodic memory network by modulating the spatial signal in the hippocampus in relation to objects in space.

2.5 Conclusions

To summarise, place cells in distal CA1 demonstrate a higher degree of spatial tuning than place cells in proximal CA1 in an environment which contains objects. Further, although place cells in distal and proximal CA1 both remap in response to object displacement, this remapping response is modulated by proximity to objects in distal CA1. Lastly, CA1 contains a sub-population of cells which express place fields at previous object locations, and only place cells in distal CA1 precisely encode the recent new location of objects in the environment. This may represent a neural mechanism for object-place memory which is driven by input from LEC L3. This possibility could be further investigated using molecular tools which permit selective

manipulation of LEC L3 input into the hippocampus. The next experimental chapter describes

the characterisation of similar tools for LEC L2.

Chapter 3: Investigating the Molecular Organisation of Layer 2 of the Lateral

Entorhinal Cortex

3.1 Introduction

The experiment presented in the previous chapter capitalised on the divergent nature of projections from MEC and LEC into CA1 of the hippocampus, using in-vivo electrophysiology to indirectly measure the influence of LEC L3 input on place cell activity. In the discussion, it was stated that the availability of molecular tools which permit precise manipulation of laminar output from LEC to the hippocampus would be instrumental to progress in the field. To this end, the experiments presented in this chapter examined the arrangement of projecting neurons in LEC L2 and identified a molecular tool which provides genetic access to a sub-population of neurons within this layer.

The superficial layers are well established as the main source of output to the hippocampal formation from the entorhinal cortex (Dolorfo & Amaral, 1998; Van Groen et al. 2003; Van Strien et al. 2009). Sections 1.2.2 and 1.2.3 of the general introduction provide a detailed overview of the immunohistochemical, electrophysiological and morphological properties of the principal neurons which constitute the layers of the entorhinal cortex (also see Witter et al. 2017 for a recent review). The present discourse focusses on LEC L2, which is a promising layer for further study given that disrupted signalling from LEC L2 to the hippocampus is explicitly associated with age-related cognitive decline (Gomez-Isla et al. 1996; Stranahan & Mattson, 2010; Stranahan et al. 2013; Khan et al. 2014), and the molecular organisation of its medial counterpart is well described (Kitamura et al. 2014; Surmeli et al. 2015).

To summarise briefly, MEC L2 is composed of two types of excitatory principal cells: 'stellate' and 'pyramidal' cells, which are distinguished by distinct morphological and electrophysiological profiles. Stellate and pyramidal cells are further dissociated by their molecular composition and the structures which they project to; stellate cells are immunoreactive for the protein reelin, and project to the DG and CA3, whereas pyramidal cells

are immunoreactive for the protein calbindin and project to CA1 and the subiculum (Varga, Lee, & Soltesz, 2010; Kitamura et al. 2014; Ray et al. 2014; Surmeli et al. 2015). Until recently, there was considerably less known about the molecular organisation of the LEC L2. Interestingly, LEC L2 bifurcates into two distinct sub-layers, L2a and L2b, which contain neurons that are immunoreactive for reelin and calbindin, respectively (Fujimaru & Kosaka, 1996; Leitner et al. 2016, Witter et al. 2017). As in the MEC, these two sub-populations of cells correspond with discrete output pathways. LEC L2a reelin-positive cells project to the DG and LEC L2b calbindin-positive cells do not project to the hippocampus, but send feedback to olfactory structures (Leitner et al. 2016).

Table 3.1

Summary of electrophysiological properties of LEC L2 neurons

Property	L2 Fan Cells (n=15)	L2 Pyramidal Cells (n=9)	L2 Multiform Cells (n=7)
Input resistance (mΩ)	57.3 ± 4.9	41.6 ± 1.6	55.7 ± 6.85
Time constant/ Tau (ms)	23.2 ± 0.94	18.6 ± 0.87	20.7 ± 1.32
'Sag' (%)	11.5 ± 0.7	0	25 (1/7)
Resting membrane potential (mV)	-65.9 ± 0.58	-75.1 ± 0.42	-70.0 ± 155
Action potential threshold (mV)	-45.4 ± 0.48	-44.6 ± 0.7	-45.8 ± 0.5
Action potential duration (ms)	1.28 ± 0.03	1.85 ± 0.1	1.64 ± 0.10
Action potential amplitude (mV)	77.2 ± 0.86	80.1 ± 2.1	78.0 ± 1.13

Note: Adapted from Tahvildari & Alonso (2005). Values are mean and SEM.

Table 3.1 summarises the key electrophysiological properties of cells in LEC L2. As discussed in the Section 1.2.2 of the introduction, in-vitro electrophysiological recordings have revealed at least three principal cell types in this layer (Tahvildari & Alonso, 2005; Canto & Witter, 2012a). The most numerous group are stellate-like 'fan' cells, which have a more depolarised resting membrane potential, slower time constant, and larger input resistance than other cell types in L2. Further, fan cells manifest a 'sag' membrane potential response to injection of depolarising current, comparable to that observed in MEC L2 stellate cells. In addition, LEC L2 also contains populations of pyramidal cells and multi-form cells, each with distinct electrophysiological and morphological profiles. Recently, it was reported that LEC L2a reelin-positive cells correspond to fan cells, whereas LEC L2b calbindin cells correspond to pyramidal and multiform cells (Leitner et al. 2016; Witter et al. 2017).

Though the MEC and LEC share clear structural similarities, research which has compared the consequences of whole lesions to either structure provide evidence that they are functionally distinct (Deshmukh & Knierim, 2011; Van Cauter et al. 2013; Hunsaker et al. 2013; Neunuebel et al. 2013). Further, contemporary work has begun to tease apart the functions of laminar outputs from the superficial MEC to the hippocampus. Early studies used selective lesions to determine a role for MEC L3 in place field generation in CA1 (Brun et al. 2002; Brun et al. 2008), and more recent work used molecular tools to precisely manipulate the superficial layers of MEC and identify laminar contributions to temporal, contextual and spatial memory (Suh, Rivest, Nakashiba, Tominaga, & Tonegawa, 2011; Kitamura et al. 2014; Tennant et al. 2018). The development of molecular tools which permit similar manipulation of populations of neurons within the LEC would be invaluable for probing the contributions of different components to memory.

Given similarities in the arrangement of projecting neurons of MEC and LEC L2, molecular tools which provide genetic access to sub-populations of neurons in MEC L2 could

potentially label similar populations in LEC L2. Recently, Surmeli et al. (2015) characterised the expression of Cre in the superficial MEC of two transgenic mouse lines, Sim1:Cre and Wfs1:CreEr. Cre expression is controlled by the Single mind homolog-1 (Sim1) promoter in Sim1:Cre mice and by Wolfram syndrome 1 homolog (Wfs1) promoter in Wfs1:CreEr mice. By surgically injecting a Cre-dependent AAV encoding a fluorescent reporter into the superficial MEC of both lines, Surmeli et al. determined that Cre is expressed in MEC L2 reelin cells in Sim1:Cre mice and in MEC L2 calbindin cells in Wfs1:CreEr mice. Therefore, these mice provide genetic access to distinct sub-populations of neurons in MEC L2 which project to the DG and CA1, respectively.

Building on this, the experiments presented in this chapter aimed to examine the anatomical organisation of LEC L2 and determine whether these molecular tools could be repurposed to label discrete sub-populations of neurons within this layer. When these experiments were conceived, the arrangement of the projecting neurons in LEC L2 had not been described. Consequently, the primary aim of these experiments was to investigate the distribution and projection pathways of neurons immunoreactive for reelin and calbindin in LEC L2. A similar set of experiments has since been published (Leitner et al. 2016), therefore our findings serve as a replication. Further, a secondary aim of these experiments was to examine Cre expression in the superficial LEC of Sim1:Cre, WfS1:CreEr and Ccdc3:Cre mice. In Ccdc3:Cre mice, Cre is expressed under the control of the coiled coil domain-containing 3 (Ccdc3) promoter. Ccdc3:Cre mice were included in these experiments due to observations of sparse Cre expression in MEC L2 in concurrent experiments within our research group. These experiments established that the Sim1:Cre mouse provides genetic access to a sub-population of neurons in LEC L2 which project to the hippocampus. Consequently, a final aim of these experiments was to examine the electrophysiology and morphology of the labelled cells to determine whether they mapped onto a neuronal sub-type previously described in this layer.

3.2 Methods

3.2.1 Animals

All mice were bred at the University of Edinburgh. Experiments with wild-type mice used C57BL6/J mice. All transgenic mice (Sim1:Cre, Wfs1:CreEr, and Ccdc3:Cre) were bred to be heterozygous for the Cre transgene. 5-11 week old male and female mice were used in all experiments. Mice were housed in groups in diurnal light conditions (12-hr light/dark cycle), and had *ad libitum* access to food and water. All experiments and surgery were approved by the University of Edinburgh animal welfare committee, conducted under a project license (62/9586) and personal license (180825F26) acquired from the UK Home Office and conducted in accordance with national (Animal [Scientific Procedures] Act, 1986) and international (European Communities Council Directive of 24 November 1986 (86/609/EEC) legislation governing the maintenance of laboratory animals and their use in scientific research.

3.2.2 Surgical Injection of Tracers and Viruses

Mice were anaesthetised with Isoflurane in an induction chamber, before being transferred to a stereotaxic frame. Mice were administered an analgesic (Carprieve, 0.03 ml) subcutaneously, and an incision was made to expose the skull. For retrograde labelling of neurons which project to the hippocampus, the retrograde tracer Fast Blue (FB; Polysciences) was injected unilaterally into the dorsal DG, CA1 or CA3 of wild-type mice. To target the molecular layer of the DG, a small craniotomy was made at 2.8 mm posterior to bregma and 1.8 mm lateral to midline. A glass pipette was lowered vertically 1.7 mm from the surface of the brain and 50-100 nl of the tracer diluted at 0.5% w/v in dH_2O was injected at this location. To reduce the spread of tracer up the injection tract, the pipette was slowly retracted after a stationary period of four minutes. To target CA1, this procedure was repeated at 2.30 mm posterior to bregma and 1.75 mm lateral to midline, injecting at a 1.15 mm depth from the

surface of the brain. To target CA3, this procedure was repeated at 2.30 mm posterior to bregma, 2.75 lateral to midline, injecting at 2.0 mm depth from the surface of the brain. For all tracer injections, experiments commenced 1-2 weeks post-surgery.

For injections of AAV into the LEC, an injection strategy was developed to target the superficial layers. A craniotomy was made 3.8 mm posterior to bregma, and 4.0 mm lateral to midline. Where necessary, coordinates were adjusted in relation to landmarks on the skull, so the craniotomy was directly adjacent to the intersection of the lamboid suture and the ridge of the parietal bone (Fig. 3.1). From these coordinates, the craniotomy was extended 0.8 mm rostrally to provide access to the mediolateral extent of the LEC.
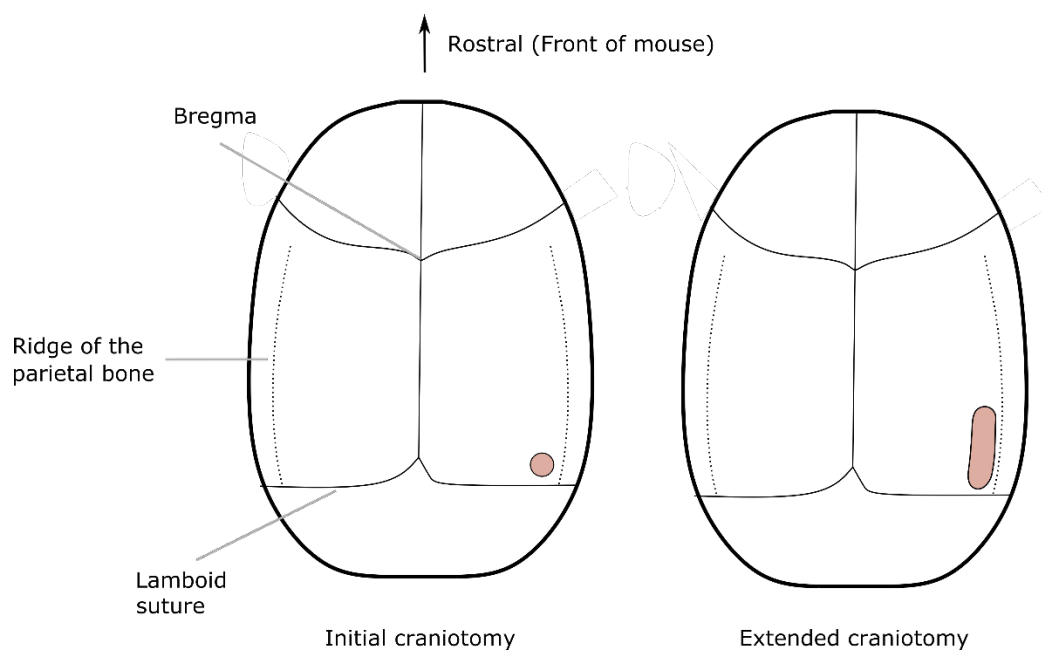
Fig 3.1 Location of craniotomy for injection into lateral entorhinal cortex. Craniotomy is made directly adjacent to the intersection of the lamboid suture and the ride of the parietal bone (left) and lengthened rostrally to extend access to the entire transverse axis of lateral entorhinal cortex (right).

At the original coordinates (3.8 mm posterior to bregma and 4.0 mm lateral to midline), dura was cut, and a glass pipette was lowered slowly from the surface of the brain at a 10°-12° angle until a slight bend in the pipette indicated an approach to dura at the side of the brain. The pipette was retracted 0.2 mm and 200-300 nl of virus was injected at this location. This protocol was repeated at a site 0.2 mm rostral to the original injection coordinates. To target ventral LEC, the angle of the pipette was adjusted to a 6°- 9° angle and a third injection was delivered at the rostral injection site. The angle was adjusted within each reported range based on the proximity of the craniotomy to the ridge of the parietal bone; the lower value was chosen for more medial craniotomies, and the higher value was chosen for more lateral craniotomies. This flexible approach was found to minimise the likelihood of accidental injection into the MEC or PER. For each injection, the pipette was slowly retracted after a stationary period of four minutes to reduce the spread of virus up the injection tract. For all surgeries, mice were administered an oral analgesic prepared in flavoured jelly for three days after surgery.

Viruses used in these experiments were AAV-Flex-GFP and AAV-hm4di-mCherry (UNC Vector Core, Chapel Hill, North Carolina). To permit adequate transfection of each virus, all experiments commenced 2-3 weeks post-surgery. Notably, Cre expression is induced by administration of the drug Tamoxifen in Wfs1:CreEr mice. To induce Cre expression, Tamoxifen (Sigma, 20mg/ml in corn oil) was administered on three consecutive days by intraperitoneal injection two weeks after virus injection and one week before sacrifice. This induction protocol is identical to that used in this line previously (Surmeli et al. 2015).

3.2.3 Histology

Mice were administered a lethal dose of sodium pentobarbital and transcardially perfused with cold PBS followed by cold PFA (4%). Brains were extracted and fixed for a minimum of 24 hours in PFA at 4°C, washed with PBS, and transferred to a 30% sucrose

solution prepared in PBS for 48 hours at 4°C. Brains were sectioned horizontally at 60 μm on a freezing microtome. For tracer injections, the whole brain was sectioned to permit visualisation of the injection site and consequential labelling. For virus injections, sectioning commenced 200-300 μm dorsal of LEC and concluded at the bottom of the brain.

For immunohistochemistry, slices were blocked for 2-3 hours in 5% Normal Goat Serum (NGS) prepared in 0.3% PBS-T (Triton). To stain against reelin and calbindin, slices were transferred to a primary antibody solution prepared in 1% NGS in 0.3% PBS-T for 24 hours. Primary antibodies were mouse anti-reelin (MBL, 1:200) and rabbit anti-calbindin D-28K (SWANT, 1:2500). Slices were washed with 0.3% PBS-T 3x for 20 minutes before being transferred to a secondary antibody solution prepared in 0.3% PBS-T for 24 hours. Secondary antibodies were AlexaFluor® Goat Anti-Mouse 488 and 546 and AlexaFluor® Goat Anti-Rabbit 555 and 647 (Invitrogen, all used at 1:500). To counterstain all cell bodies, Neurotrace 640/660 (Invitrogen, 1:800) was included in the secondary antibody solution. Slices were washed with 0.3% PBS-T 3x for 20 mins and then mounted and cover-slipped with Mowiol. Slides were stored at 4°C for microscopy. For staining against biocytin after slice electrophysiology, slices were washed with PBS 4x for 10 minutes and transferred to a AlexaFluor® Streptavidin 488 (Invitrogen, 1:1000) and Neurotrace 640/660 (Invitrogen, 1:1000) solution prepared in 0.3% PBS-T for 24 hours. Slices were washed with PBS-T 4x for 20 mins and then mounted and cover-slipped with Mowiol.

3.2.4 Quantification of Fractions of Labelled Cells

All images were acquired using a Nikon A1 confocal microscope and NIS elements software. Images were taken at 10x or 20x magnifications. For quantification of cells immunolabelled for reelin, calbindin, or labelled by retrograde tracer or fluorescent reporter, 20x Z-stacks were acquired of regions of interest (ROI) at 1–2 μm steps. ROIs were regions of

L2 of various sizes within the borders of LEC. The borders of the LEC were determined by referencing an atlas of the mouse brain (Paxino & Franklin, 2007). ROIs were chosen based on the integrity of the tissue and quality of staining or labelling. All neurons within each ROI were counted manually. Fractions of labelled cells were determined by calculating the proportion of labelled cells in each ROI as n labelled cells divided by total n cells. Proportions were averaged across all ROIs from all mice to yield an overall percentage of labelled cells. Values are presented as the mean ± SEM.

3.2.5 Slice Electrophysiology

Horizontal brain slices were prepared from 5-8 week old Sim1:Cre mice injected with AAV-hm4di-mCherry. Mice were sacrificed by cervical dislocation and decapitated. The brains were rapidly removed and submerged in cold cutting artificial cerebrospinal fluid (ACSF) at 4°C. The cutting ACSF was comprised of the following (in mM): NaCl 86, NaH_2PO4 1.2, KCl 2.5, $NaHCO_3$ 25, Glucose 25, Sucrose 50, $CACl_2$ 0.5, $MgCI_2$ 7. The brain was split into hemispheres, glued to block submerged in cold cutting ACSF with the dorsal surface facing the block, and sectioned horizontally at 300-400 μm on a vibratome. Slices were transferred to normal ACSF at 37°C for 15 minutes, then incubated at room temperature for a minimum of 45 minutes. Normal ACSF was comprised of the following (in mM): NaCl 124, NaH2PO4 1.2, KCI 2.5, NaHCO3 25, Glucose 25, CaCI2 2, MgCI2 1).

For recordings, slices were transferred to a submerged chamber and maintained in normal ACSF at 35-37°C. Labelled neurons were identified by their expression of mCherry. Whole cell patch-clamp recordings were made using boroscillate electrodes with a resistance of 4-8 MΩ and filled with an intracellular solution comprised of the following (in mM): K gluconate 130, KCI 10, Hepes 10, $MgCl_2$ 2, EGTA 0.1, Na_2ATP 4, Na_2GTP 0.3, phosphocreatine 10, and 5% biocytin (w/v). Appropriate bridge balance and capacitance

neutralisations were applied. Upon completion of all recording protocols, each cell was left stationary with the electrode attached for one hour before being transferred to PFA (4%) and stored at 4°C for at least 24 hours before histological processing.

3.2.6 Recording Protocols

A series of customised protocols developed within the lab were used to determine the electrophysiological properties of each cell (as described in Nolan et al. 2007; Garden et al. 2008). Intrinsic membrane properties of the cell were measured by examining the voltage response to the injection of current in hyperpolarising and depolarising steps (-160 to 160 pA in 40 pA increments, each 3 s). To determine the rheobase of each cell, depolarising current was applied to the cell in a constantly increasing manner to induce action potentials (50 pA/s, 3s). To determine the resonance properties of the cell, membrane voltage was recorded as an oscillatory current with a linearly varying frequency was applied to the cell (ZAP protocol; Erchova et al. 2004). Upon completion of these investigatory protocols, the diffusion of biocytin into the cell was encouraged using a protocol which injected current into the cell in increasing amounts (Jiang et al. 2015).

3.2.7 Electrophysiological Data Analysis

Electrophysiological data were analysed using AxoGraph (axographx.com), IGOR Pro (Wavemetrics, USA) using Neuromatic (http://www.neuromatic.thinkrandom.com) and customised MATLAB scripts developed within the lab (Hugh Pastoll & Li Wen Huang). To determine the morphology of filled cells, 20x Z-stacks were acquired at 1-2 μm steps. Cells were classified as fan, pyramidal or multi-form cells by visual comparison of the shape of the soma and arrangement of dendrites to published morphological descriptions (Tahvildari & Alonso, 2005; Canto & Witter, 2012; Leitner et al. 2016; Witter et al. 2017). Briefly, fan cells

were identified by a polygonal soma and the 'fan-like' arrangement of primary dendrites, branching repeatedly from the soma towards L1. Pyramidal cells were identified by a pyramid-shaped soma and bi-directional arrangement of dendrites towards superficial and deep layers. Multi-form cells were identified by a non-pyramid-shaped soma, with multiple primary dendrites oriented in all directions, dissimilar to the arrangement of fan or pyramidal cells.

3.3 Results

3.3.1 Two Distinct Sub-Layers in LEC L2

Figure 3.2 shows the arrangement of neurons in LEC L2. Staining with Neurotrace revealed that LEC L2 contains two distinct sub-layers, L2a and L2b, as described previously (Fujimaru & Kosaka, 1996; Leitner et al. 2016). The layer which was identified as L2b is unlikely to be L3 given the visible extension from MEC L2 and the observation of a further cortical layer prior to the lamina dissecans which separates L3 and L5 of entorhinal cortex. Bifurcation of LEC L2 persists across the dorsoventral and posterior-anterior extent of the LEC, and thus functions as a clear anatomical marker of LEC borders in horizontal slices (Panel A, Fig 3.2, also see Appendix E). Immuno-labelling with antibodies against reelin and calbindin revealed that the majority of neurons in L2a were positive for reelin (Panel B, Fig 3.2; 90.0 ±1.3%, 2018/2273 cells, n = 4 mice, 11 sections). L2a also contained sparse populations of neurons which were positive for calbindin (4.0 ± 0.4%, 90/2273 cells) or positive for both reelin and calbindin (2.3 ± 0.4 %, 48/2273 cells). In contrast, the majority of neurons in L2b were positive for calbindin (61.9 ± 2.4%, 1270/2103 cells), with a smaller population of neurons positive for reelin (15.9 ± 1.6%, 347/2103 cells) or both reelin and calbindin (4.8 ± 0.3%, 104/2103 cells).
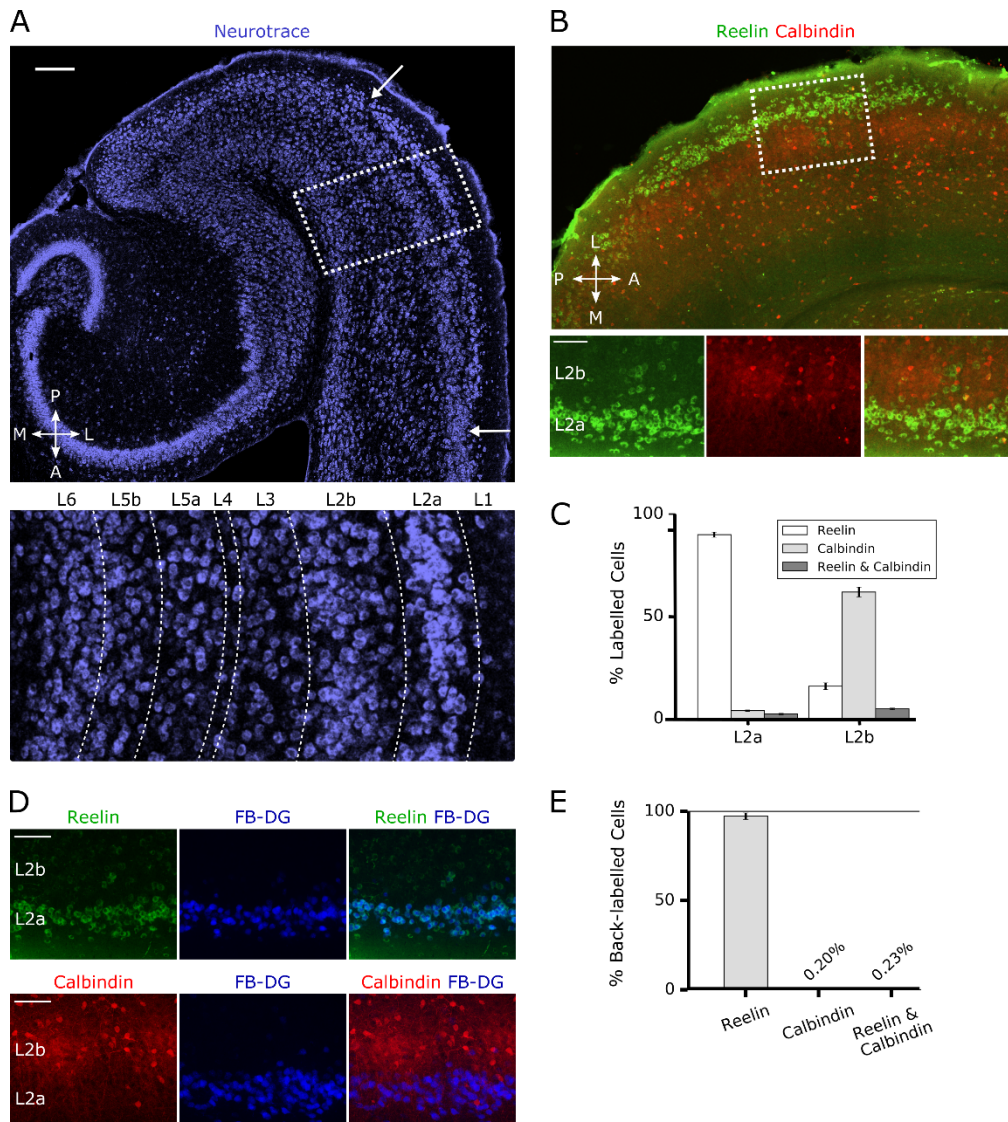
Figure 3.2: LEC L2 bifurcates into two distinct sub-layers. (A) Horizontal brain section (x10 magnification) showing the distribution of neurons in the LEC. Inset shows laminar demarcation. Arrows indicate LEC borders. Scale bar represents 250 μm. (B) Horizontal brain section (x10 magnification) showing immunolabelling against reelin (green) and calbindin (red) in LEC L2. Scale bar represents 100 μm. (C) Quantification of neurons positive for reelin (white), calbindin (light grey) and both (dark grey). Error bars represent SEM. (D) Cells labelled in LEC L2 by tracer injections to the dentate gyrus (blue) overlaid with cells counterstained for reelin and calbindin. Image is at 20x magnification and scale bars represent 100 μm. (E) Quantification of back-labelled cells immunolabelled by reelin, calbindin or both. Error bars represent SEM. Abbreviations: A, anterior; DG, dentate gyrus; FB, Fast Blue; L, lateral; M, medial; P, posterior.

3.3.2 Neurons in LEC L2a Project to the Dentate Gyrus

To investigate whether LEC L2a and L2b corresponded to discrete projections to the hippocampus, retrograde tracer was injected into the dorsal DG of wild-type mice (n = 4) which has previously been shown to receive input from the superficial LEC (Dolorfo & Amaral, 1998; Van Groen et al. 2003). Figure 3.2 shows the neurons labelled by these injections. Back-labelled cells were located primarily in LEC L2a (Panel D, Fig. 3.2; 95.8 ± 1.0%, 1025/1077 cells, 8 sections) with sparse labelling in LEC L2b (4.3 ±1.0%, 52/1077 cells). There was no apparent labelling in the contralateral hemisphere. Back-labelled neurons were positive for reelin (Panel E, Fig. 3.2; 93.1 ± 1.8%, 1008/1077 cells), but not calbindin (0.2 ± 0.1%, 2/1077 cells). A few neurons were triple-labelled for reelin, calbindin, and the tracer (0.2 ± 0.1%, 3/1077 cells). Unfortunately, all tracer injections into CA3 and CA1 resulted in some unintended spread to adjacent hippocampal sub-regions (n = 6 mice). Consequently, back-labelled cells from these injections were not quantified, though there was no apparent labelling of LEC L2b in any case. Therefore, the sub-layers of LEC L2 are further discriminated on the basis of their projections; L2a contains a population of reelin-positive cells which project to the DG, whereas L2b contains a population of calbindin-positive cells which do not project to the hippocampus.

3.3.3 Sim1:Cre Mice Label Reelin Positive Cells in L2A

To characterise the expression of Cre in the Sim1:Cre mouse line, a Cre-dependent AAV encoding green flourescent protein (AAV-Flex-GFP) was injected into the superficial LEC of Sim1:Cre mice (n = 4). Figure 3.3 shows the resultant expression of the reporter gene (GFP) in a Sim1:Cre mouse. Labelled neurons were primarily located in L2a (Panel A, Fig 3.3; 87.4 ± 1.6%, 1282/1490 cells, n = 14 sections) but also occurred sparsely in L2b (12.6 ± 1.6%,
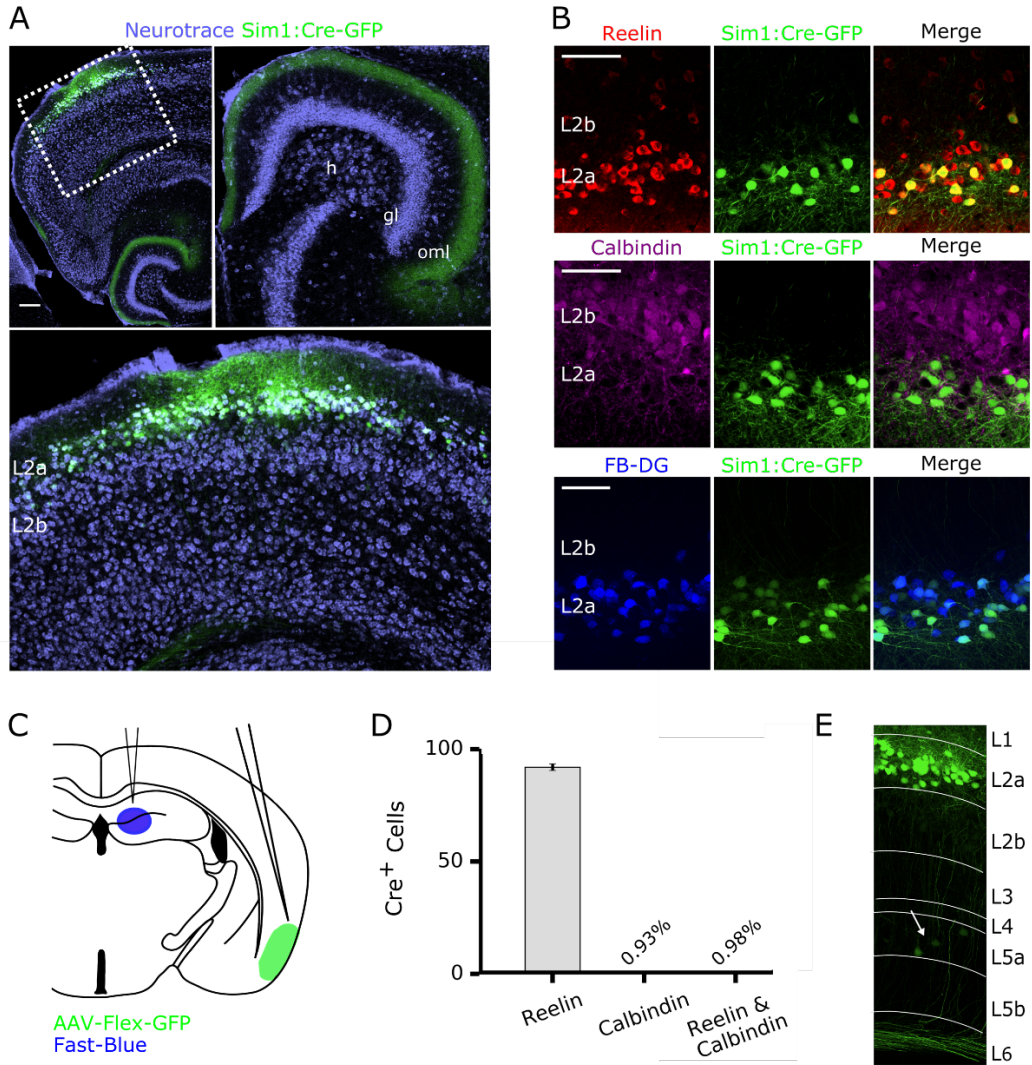
Figure 3.3: Sim1:Cre mouse gives genetic access to L2a reelin cells which project to the dentate gyrus. (A) Top left: Horizontal brain section (x10 magnification) showing reporter gene expression (GFP, green) in LEC L2a of the Sim1:Cre mouse following injections of AAV-Flex-GFP. Scale bar represents 250 μm. Neurons are counterstained with Neurotrace (violet). Top right: Axonal labelling of the DG oml. Bottom: Inset shows L2a specificity. (B) Injections label cells which are immunolabelled for reelin (green, top) but not calbindin (purple, middle) and project to the dentate gyrus (blue, bottom). Images are at 20x magnification and scale bar represents 100 μm. (C) Schematic injections into the dorsal DG and superficial LEC. (D) Quantification of overlap between neurons expressing the reporter gene and immunolabellng against reelin, calbindin, and both reelin and calbindin. (E) Representative example of labelling in LEC L5a. Arrow indicates L5a neurons which express the reporter gene. Abbreviations: DG, dentate gyrus; h, hilus; gl; granular layer; oml, outer molecular layer.

207/1490 cells). Labelling in the deep LEC was observed in a few sections, but this was restricted to < 5 neurons in all cases (Panel E, Fig. 3.3).

Neurons expressing the reporter gene in L2a were positive for reelin (Panel B, Fig 3.3; 98.2 ± 0.4%, 1260/1282 cells, n = 14 sections) but not calbindin (0.1 ± 0.4%, 1/1282 cells). A small sub-set of cells were triple-labelled by reelin, calbindin, and the reporter gene (0.3 ± 0.2%, 4/1282). Most neurons expressing the reporter gene in L2b were positive for reelin (52.0 ± 5.7%, 97/207 cells), but some calbindin-positive neurons were also labelled (7.1 ± 2.8%, 17/207 cells). Further, a small sub-set of cells in L2b were triple-labelled by reelin, calbindin and the reporter gene (4.6 ± 1.9%, 13/207 cells). Overall, the majority of neurons expressing the reporter gene across both layers were positive for reelin (Panel D, Fig 3.3; 92.0 ± 1.5%, 1357/1490 cells), with small sub-sets of labelled cells positive for calbindin (1.0 ± 0.3%, 18/1490 cells) or triple-labelled by reelin, calbindin, and the reporter gene (1.0 ± 0.3%, 17/1490 cells). Further, to determine the density of virus expression in LEC L2, proportions of infected neurons were quantified across entire regions of expression for three mice. Within regions of expression, 48-74% of LEC L2a cells were expressed the reporter gene (54.4 ± 2.8%, 1173/2153 cells, n = 9 sections), and 3-13% of LEC L2b cells expressed the reporter gene (8.0 ± 1.4%, 258/3007 cells).

Lastly, to investigate whether the population of neurons labelled in LEC L2 overlapped with the reelinergic neurons projecting to the DG, an injection of AAV-Flex-GFP was paired with an injection of a retrograde tracer in the dorsal DG (n = 3 mice). The majority of neurons expressing the reporter gene co-localised with neurons labelled by the retrograde tracer (Panel B, Fig 3.3; 74.3 ± 4.4%, 331/441 cells, n = 8 sections). Therefore, the Sim1:Cre line provides genetic access to a population of neurons in LEC L2a which are positive for reelin and project to the DG.
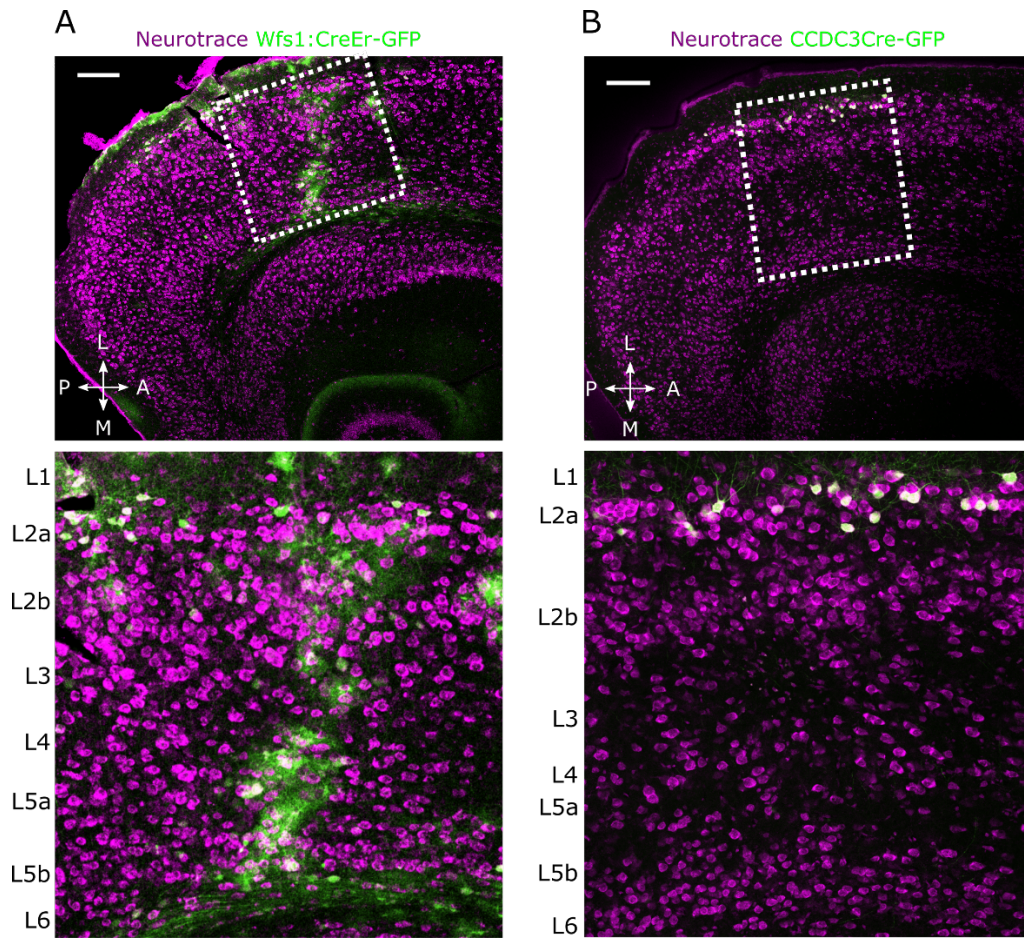
Figure 3.4: Expression of the reporter gene in Wfs1:CreER and Ccdc3:Cre mice. All images are at a 10x magnification. (A) Horizontal brain section showing reporter gene expression (GFP, green) in the superficial and deep LEC of a Wfs1:CreER mouse following injection of AAV-Flex-GFP. (B) Horizontal brain section showing sparse reporter gene expression (GFP, green) in LEC L2a of a Ccdc3:Cre mouse following injection of AAV-Flex-GFP. Neurons are counterstained with Neurotrace (purple). Bottom: Insets show laminardemarcation. Scale bars represent 200 μm.

3.3.4 Expression of Cre in Wfs1:CreEr and Ccdc3:Cre Mice

To characterise the expression of Cre in the Wfs1:CreEr and Ccdc3:Cre mouse lines, AAV-Flex-GFP was also injected into the superficial LEC of these mice. Figure 3.4 shows the expression of the reporter gene in brain sections extracted from Wfs1:CreEr and Ccdc3:Cre mice following injections of Cre-dependent AAV-Flex-GFP. In Wfs1:CreEr mice (n = 4), sparse reporter gene expression occurred in LEC L2a and L2b, and there was glial expression in superficial and deep LEC (Panel A, Fig 3.4). Given the apparent lack of specificity of reporter gene expression in Wfs1:CreEr mice, this line was not investigated further. In a Ccdc3:Cre mouse (n = 1), reporter gene expression was restricted to LEC L2a, but was extremely sparse (Panel B, Fig 3.4). Therefore, the Ccdc3:Cre line was not investigated further.

3.3.5 LEC Neurons Labelled in Sim1:Cre Mice are Fan Cells

Sim1:Cre mice provide genetic access to a distinct population of neurons in LEC L2a, but it was unclear whether the labelled population maps onto a specific type of cell. To investigate this, the electrophysiology and morphology of labelled cells was investigated by patch-clamp recording in slices extracted from Sim1:Cre mice (n = 9) injected with an AAV encoding a fluorescent reporter (AAV-hm4di-mCherry).

Table 3.2 summarises the electrophysiological properties as averaged across all recorded cells, and Figure 3.5 (Panels A, B, and C) shows the morphology and electrophysiological traces from a representative recorded cell. Labelled neurons (n = 15) were recorded from 5/9 mice. The quality of biocytin fills was sufficient to confirm morphology for 12/15 of the recorded neurons. Of these neurons, 11/12 were morphologically matched to fan cells, and 1/12 was morphologically matched to a multi-form cell. All recorded cells were located in LEC L2a (Fig 3.5, Panels D and E).

Table 3.2

Electrophysiological properties of Cre+ LEC L2 cells in Sim1:Cre mice

Property	L2a Cells (n = 15)
Input resistance - (mΩ)	130.47 ± 11.9
Time constant/ τ (ms)	24.19 ± 1.7
Sag Ratio	0.85 ± 0.07
Resting membrane potential (mV)	-68.47 ± 1.4
Action potential threshold (mV)	-37.95 ± 1.5
Action potential duration (ms)	0.67 ± 0.09
Action potential amplitude (mV)	88.19 ± 0.9
Rheobase (pA)	126.43 ± 8.9
Resonance Frequency (Hz)	1.15 ± 0.09

Note: Time constant and input resistance values are reported based on the membrane response to hyperpolarising current steps.

Consistent with the electrophysiological parameters of fan cells, recorded cells had a relatively depolarised resting membrane potential (-68 mV), high input resistance (130 mΩ), relatively slow time constant (24 ms) and consistently demonstrated a sag membrane potential response to injection of depolarising current. Recorded cells reached depolarisation threshold (rheobase) with application of <130 pA of depolarising current, and had an action potential threshold of -38 mV. Further, the recorded cells were resonant at a frequency around 1 Hz. Lastly, these cells always demonstrated tonic firing patterns (no phasic firing or spike bursts were observed) with relatively short action potentials (0. 7 ms).
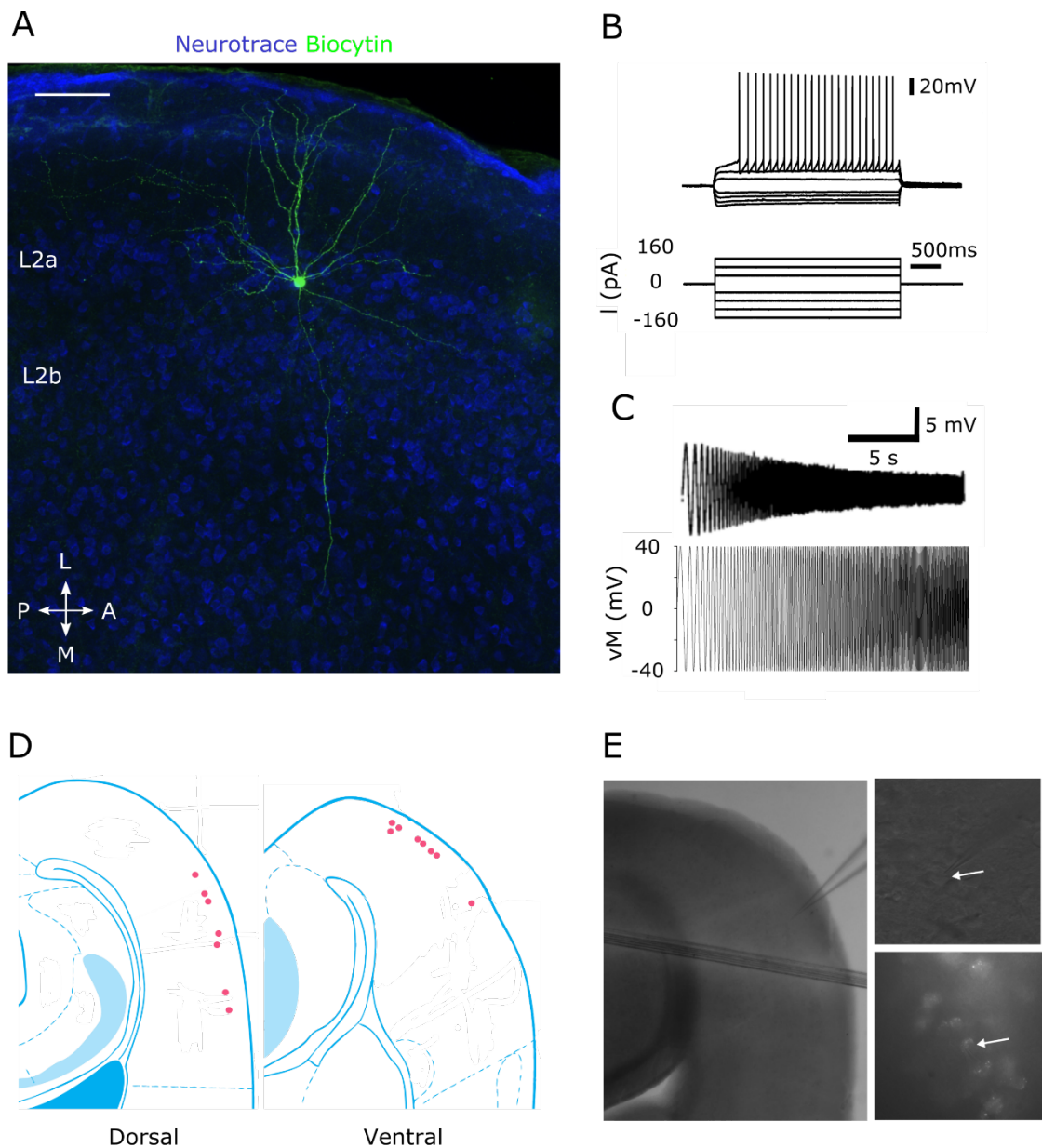
Figure 3.5. Neurons labelled in Sim1:Cre mice are fan cells. (A) Example of a fan cell in L2a filled with biocytin (green). Neurons are counterstained with Neurotrace (blue). Note axon leading towards the dentate gyrus. Image is at 20x magnification and scale bar represents 100 μm.(B) Examples of sag membrane response and action potentials (top) to the injection of negative and positive current steps, respectively (bottom). (C) Example of resonance of a recorded cell (top) in response to the ZAP protocol (bottom). (D) Location of recorded cells in dorsal and ventral LEC. Schematic of the brain is adapted from Paxino & Watson (2007). (E) Example horizontal section with electrode attached to cell in LEC L2a (left). Insets show whole-cell patch clamping (top) and example of mCherry expression in a slice (bottom). White arrows indicate locations of patched cells.

3.4 Discussion

The primary aim of these experiments was to describe the arrangement of projecting neurons in LEC L2, and determine whether their organisation resembled that of MEC L2, which contains discrete populations of neurons which are immunoreactive for the proteins reelin and calbindin, and project to the DG and CA1, respectively (Kitamura et al. 2014; Surmeli et al. 2015; Witter et al. 2017). Indeed, it was observed that LEC L2 also contains populations of reelin-positive and calbindin-positive cells, yet in contrast to the MEC, these are arranged across two distinct sub-layers within L2. L2a, the most superficial layer of L2, contains predominantly reelinergic cells, whereas L2b, the deeper layer of L2, contains predominantly calbindin-positive cells. The bifurcation of LEC L2 is consistent with previous reports (Fujimara & Kosaka, 1996; Leitner et al. 2016; Witter et al. 2017). Further, injections of a retrograde tracer into the DG, CA1 and CA3 subregions of the hippocampus confirmed that L2a reelin cells project to the DG, but L2b calbindin cells do not project to the hippocampus. These findings are consistent with the observations of Leitner et al. (2016), who further determined that LEC L2b provides feedback to the olfactory cortex. This contrasts with the projections from calbindin cells in MEC L2, which innervate CA1 (Surmeli et al. 2015).

Interestingly, experiments conducted in our research group after the completion of this project further suggest that the molecular organisation of LEC L5 also bears resemblance to MEC L5 (Christina Brown, unpublished observations). MEC L5 contains two sub-layers, L5a and L5b, which are discriminated by the transcription factors Etv1 and Ctip2, respectively (Surmeli et al. 2015). In these experiments, it was observed that LEC L5 also bifurcates in L5a and L5b, and these layers are also discriminated by Etv1 and Ctip2. Further, in the superficial LEC, it was observed that Ctip2 was expressed in LEC L2a, but not MEC L2, and this expression co-localised with immunolabelling against reelin. These findings complement the

113

data presented in this chapter, and offer a further method for demarcating the border between MEC and LEC in superficial and deep layers.

The secondary aim of these experiments was to determine whether existing molecular tools which provide genetic access to discrete sub-populations of neurons in MEC L2 could be repurposed for labelling sub-populations of neurons in LEC L2. To investigate this, AAV encoding a fluorescent reporter was injected into the LEC of Sim1:Cre, Wfs1:CreEr, and Ccdc3:Cre mice. These injections determined that Sim1:Cre mice express Cre in L2a reelin-positive cells which project to the DG. Axonal labelling in the outer molecular layer of the DG is consistent with the organisation of projections from LEC to this layer which have been described previously (Witter & Amaral, 1998; Van Strien et al. 2009; See Section 1.2.1 of the General Introduction). Further, our findings are consistent with the pattern of reporter gene expression observed after similar injections into MEC L2 of Sim1:Cre mice (Surmeli et al. 2015). Therefore, the Sim1:Cre mouse line provides a novel opportunity to selectively target a sub-population of cells within the LEC which correspond to a discrete projection to the hippocampus. The development of this tool has enormous implications for research investigating the functional circuitry of the entorhinal-hippocampal network, and complements recent work using similar molecular tools to manipulate sub-populations of MEC L2 (Suh et al. 2011; Kitamura et al. 2014; Tennant et al. 2018).

Notably, there was sparse labelling in L2b in Sim1:Cre mice. However, this was restricted to a small proportion of the population and usually co-localised with immunoreactivity against reelin. It is possible that this labelling corresponds with the small population of neurons in L2b which are retrogradely labelled by tracer injections into the DG, yet this cannot be determined from the dataset presented in this chapter. Further, labelling of LEC L5a neurons was observed in a few sections, as has been reported for MEC L5a in the Sim1:Cre mouse (Surmeli et al. 2015). This is unlikely to affect the utility of the Sim1:Cre line

for targeting LEC L2, given that the spread of virus to LEC L5 should be minimal with the injection strategy developed for these experiments. However, this observation does inspire further characterisation experiments to determine whether Sim1:Cre mice label a specific sub-population of LEC L5. Specifically, future work could examine whether Cre expression co-localises with Etv1 or Ctip2 in this layer, which might raise the possibility of using this line to examine functional circuits which incorporate the deep LEC.

In Wfs1:CreEr mice, reporter gene expression was sparse and non-specific to a single layer, which contrasts with the specificity observed in MEC L2 (Surmeli et al. 2015). The lack of specificity is surprising given recent reports that the Wfs1 gene co-localises with calbindin-positive neurons in LEC L2b (Leitner et al. 2016). Although the tamoxifen induction protocol used in our experiment was identical to that of Surmeli et al. (2015), it is possible that different results could be obtained by altering the concentration of the drug or extending the period of administration. Repetition of these characterisation experiments with Wfs1:CreEr mice which are crossed with a reporter line may be worthwhile to assess the validity of our findings. Further, pilot injections in Ccdc3:Cre mice revealed that reporter gene expression was restricted to a subset of LEC L2a, but was extremely sparse. This line was not investigated further within the scope of this project, but could be revisited in future experiments. It is possible that this line labels one of the small sub-populations of pyramidal or multi-form cells in LEC L2a, which could prove beneficial for future research.

The final aim of these experiments was to examine the morphology and electrophysiology of the neurons labelled in Sim1:Cre mice, and determine whether these properties mapped on to a previously described cell type in LEC L2 (Tahvildari & Alonso, 2005; Canto & Witter, 2012; Leitner et al. 2016; Witter et al. 2017). Indeed, most recorded cells were morphologically matched to 'fan cells', with apical dendrites arranged in a 'fan-like' shape towards the pia, branching within L1 and L2. Further, these cells exhibited

electrophysiological profiles similar to those reported for fan cells, including a relatively depolarised resting membrane potential, slower tau, and a clear sag membrane potential response to injection of depolarising current (Tahvildari & Alonso, 2005; Leitner et al. 2016). Further, values reported for rheobase, input resistance, action potential threshold and action potential amplitude were very similar to those reported for reelinergic fan cells by Leitner et al. (2016). There are currently no explicit descriptions of the resonance properties of LEC L2 fan cells in the literature, therefore our observation of resonance at approximately 1 Hz is the first. Interestingly, one recorded neuron matched the morphology of a multi-form cell. In the literature, multi-form cells do not have a consistent electrophysiological profile, and this category encompasses neurons which do not meet the morphological criteria for fan or pyramidal cells. Importantly, the electrophysiological properties of this cell did not differ from fan cells. Therefore, it is possible that this cell is one of the calbindin-positive neurons in L2a which are labelled in the Sim1:Cre mouse, or, given that some multi-form cells co-localise with reelin, it is possible that reelinergic multi-form cells contribute to the LEC L2a projection to the DG.

Overall, while these data reveal a great deal about the anatomy of LEC L2, it is difficult to infer how information is processed in the network from the molecular and electrophysiological descriptions of neurons in LEC L2 alone. Future electrophysiological work could perform paired recordings of neurons in LEC L2 to examine how, and if, fan cells communicate with one another and further determine how information might be processed within an LEC L2 microcircuit, as has been described for MEC L2 (see Witter et al. 2017). Further, future experimental approaches might combine in-vitro manipulations with molecular tools, such as the Sim1:Cre line, to ask sophisticated questions about the functional connectivity of neurons in the superficial LEC.

3.5 Conclusion

To summarise, the principal cells of LEC L2 are arranged across two sub-layers, each with distinct molecular profiles. Further, the Sim1:Cre mouse can be used to label a sub-population of LEC L2 neurons which project to the DG. This tool permits precise manipulation of the projection from LEC L2 to the hippocampus. Recent experiments combined the Sim1:Cre line and behavioural paradigms to study the contribution of MEC L2 stellate cells to spatial memory (Tennant et al. 2018). Relatedly, the next experimental chapter of this thesis presents an experiment which combined the Sim1:Cre mouse and object-based memory tasks to determine how projections from LEC L2a fan cells functionally contribute to associative memory processes.

Chapter 4: Layer 2 of the Lateral Entorhinal Cortex is Required for Episodic Memory in Mice

4.1 Introduction

The previous experimental chapter examined the molecular organisation of LEC L2, and presented a novel tool (Sim1:Cre mouse) which provides genetic access to a population of reelinergic neurons in LEC L2 that project to the hippocampus. The current experiment built on this research by using this tool to investigate how information processing between LEC L2 and the hippocampus facilitates episodic memory processes.

This experiment was inspired by a reliance on non-specific manipulations of the LEC to make inferences about the function. As detailed in Section 1.5.2 of the General Introduction, several studies have used complete LEC lesions in rodents to investigate whether the LEC is required for performance on various types of memory tasks. LEC lesions do not impair performance on navigational spatial memory tasks, such as the Morris water maze (Ferbinteanu et al. 1999; Burwell et al. 2004; Van Cauter et al. 2013), but do severely impair performance on memory tasks which require the animal to associate information about objects in an open field with spatial and/or contextual information (Van Cauter et al. 2013; Wilson et al. 2013a; 2013b). However, LEC lesions do not impair the ability to recognise a novel object (Van Cauter et al. 2013; Wilson et al. 2013b) unless the task demands the animal to identify the novel object from a field containing > 2 objects (Hunsaker et al. 2007; Van Cauter et al. 2013; Hunsaker et al. 2013, but see Kesner et al. 2001).

These experiments have identified which types of memory require the LEC, but are limited by the non-specificity of the lesion approach; it is unclear how damage to discrete projection pathways to and from the LEC relate to the observed pattern of memory impairment. It might be possible to dissociate between animals with lesion damage localised to superficial or deep LEC, but there is no evidence of this analysis in the published research. Where the LEC is reversibly inactivated using an implanted cannula, it is possible to determine whether the cannula tip is located in the superficial or deep LEC during histology. Indeed, Yoo & Lee

(2017) noted that animals with cannulas terminating in the deep LEC were significantly impaired in a scene-based choice task relative to animals with cannulas terminating in the superficial LEC. This finding provides evidence that the input and output pathways between the LEC and the hippocampus are functionally dissociable, but highlights the fact that the field currently lacks a refined methodology for teasing apart precise circuit components.

The use of immediate early gene (iEG) imaging has made some progress in addressing the roles of discrete pathways to memory function. Wilson et al. (2013a) compared the expression of the iEG *c-fos* across the projection bands of LEC in rats that experienced a single context, multiple contexts, or a novel configuration of object and context. They observed increased *c-fos* in the VIE subdivision of LEC in rats that experienced the novel object-context configuration relative to the single or multiple context groups, and increased *c-fos* expression in the DIE subdivision in all rats that experienced multiple contexts in comparison to those that experienced a single context. This suggests that projections to the hippocampus from the VIE and DIE bands of the LEC may be critical for integrating object and context information and processing information about multiple contexts, respectively. Unfortunately, this experiment was conducted using sagittal sections of brain tissue, which did not permit clear discrimination between the individual layers of the LEC.

Examining the functional role of reelin signalling from the entorhinal cortex may provide further clues regarding the contribution of discrete projection pathways from the LEC to the hippocampus in memory. As discussed in Chapter 3 (see also Fujimara & Kosaka, 1996; Surmeli et al. 2015; Leitner et al. 2016), reelin signalling from the entorhinal cortex largely originates from L2. Complete knockdown of LEC reelin signalling in rats results in profound impairment on the Morris water maze task (Stranahan et al. 2011b), which contradicts earlier reports of intact performance on this task with complete lesions of LEC (Ferbinteanu et al. 1999; Burwell et al. 2004; Van Cauter et al. 2013). Further work from the same research group

demonstrated that there is a relationship between a reduced number of reelinergic cells in the entorhinal cortex and spatial memory impairment (Stranahan et al. 2011a). In this experiment, a cohort of young and aged rats were trained on the Morris water maze task, and their performance was examined in relation to the number of reelin-positive cells in the LEC & MEC. Aged rats that were impaired on the task had significantly fewer reelin-positive cells in the LEC relative to young controls and aged rats that were unimpaired on the task. There was no difference in the number of reelin-positive cells in the MEC across groups. Unfortunately, these experiments were not extended to include other memory tasks, such as the object-based associative memory tasks used by Wilson et al. (2013a; 2013b). Further, while reelin signalling largely originates from L2, some reelin-positive cells are observed in other LEC layers. Therefore, these data cannot be interpreted explicitly as the consequence of reduced reelin signalling in any discrete pathway.

To date, only one experiment explicitly links activity in a layer of LEC to behaviour. Leitner et al. (2016) used calcium imaging of LEC L2 to demonstrate that reelin-positive cells in L2 may play a role in discriminating between different olfactory stimuli. However, this experiment required the animal to be head-fixed and under general anaesthetic, which precludes extrapolation of these findings to active memory processes. Further, the calcium imaging approach requires a transparent window to be implanted in the skull immediately above the region of interest. Given the lateral location of LEC, this method would be difficult extend to free-moving behaviours.

Therefore, the Sim1:Cre mouse provides a novel opportunity to selectively manipulate a single input pathway from the LEC to the hippocampus and observe the behavioural consequences. The use of a precise molecular tool circumvents the limitations of the previous research outlined here. In the current experiment, output from LEC L2a was selectively inhibited in a cohort of Sim1:Cre mice using the tetanus-toxin light chain (TeLC). Briefly,

TeLC is derived from tetanus toxin, a neurotoxin composed of heavy and light chains which are connected by a disulphide bridge. When a cell is infected, the light chain cleaves the vesicle docking protein synaptobrevin-2, which effectively prevents neurotransmitter release from the pre-synaptic terminals of the cell (Schiavo et al. 1992; Link et al. 1992). When the TeLC is packaged into an AAV, it can be used to inactivate populations of neurons (eg. Murray et al. 2011; Tennant et al. 2018). In this experiment, a Cre-dependent AAV encoding TeLC was injected into the superficial LEC of Sim1:Cre mice, which suppressed the output from reelin-positive cells in LEC L2 to the DG. These mice were tested on a novel object recognition task and a series of associative recognition memory tasks, replicating the behavioural protocol used in LEC-lesioned rats (Wilson et al. 2013b). Given evidence that the LEC is critical for associative recognition memory and that disrupted reelin signalling in the LEC contributes to spatial memory impairment and age-related cognitive decline (Stranahan et al. 2011a; 2011b), it was hypothesised that suppression of LEC L2a would result in impaired associative recognition memory, but have no effect on novel object recognition.

4.2 Methods

4.2.1 Animals

Adult Sim1:Cre mice (n = 21 experimental, 17 control) of mixed gender (18 male) were used in this experiment. The experiment was run in two cohorts (first cohort, n = 12 experimental, 9 control; second cohort, n = 9 experimental, 8 control). All mice were bred to be heterozygous for the Cre transgene. Mice were aged between 3-8 months at the time of surgery. Throughout the experiment, mice were housed in groups of 2-4 in diurnal light conditions (12-hr light/dark cycle). All habituation and testing occurred during the light phase. Animals had *ad libitum* access to food and water throughout the study. All experiments and surgery were conducted under a project license (70/8306) and personal license (180825F26)

acquired from the UK home office (70/8306) and in accordance with national (Animal [Scientific Procedures] Act, 1986) and international (European Communities Council Directive of 24 November 1986 (86/609/EEC) legislation governing the maintenance of laboratory animals and their use in scientific research.

4.2.2 Viral Vectors

Viruses were purchased from Vector Core (University of Edinburgh) and prepared as described previously (McClure, Cole, Wulff, Klugmann & Murray, 2011). This experiment utilised two Cre-dependent AAVs: AAV-Flex-TeLC (titre: 7.55 x 10E12 Cps/ml), and AAV-Flex-GFP (titre: 5.07x10E12 Cps/ml).

4.2.3 Surgery

Mice were administered pre-operative oral analgesic (Metacam) prepared in flavoured jelly approximately 24 hours before surgery. Mice were anaesthetised with Isoflurane before being transferred to a stereotaxic frame. Mice were administered an analgesic (Carprofen, 0.03 ml) subcutaneously, and an incision was made to expose the skull. The superficial LEC was targeted using an injection strategy described previously (see Section 3.2.2 of Chapter 3). For injections of AAV-Flex-TeLC, 200-500 nl of undiluted virus was injected at each injection site. For injections of AAV-Flex-GFP, 100-150 nl of undiluted virus was injected at each injection site. Mice were administered post-operative oral analgesic (Metacam) for three days after surgery.

4.2.4 Apparatus

The test environment was a rectangular wooden box (length 32 cm, width 25.5 cm, height 22 cm) which could be configured to provide two distinct contexts. Context A had black and white vertically striped walls with a smooth white floor. Context B had grey walls with a wire-mesh floor. The wall and floor of the box was cleaned with veterinary disinfectant before each trial to remove waste and olfactory information. To secure objects in place within the environment, square sections of white fastening tape (Dual Lock, 3M) were attached to the upper left and right quadrants of the box floor. The test room was lit by two lamps positioned at equal distances from the test box. This arrangement diffused light evenly throughout the test environment without creating shadows to reduce any stress induced by a bright overhead light. Stable global cues in the room (eg. lamps) were visible to the animal throughout testing.

4.2.5 Objects

This experiment used an array of household objects which were approximately the same size as a mouse and varied in colour, shape, and texture. Objects were matched for similarity in size and interest to the animal when paired for testing. Objects were cleaned thoroughly with veterinary disinfectant before each trial. Objects used during habituation were not recycled during testing. To avoid the use of odour cues, new identical copies of each object were used for each trial.

4.2.6 Habituation

In the week before surgery, the experimenter handled each animal every day for 10 minutes in the testing room. Habituation to the test environment commenced one week after surgery and lasted for 5 consecutive days. On day 1, the mice explored each context for 10 minutes with their cage mates. On days 2-5 the mice explored each context for 10 minutes

individually. On days 4-5, junk objects were introduced in the upper left and right quadrants of the test environment.

4.2.7 Behavioural Task

Testing occurred in four stages (Fig. 4.1): Novel object recognition (NOR), novel object-place (OP) recognition, novel object-context (OC) recognition, and novel object-place-context (OPC) recognition. Each stage lasted for 4 days. For all sample and test trials, the animal was allowed to explore the environment freely for 3 mins. Between trials, mice were removed to a holding cage for approximately 1 min while the experimenter reconfigured the test environment for the subsequent trial. For each task, the object that was novel at test, the context, and the quadrants where the novel object or configuration occurred were counterbalanced across animals and conditions (TeLC and GFP control). For OC and OPC tasks, the presentation order of context A and B in the sample phase, the context used at test, and the context in which each object was presented during the sample phase were also counterbalanced across animals and conditions. The four stages are described here in the order in which they occurred:

1. NOR Task: In the sample trial, mice were presented with two copies of a novel object in one of the contexts (striped or grey walls). In the test trial, mice were presented with a new copy of the object from the sample trial (now familiar) and a novel object in the same context as the sample trial.

2. OP Task: In the sample trial, mice were presented with two different novel objects in one of the contexts. In the test trial, mice were presented with two copies of one of these objects in the same context as the sample trial. One of these copies was

125
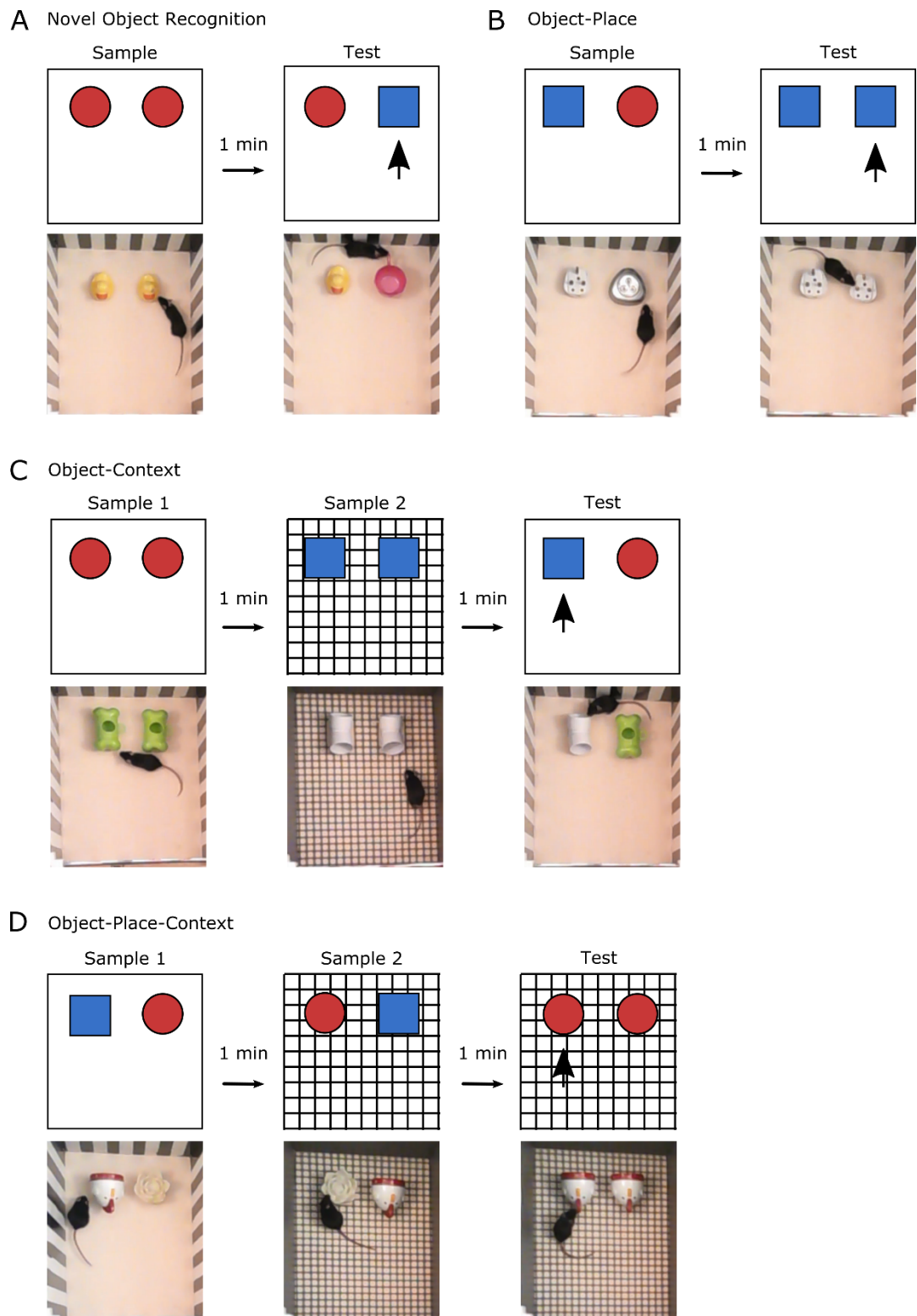
Figure 4.1: Schematic of the four object recognition tasks. The four tasks are shown separately: A) Novel Object Recognition, B) Object-Place, C) Object-Context, D) Object-Place-Context. Each task is illustrated with cartoon diagrams (top) and photographic examples of a mouse exploring the environment (bottom). A black arrow indicates the novel object or configuration in the test trial.

126

presented in the same location as in the sample phase (familiar OP configuration) whereas the other copy is in a new location (novel OP configuration).

3. OC task: In the first sample trial, mice were presented with two copies of a novel object in context A. In a second sample trial, mice were presented with two copies of a different novel object in context B. In the test trial, mice were presented with a single copy of each object within one of the contexts (A or B). At test, both objects are familiar and have been encountered at both locations, but one object has previously been encountered in the test context (familiar OC configuration), whereas the other one has not been encountered in the test context (novel OC configuration).

4. OPC task: In the first sample trial, mice were presented with two different novel objects in context A. In a second sample trial, mice were presented with the same objects in opposite locations in context B. In the test trial, mice were presented with two copies of one of the objects within one of the contexts (A or B). At test, one copy of the object is in a novel location for the test context (novel OPC configuration), whereas the other copy is in a familiar location for the test context (familiar OPC configuration).

4.2.8 Behavioural Data Analysis

All trials were recorded by a camera positioned above the test environment. Footage was scored offline by an experimenter who was blind to experimental condition. The amount of time spent exploring each object was measured. Exploration was defined as periods where the animals nose is oriented towards the object, but the animal was not interacting with the object (eg. biting) or rearing against the object to look out of the test environment. To determine whether the animal had an exploratory preference for the novel object or configuration, a

discrimination ratio (D') was calculated for each test trial, as described previously (Section 2.2.10 of Chapter 2). For each animal, average discrimination ratios were calculated for each task. A population mean was then calculated for experimental and control groups. Trials where the total exploration time was <5 seconds during sample or test were excluded. Where ≥ 3 trials of a task met the criteria for exclusion for an animal, the animal was removed from the dataset for that task (NOR, n = 3, 2 TeLC and 1 GFP control; OP, n = 2, both GFP control; OC, n = 3, 2 TeLC and 1 GFP control; OPC, n = 7, 2 TeLC and 5 GFP control).

4.2.9 Histology

Mice were administered a lethal dose of sodium pentobarbital (0.1 ml) and transcardially perfused with cold PBS followed by cold PFA (4%). Brains were fixed for 24 hours in PFA at 4°C, washed with PBS, and transferred to a 30% sucrose solution prepared in PBS for 48 hours at 4°C. Brains were then sectioned horizontally at 60μm on a freezing microtome, commencing from 200-300 μm dorsal of LEC and concluding at the bottom of the brain. Slices were washed in 0.3% PBS-T (Triton) 3 x for 20 minutes, before being transferred to a solution containing Neurotrace 640/660 (Invitrogen, 1:800) prepared in 0.3% PBS-T for 2-3 hours at room temperature. Slices were washed with 0.3% PBS-T 3 x for 20 minutes before being mounted and cover-slipped with Mowiol. Mounted sections were stored at 4°C.

4.2.10 Quantification of Virus Expression

All images were acquired using a fluorescent microscope (Zeiss ApoTome) and ZenPro software. To confirm the location and extent of virus expression in each animal, 1:4 sections which contained LEC were imaged at a 10x magnification. Coordinates for each section were determined by referencing an atlas of the mouse brain (Franklin & Paxinos, 2007).

Unfolded representations of LEC L2a were generated by adapting procedures previously used to quantify lesions of the entorhinal cortex (Insausti et al. 1997; Steffenach et al. 2005). The anterior and posterior borders of the LEC were determined by the bifurcation of L2, which is absent in adjacent structures. Where bifurcation was unclear, borders were determined through comparison to a slice from another animal at the same dorsal-ventral coordinates. The length of L2a was measured in ImageJ (https://fiji.sc) using a built-in tool calibrated to the scale of the image. For sections with virus expression, three measurements were extracted: the distance of the region of expression from the anterior LEC border, the length of the region of expression, and the distance of the region of expression from the posterior LEC border. The region of expression was defined as the length of L2a between the most anterior infected neuron and the most posterior infected neuron. These values were used to calculate the proportion of LEC L2a in which the virus was expressed for each animal. Any unintended spread of virus to adjacent structures was noted.

To determine the density of virus expression in each slice, the region of expression was imaged at a 20x magnification. For each region, the number of neurons expressing the reporter gene (GFP) and the number of counterstained neurons were quantified manually. From these values, the percentage of infected neurons with each region of expression was calculated as *n* labelled cells divided by total *n* cells in the region. Density measurements were calculated for every section with virus expression. These values were averaged across all quantified sections to produce a single density value for each mouse.

4.2.11 Statistical Analysis

Prior to analysis, normality of data was tested using the Shapiro-Wilk statistic. Where the data was found to be non-normally distributed, an appropriate non-parametric alternative was used. All statistical analyses were conducted using SPSS (IBM, version 24). To compare

data across cohorts, independent sample *t*-tests were conducted for each task using the discrimination ratios from each experimental group (TeLC and GFP control) in each cohort (first and second). To determine whether there was an effect of experimental group, univariate ANOVAs or Kruskal-Wallis *H*-tests were conducted with group (TeLC and GFP control) as a between-subjects factor for each task. To determine whether the average discrimination ratios for each group were different from chance, one-sample *t*-tests were conducted against a value of 0 for each task. Further univariate ANOVAs were conducted to determine whether there was a group effect for virus expression (unilateral versus bilateral) in the TeLC group. For these analyses, an animal was classified as unilateral if the virus expression covered <10% of LEC L2a in one hemisphere and >10 % in the contralateral hemisphere. An animal was classified as bilateral if virus expression covered >10% of the area of LEC L2a in both hemispheres. To determine whether there was a relationship between the extent of virus expression and behaviour, Pearson's product-moment correlation coefficients were calculated with percentage area of expression as a variable against the average discrimination ratio of each task for each animal. Where sections were categorised into dorsal, intermediate, and ventral LEC, coordinates were grouped using the following dorsoventral coordinates from bregma, respectively: -3.28 to -4.12, -4.28 to -4.44 and -4.56 to -4.88 mm.

4.3 Results

4.3.1 Collapsing of Cohorts

To permit collapsing of the two cohorts for statistical analysis, it was necessary to verify that the discrimination ratios for each task were not significantly different across cohorts for the either experimental group. There was no significant difference in performance across cohorts in the TeLC group for the OP task (t (19) = 0.325, P =0.748), OC task (t (17) = -0.013, P = 0.990), or OPC task (t (17) = 1.007, P = 0.328). However, there was a significant difference

between the discrimination ratios of the first and second cohort for the NOR task (t (17) = 2.943, P = 0.009). Mice in the first cohort performed above chance on the NOR task, (t (11) = 6.618, P < 0.001), but mice in the second cohort did not (t (8) = 1.584, P = 0.157). Therefore, for the NOR task, statistical analysis was conducted across both cohorts and individually. There was no significant difference in performance across cohorts in the GFP control group for the NOR task (t (14) = -0.954, P = 0.357), OP task (t (13) = -1.469, P = 0.168), OC task (t (14) = -0.082, P = 0.936), or OPC task (t (10) = -1.922, P = 0.084).

4.3.2 Histology

A subset of brains (1 TeLC, 4 GFP) suffered mechanical damage to LEC L2 in > 30% of sections during histology. Removal of these mice from the dataset does not change the statistical significance of comparisons between groups (see Appendix F), therefore they were included in the analysis of behaviour, yet excluded from analyses which address the relationship between virus expression and behaviour. Table 4.1 shows the area percentage of virus expression for animals in the TeLC group. Most had bilateral expression (n = 14), with unilateral expression in a minority (n = 6). One mouse was not classified due to extensive damage to the left hemisphere. Figure 4.2 shows virus expression in the TeLC group (Panel A and C). Virus expression covered similar percentages of LEC L2a in mice in the TeLC ($\bar{x}$ = 30.42 ± 2.3%) and GFP group ($\bar{x}$ = 35.71 ± 4.9%; $F_{(1, 31)}$ = 1.104, P =0.301) at expression densities of 22.91 ± 0.9% and 38.11 ± 2.56%, respectively (Fig 4.2, Panels D and E). Expression densities were significantly higher in the GFP group ($F_{(1, 31)}$ = 43.112, P < 0.001).

Table 4.1

Quantification of virus expression for mice in the TeLC group.

Mouse	Classification	LEC (%)	dLEC (%)	iLEC (%)	vLEC (%)
40	Bilateral	27.84	34.30	39.01	9.31
4	Bilateral	19.76	24.59	26.10	6.88
6	Bilateral	21.37	22.10	28.55	14.34
27	Unilateral	28.15	33.91	24.10	21.19
69	Unilateral	24.48	22.44	15.49	35.22
1	Bilateral	38.63	51.08	28.77	22.86
48	Bilateral	31.39	47.04	31.58	2.93
32	Unilateral	17.62	19.17	12.13	19.23
31	Bilateral	33.77	38.10	36.98	24.19
58	Bilateral	31.47	37.03	29.97	22.78
55	Bilateral	27.59	38.51	23.08	7.77
38	Unilateral	17.01	19.27	9.56	19.34
28	Bilateral	22.42	36.28	14.54	4.39
10	Unilateral	25.49	28.46	20.68	24.26
32	Unilateral	19.79	22.06	19.80	15.86
30	Bilateral	43.95	55.016	42.53	28.07
44	Bilateral	41.56	56.23	32.52	23.06
41	Bilateral	30.82	31.33	17.82	29.05
61	Bilateral	52.23	61.94	40.52	48.42
64	Bilateral	50.07	62.64	30.43	41.04
Average		**30.42 (±2.3)**	**37.32 (±3.1)**	**26.27 (±2.1)**	**21.01 (±2.6)**

Note: Numbers reflect the total percentage area of virus expression across both hemispheres for LEC L2a, dorsal LEC (dLEC), intermediate LEC (iLEC) and ventral LEC (vLEC). Average percentages with SEM across all animals are shown in the bottom row of the table in bold.
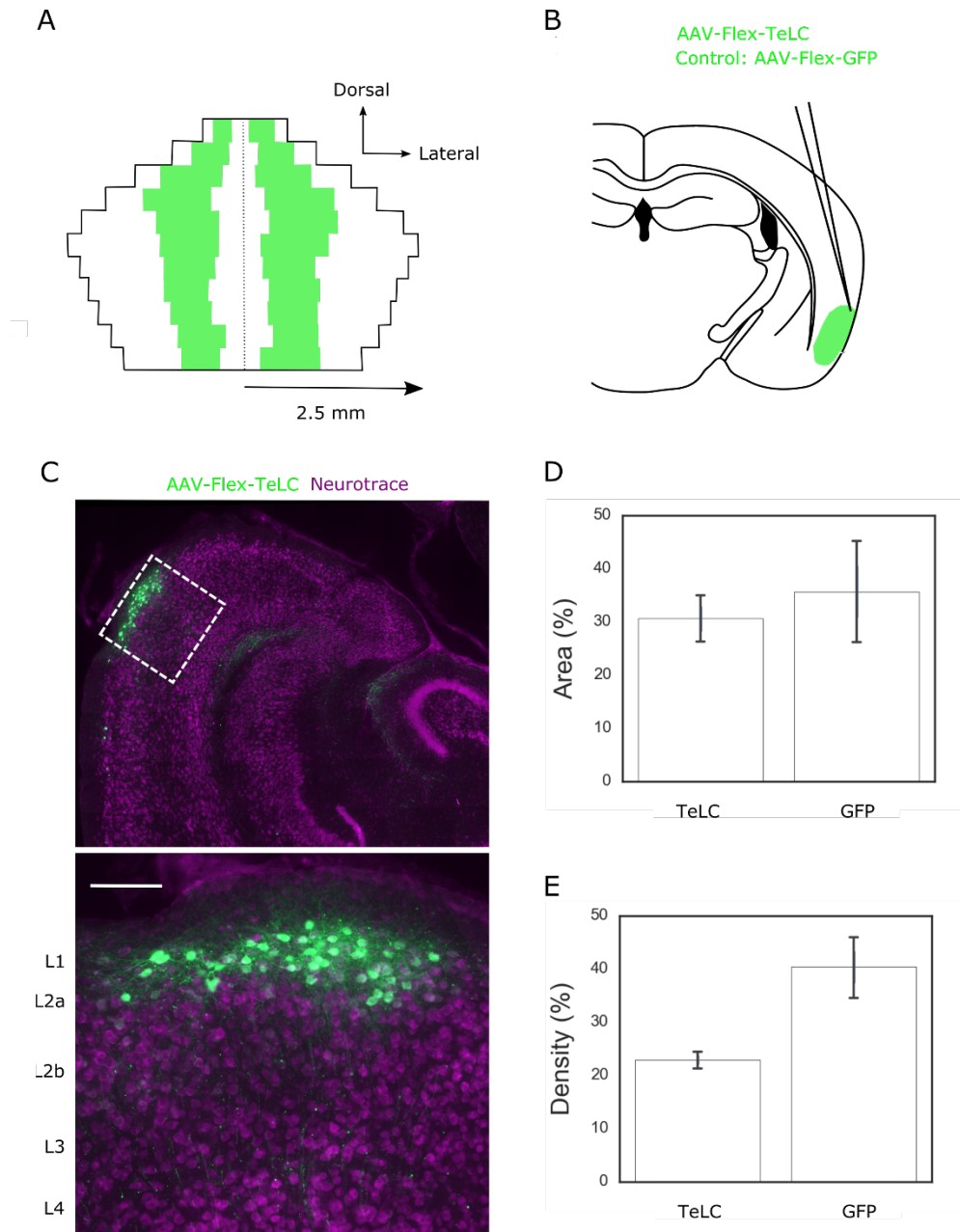
Figure 4.2. Quantification of virus expression. A) Unfolded representation of LEC L2a overlaid with average location and spread of virus (green) across mice in the TeLC group; A=Anterior border, P=Posterior border, D= Dorsal, V=Ventral. B) Illustration of injection strategy. C) (Top) Horizontal section from a Sim1:Cre mouse injected with AAV-Flex-TeLC-GFP. (Bottom) Extract depicting virus expression (green) in LEC L2a. Scale bar represents 100 um. D) Bar graph showing the average areas of LEC L2a infected in TeLC and GFP groups. E) Bar graph showing the average densities of expression in TeLC and GFP groups. All error bars represent SEM.

In all mice, there was sparse labelling of L2b in at least one section, as observed previously during the characterisation of the Sim1:Cre line (see Section 3.3.3 of Chapter 3). In the TeLC group, there was labelling of LEC L5 in a subset of mice (n = 11). In most cases (n= 8) this was negligible, summating to <10 cells across all sections. In the other cases (n = 3), this was approximated to be <5 % of LEC L5. There was no significant difference between performance of mice with L5 expression and other mice in the TeLC group on the NOR task ($F_{(1, 17)}$ = 0.009, P = 0.927), OP task ($F_{(1, 19)}$ = 0.302, P =0.589), OC task ($F_{(1, 17)}$ = 0.264, P = 0.614), or OPC task ($F_{(1, 17)}$ = 0.480, P =0.498). Further, there was minor spread of virus to portions of MEC L2 directly adjacent to LEC L2 in a subset of mice (n = 8). This was approximated to be <5 % of MEC L2 in all cases. There was no significant difference between the performance of mice with MEC L2 expression and other mice in the TeLC group on the NOR task ($F_{(1, 17)}$ = 1.567, P = 0.229), OP task ($F_{(1, 19)}$ = 0.012, P = 0.914), OC task ($F_{(1, 17)}$ = 0007, P = 0.932), or OPC task ($F_{(1, 17)}$ = 0.024, P = 0.880). These analyses indicate that any findings were not driven by expression in LEC L5 or MEC L2, therefore data from these animals was included in statistical analyses.

4.3.2 Novel Object Recognition

Figure 4.3 shows the discrimination ratios for the TeLC group and GFP controls for the NOR task. There was a significant difference between the performance of the TeLC and GFP groups ($F_{(1, 33)}$ = 4.542, P = 0.041, η^2 = 0.121; Panel A, Fig 4.3). Although the TeLC group had significantly lower discrimination ratios than the control group, they still explored the novel object significantly more than expected by chance ($\bar{x}$ D' = 0.22 ± 0.04, t (18) = 5.001, P = < 0.001). The GFP control group also performed significantly above chance on this task ($\bar{x}$ D' = 0.35 ± 0.05, t (15) = 7.922, P = < 0.001).

Figure 4.3. Average discrimination ratios and exploration times on the NOR task. (Left) Bars indicate average discrimination index for each group (TeLC and GFP control). Each blue dot indicates the discrimination index for a single animal. Asterisks indicates a significant difference between the two groups ($p < 0.05$). (Right) Bars indicate average exploration time in seconds during the test trials for each group. All error bars represent SEM.

Due to the significant difference between cohorts of the TeLC group for the NOR task, these analyses were repeated for each cohort individually (Panel B, Fig. 4.3). There was no significant difference between the performance of the TeLC group and GFP controls in the first cohort ($F_{(1, 22)} = 0.368$, $P = 0.550$), but there was a significant difference between the performance of the two groups in the second cohort ($F_{(1, 14)} = 9.591$, $P = 0.008$, $\eta^2 = 0.407$). The difference across cohorts might be explained by the location and extent of virus expression in each group, a possibility which is examined later in this chapter (see Section 4.3.8). Considered together, these data suggest that the mice in the TeLC group can recognise a novel object, yet are impaired in novel object recognition in comparison to controls.

4.3.3 Performance on the Object-Place Task

Figure 4.4 shows the discrimination ratios for the TeLC group and the GFP controls for the associative object recognition tasks: OP, OC, & OPC. There was no significant difference between the performance of the two groups on the OP task ($F_{(1, 34)} = 1.608$, $P = 0.213$). However, the TeLC group did not perform above chance on the OP task ($\bar{x}$ D'= 0.03 ± 0.03, t (20) = 1.067, $P = 0.299$). In contrast, the GFP control group performed significantly above chance on this task ($\bar{x}$ D' = 0.12 ± 0.05, t (14) = 2.152, $P = 0.049$). Therefore, although the two groups do not perform significantly differently from each other, comparison to chance performance demonstrates that recognition of the novel object-place configuration is not robust in the TeLC group.

4.3.4 Performance on the Object-Context Task

There was no significant difference in performance between the two groups on the OC task ($F_{(1,33)} = 0.275$, $P = 0.603$). Mice in the TeLC group and control group performed significantly above chance on this task (TeLC: $\bar{x}$ D' = 0.10 ± 0.04, t (18) = 2.742, $P = 0.013$; GFP Control: $\bar{x}$ D' = 0.12 ± 0.04, t (15) = 3.340, $P = 0.004$). These data suggest that mice in the TeLC group are not impaired at recognising novel configurations of object and context.

4.3.5 Performance on the Object-Place-Context Task

There was a significant difference in performance between the two groups on the OPC task, $F_{(1, 29)} = 10.319$, $P = 0.003$, $\eta^2 = 0.262$. Mice in the TeLC group did not perform above chance on the OPC task ($\bar{x}$ D' = -0.05 ± 0.04, t (18) = -1.183, $P = 0.252$). In contrast, the control group performed significantly above chance on this task ($\bar{x}$ D' = 0.12 ± 0.03, t (11) = 4.274, $P = 0.001$). These data suggest that mice in the TeLC group are impaired at recognising novel configurations of object, place, and context in comparison to controls.
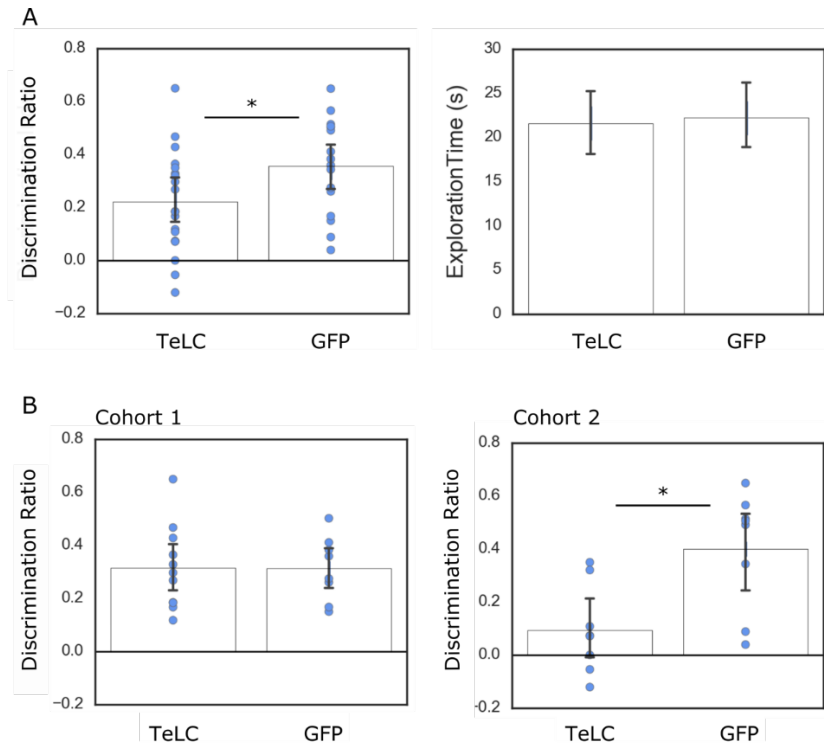
136
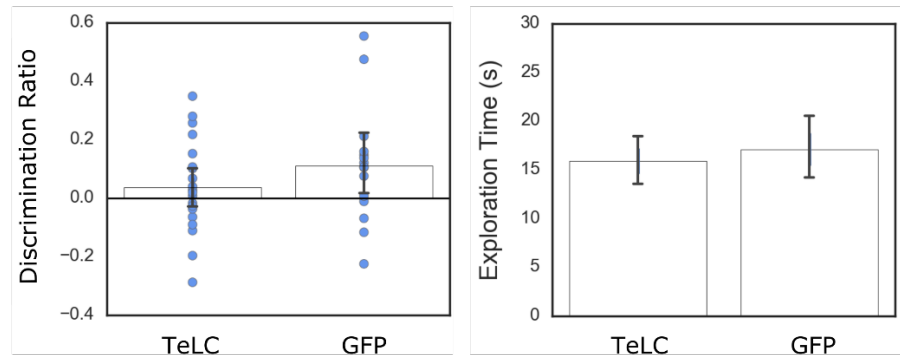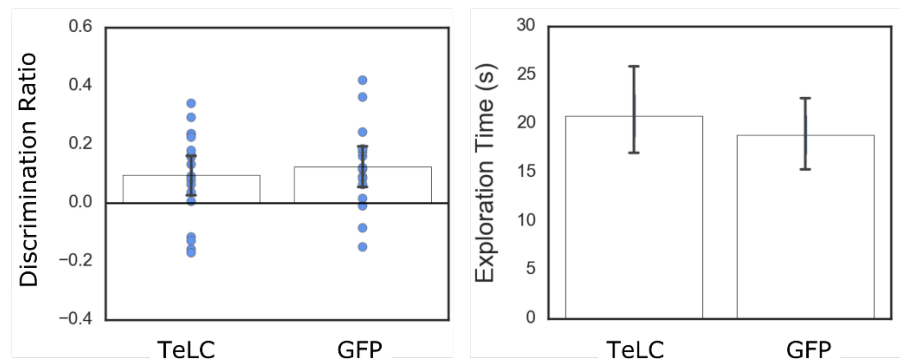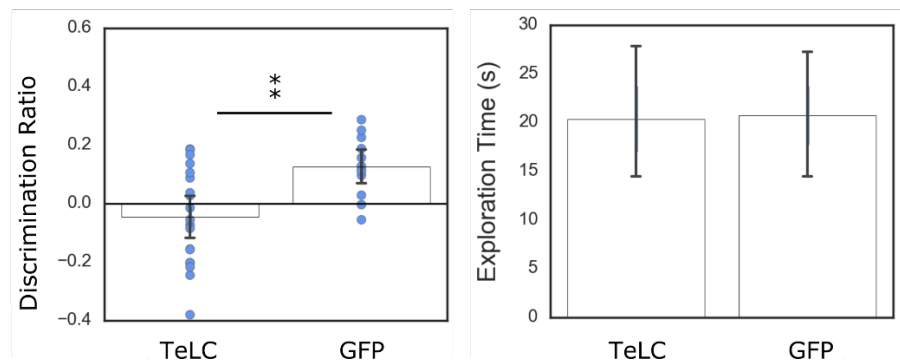
Figure 4.4. Average discrimination ratios and exploration times for OP, OC, & OPC tasks. (Left) Bars indicate average discrimination index for each group (TeLC and GFP control). Object-Place (A), Object-Context (B), and Object-Place-Context (C) are shown individually. Each blue dot indicates the discrimination index for a single animal. Asterisks indicates a significant difference between the two groups ($p < 0.01$). (Right) Bars indicate average exploration time in seconds during the test trials for each group. All error bars represent SEM.

4.3.6 Similar Exploration Times Across Experimental Groups

A possible explanation for impaired performance on the NOR, OP task and OPC task is that animals in the TeLC group explore the objects less than the GFP control group. To investigate this possibility, the time spent exploring the objects in the test and sample trials for each task were compared across groups.

For sample trials, there was no significant difference in exploration times between the two groups for the NOR (H (1) = 0.922, P = 0.337) or OP task (H (1) = 0.521, P = 0.470). Further, there was no significant difference in exploration times between groups for the OC task in the first (H (1) = 3.689, P = 0.055) or second sample trial (H (1) = 2.220, P = 0.136), or for the OPC task in the first (H (1) = 2.502, P = 0.114), or second sample trial ($F_{(1,29)}$ = 2.438, P = 0.654). There was no significant difference between the time spent exploring the objects during the test trials for the NOR ($F_{(1,33)}$ = 0.050, P = 0.825), OP task ($F_{(1,34)}$ = 0.802, P = 0.377), OC task (H (1) = 0.001, P = 0.974), or OPC task (H(1) = 0.081, P = 0.776).

Lastly, given the low performance on novel object recognition in the second cohort of the TeLC group, these analyses were repeated for the sample and test trial of the NOR task for this cohort. There was no difference in exploration times between the TeLC and control animals at sample (H (1) = 0.044, P = 0.834) or test ($F_{(1,14)}$ = 2.438, P = 0.141), which indicates that low performance in the TeLC group of this cohort was not due to lower exploration at test.

4.3.7 No Relationship Between Laterality of Virus Expression and Behaviour

The extent and location of virus expression was variable across animals in the TeLC group (see Table 4.1). To determine whether there was a relationship between virus expression and behaviour, discrimination ratios were compared across animals with bilateral and unilateral virus expression. Figure 4.5 shows the discrimination ratios within these subgroups for all tasks. Although the average discrimination ratios were slightly higher for animals with

unilateral relative to bilateral expression for the OP, OC & OPC tasks, there was no significant difference between performance between the two groups for any task (NOR: $F_{(1,16)} = 0.052$, $P = 0.823$; OP task: $F_{(1,18)} = 0.498$, $P = 0.489$; OC task: $F_{(1, 17)} = 0.408$, $P = 0.531$; OPC task: $F_{(1, 16)} = 0.008$, $P = 0.928$).

4.3.8 Correlation Between Extent of Virus Expression and Object-Place-Context Memory

Figure 4.5 contains scatterplots demonstrating the correlation between virus expression and performance for all tasks. There was a significant negative correlation between the overall percentage area of virus expression and performance on the OPC task ($r = -0.483$, n = 18, p = 0.042). When virus expression was further grouped by hemisphere, a significant negative correlation between performance on the OPC task and expression in the left hemisphere was revealed ($r = -0.636$, n = 18, $P = 0.005$). There were no other significant correlations between discrimination ratios and virus expression for any other task.

When virus expression was grouped into area percentages of dorsal, intermediate, and ventral LEC, there was a significant negative correlation between the extent of virus expression in dorsal LEC L2a and performance on the OPC task ($r = -0.563$, n = 18, $P = 0.015$). There were no other significant correlations between virus expression and performance on any other task, but the negative correlation between virus expression and performance on the NOR task did approach significance ($r = -0.413$, n= 18, $P = 0.088$). Yet when expression was grouped by hemisphere and location on the dorsoventral axis, significant negative correlations between virus expression and performance on the OPC task were revealed for the dorsal ($r = -0.636$, n = 18, $P = 0.015$) and ventral ($r = -0.563$, n = 18, $P = 0.015$) left hemisphere. The negative correlation between performance on the NOR task and expression in dorsal LEC also approached significance ($r = -0.413$, n = 18, $P = 0.089$).

139
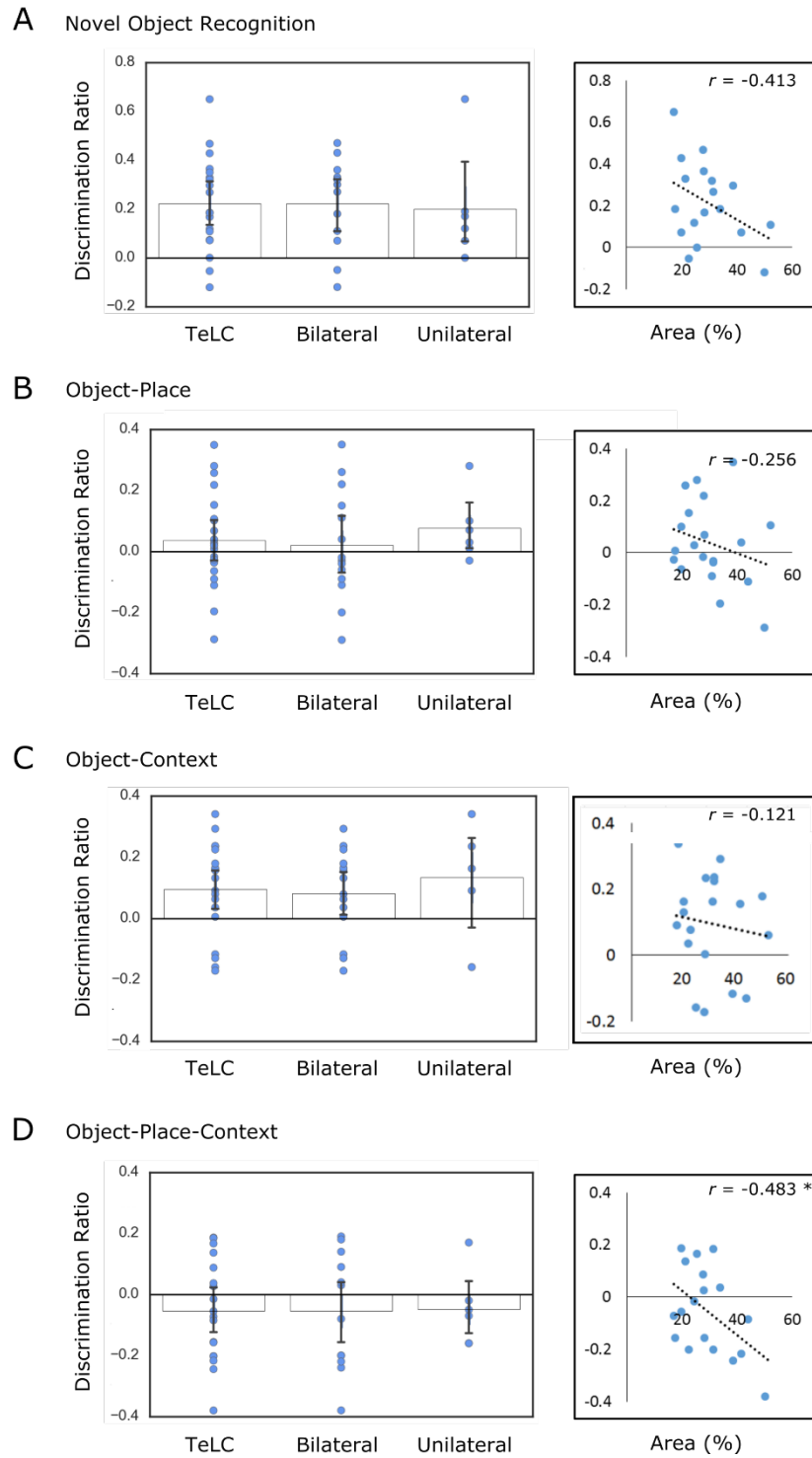
Figure 4.5. Relationship between virus expression and performance for tall tasks. (Left) Bars indicate average discrimination ratios for TeLC group and subgroups (bilateral and unilateral). Each blue dot indicates the discrimination index for a single animal. Error bars represent SEM. (Right) Scatterplots of discrimination ratios for the TeLC group against the percentage area of virus expression in LEC. Dashed line indicates line of best fit. Asterisks indicate a significant correlation ($p < 0.05$).

Lastly, these analyses were repeated for the NOR task for both cohorts of the TeLC group to determine whether the difference in performance was driven by different patterns of virus expression. Indeed, the percentage area of virus expression across LEC L2a was significantly higher in the second cohort (First cohort: $\bar{x} = 26.6 \pm 1.9$ %, Second cohort: $\bar{x}$ 35.8 $\pm$ 4.5%; $F_{(1,19)} = 4.465$, $P = 0.049$, $\eta^2 = 0.199$). Although the second cohort had higher expression in both hemispheres, this difference was significant for the left hemisphere (First cohort: $\bar{x} = 23.4 \pm 4.1\%$, Second cohort: $\bar{x}$ 38.0 $\pm$ 5.8%; $F_{(1,19)} = 4.499$, $P = 0.048$, $\eta^2 = 0.200$). Further, the percentage area of virus expression in dorsal LEC was higher in the second cohort, a difference which approached significance (First cohort: $\bar{x} = 32.3 \pm 10.8\%$, Second cohort: $\bar{x}$ 44.3 $\pm$ 5.8%; $F_{(1,19)} = 4.746$, $P = 0.064$), and the second cohort had significantly higher virus expression in the left dorsal LEC (First cohort: $\bar{x} = 30.7 \pm 18.2\%$, Second cohort: $\bar{x}$ 49.6 $\pm$ 7.2%; $F_{(1,19)} = 4.746$, $P = 0.043$, $\eta^2 = 0.209$). However, there was no significant correlation between discrimination ratios and the extent of expression in LEC L2a or dorsal LEC L2a for either cohort. Together, these data suggest that increased virus expression in LEC L2a, particularly in the left hemisphere, might drive a lower capacity for novel object recognition, yet this effect is not robust.

4.4 Discussion

The aim of this experiment was to determine whether the reelinergic projection from LEC L2 to the hippocampus (DG) is required for associative recognition memory. To investigate this, a Cre-dependent AAV encoding tetanus toxin was injected into the superficial LEC of a group of Sim1:Cre mice, suppressing the output from LEC L2a to the dentate gyrus. Subsequently, performance on a series of object-based memory tasks was measured in comparison to a group of control mice which were injected with an AAV encoding a fluorescent reporter. Given that LEC lesions result in profound associative memory impairment

(Wilson et al. 2013a; 2013b), and evidence that reduced reelin signalling from the entorhinal cortex contributes to spatial memory deficits and age-related cognitive impairment (Stranahan et al. 2011a; 2011b), it was hypothesised that suppression of LEC L2a would impair performance on tasks which measure associative recognition memory (OP, OC, or OPC), but was unlikely to impair novel object recognition.

Animals in the TeLC group demonstrated impaired recognition of novel objects and novel object-place-context configurations in comparison to animals in the control group, yet there was no difference in recognition of novel object-place and object-context configurations between groups. Comparison of the performance of each group to chance revealed that animals in the TeLC group still recognised a novel object at a level higher than predicted by chance, though they did not perform as well as animals in the control group. Further, animals in the TeLC group did not recognise novel configurations of object-place or object-place-context at a level higher than predicted by chance. Together, these findings indicate that projection from LEC L2 to the hippocampus is required for episodic memory in mice, and may also contribute to novel object recognition and object-place memory.

The observation of an impairment on the NOR task is surprising, although not entirely unsupported by the literature. This finding is consistent with observations that LEC neurons encode information about objects in the environment (Deshmukh & Knierim, 2011; Deshmukh et al. 2012; Tsao et al. 2013) and LEC lesions impair novel object recognition in versions of the task with >2 objects in the environment (Hunsaker et al. 2013; Van Cauter et al. 2013). Further, Albasser et al. (2010) combined iEG imaging of *c-fos* and structural equation modelling to demonstrate that the perforant pathway to the DG is involved in novel object recognition in concert with several other pathways in the medial temporal lobe. Although the relationship between virus expression and performance on the NOR task was not statistically significant, this correlation did approach significance for overall expression and

expression in dorsal LEC L2. Similarly, the pattern of virus expression may have driven lower performance on the NOR task in the second cohort, which had higher expression of virus overall than animals in the first cohort, particularly within the dorsal left hemisphere. Interestingly, Hunsaker et al. (2013) observed that their lesions primarily affected the region of LEC which projects to the dorsal hippocampus, and the same research group previously observed that pharmacological inactivation of LEC input to the dorsal hippocampus produces a similar deficit (Hunsaker et al. 2007). It is possible that a role for the dorsal LEC in novel object recognition is also suggested by the data presented in this chapter. Importantly, the mice in the present study were mildly impaired in comparison to controls, but still performed significantly above chance. This suggests that projections from LEC L2 to the hippocampus may be involved in novel object recognition, but this type of memory can be supported by other components of the circuit, such as projections from LEC L3 and the direct projections to the hippocampus from the PER (Van Strien et al. 2009).

Impaired performance on the OP & OPC task is consistent with previous reports of chance performance on these tasks in rats with whole LEC lesions. This impairment was severe irrespective of the laterality of virus expression, which is consistent with impairment on these tasks in rats with unilateral LEC lesions (Wilson et al. 2013b). Given that the majority of inactivated cells were positive for reelin, this pattern of impairment is also consistent with a role of reelinergic output from LEC L2 in learning and memory.

Although mice in the GFP group performed above chance on the OP task, performance was not significantly different from the TeLC group. It is possible that methodological differences between our study and previous studies which used this task in mice (eg. Davis et al. 2013; Belblidia et al. 2015), such as choice of objects or trial length, may have contributed to low performance in the control group. A systematic investigation of the relationship between these factors and performance on the OP task would be valuable to the field. Irrespective of

low performance in the control group, loss of performance in the TeLC group extends the previous finding of impaired spatial memory after knockdown of reelin signalling in the LEC (Stranahan et al. 2011a; 2011b) to an object-based associative memory task. It is possible that reelin signalling originating from LEC L2 plays a critical role in both types of spatial memory. Future studies could expand on this finding by incorporating other spatial memory tasks, such as object dislocation within an environment or reward-based choice tasks in a radial arm maze. Given that the Sim1:Cre also provides genetic access to MEC L2 (Surmeli et al. 2015), this mouse line could be a particularly beneficial tool for projects aimed at investigating functional dissociations between MEC and LEC.

For the OPC task, there was a significant negative correlation between the extent of virus expression and performance, which indicates that mice with larger regions of virus expression have a larger episodic memory deficit. Interestingly, this relationship appears to be driven by virus expression in the left hemisphere. While lateralisation of entorhinal contributions to memory have not been identified in the human or animal literature, our findings are consistent with evidence that left hemisphere hippocampal damage corresponds with impairment in humans performing a virtual-reality episodic memory task (Spiers et al. 2001). Futher, in mice, it was recently demonstrated that the left, but not right, hippocampus is required for associative long-term memory for reward location in relation to extra-maze cues (Shipton et al. 2015). It is possible that the present finding complements this research by suggesting that input into the left hippocampus from LEC L2 is required for episodic memory in mice. Further, the significant negative correlation between expression in ventral LEC and performance on the OPC task is consistent with previous reports of higher expression of c-*fos* in the VIE sub-division of the LEC in rats who experienced novel object-context configurations (Wilson et al. 2013a). Interestingly, impaired performance on the OPC task was not paired with a deficit for recognising novel configurations of object and context. Therefore, it is possible

that while L2a projections are required for associating all aspects of an experience (object, place, and context), object and contextual information is integrated elsewhere within the network.

4.5 Conclusion

In summary, the present experiment demonstrated that selective inactivation of LEC L2 results in episodic memory impairment in mice, but has no effect on the ability to integrate object and context information. Further, suppression of this layer results in impaired novel object recognition and less robust performance on an object-place recognition task. These findings suggest that output from LEC L2a to the DG is critical for integrating object, location, and context information and may help support novel object recognition.

Chapter 5: General Discussion

5.1 Thesis Overview

The overarching aim of the current thesis was to examine how information about an episode is processed between the LEC and hippocampus, specifically within the projections reaching the hippocampus from the superficial layers of entorhinal cortex. The experiments presented in this thesis were driven by previous work which used whole lesions and electrophysiological methods to determine that the LEC is required for associative recognition memory (Wilson et al. 2013a; 2013b) and contains spatially modulated cells which encode information about local cues in the environment (Tsao et al. 2013; Keene et al. 2016). These findings suggested that some integration of spatial and non-spatial content occurs upstream of the hippocampus within the LEC. However, it remained unclear how the individual layers of the LEC contribute to cognition. Given that cortical projections from the entorhinal cortex to the hippocampus arise largely from L2 and L3, it is possible that inputs to the hippocampus from these components make differential contributions to an entorhinal-hippocampal circuit which underlies episodic memory. To this end, the experiments described in this thesis combined behavioural, electrophysiological and molecular methods to examine the function of the superficial layers of LEC.

Firstly, the experiment presented in Chapter 2 capitalised on the divergent nature of projections from L3 of the entorhinal cortex into CA1 of the hippocampus. Rats were implanted with electrodes targeting the distal or proximal CA1, and place cell activity was recorded as these animals explored an environment which contained objects. Given that the LEC is connected to a network of structures associated with object perception (see Section 1.2.1 of the General Introduction), and contains cells which demonstrate spatial tuning in relation to objects (see Section 1.5.2 of the General Introduction), it was predicted that the different types of input from L3 of the entorhinal cortex would drive differences in the characteristics and object modulation of place cells across the proximodistal axis of CA1.

Indeed, place cells which receive input from LEC L3 demonstrated higher spatial tuning than place cells which receive input from MEC L3, contradicting previous reports of increased spatial tuning of place cells which receive input from MEC L3 in empty environments (Henriksen et al. 2010). Surprisingly, similar proportions of place cells in distal and proximal CA1 remapped in response to the displacement of objects, and place cells which receive input from MEC L3 were more likely to express place fields in quadrants of the environment which contained objects. However, remapping in place cells which receive input from LEC L3 was modulated by the proximity of place fields to object locations, and only place cells receiving LEC input encoded precise memory traces of recent new object locations in the environment.

These data suggest that in environments where objects are present, the spatial tuning of place cells in CA1 is driven by input from LEC L3, yet object-modulation of place cell activity is not clearly influenced by the type of entorhinal input each region receives. However, remapping in place cells which receive input from LEC L3 was more precisely tied to previous and current object locations within the environment, which indicates that the selectivity of remapping across the proximodistal axis of CA1 is subtly driven by input from the entorhinal cortex; global spatial signalling originating from the MEC drives remapping across the entire environment, whereas spatial signalling originating from object-responsive cells in the LEC might drive patterns of remapping which are more selective for local landmarks. These data complement previous experiments which demonstrated that LEC input modulates place cell firing in environments which are rich in local cues (Burke et al. 2011; Lu et al. 2013; Scaplen et al. 2017), and indicates that damage to LEC L3 may contribute to the impaired performance observed in object-place recognition memory after whole LEC lesions (Wilson et al. 2013b). However, further testing of this hypothesis was precluded by the lack of available tools for precisely manipulating output from LEC L3.

Therefore, the experiments presented in Chapters 3-4 aimed to identify and utilise a sophisticated tool for manipulating LEC L2. In Chapter 3, the arrangement of projecting neurons in LEC L2 was examined, and it was observed that LEC L2 projections to the hippocampus arise from a sub-population of cells which are positive for the protein reelin and located in the superficial aspect of L2, as described previously (Leitner et al. 2016). Given that the molecular organisation of LEC L2 bore similarity to the organisation of MEC L2, it was hypothesised that molecular tools which provide genetic access to neuronal sub-populations in MEC L2 (Surmeli et al. 2015) could be re-purposed to label sub-populations of LEC L2. To this end, an injection strategy was developed to deliver Cre-dependent adeno-associated virus which encodes a fluorescent reporter into the superficial LEC of Sim1:Cre, Wfs1:CreEr, and Ccdc3:Cre mice. Indeed, the Sim1:Cre mouse labelled a sub-population of cells in LEC L2 which are positive for reelin and project to the dentate gyrus. However, labelling in the Wfs1:CreEr and Ccdc3:Cre mice was either non-specific to LEC L2 or extremely sparse. Whole-cell patch clamping of labelled cells in the Sim1:Cre mouse confirmed that these cells corresponded to 'fan cells', an excitatory principal cell type previously described in the superficial LEC (Section 1.2.2 of the General Introduction, Tahlvidari & Alonso, 2005; Leitner et al. 2016). Therefore, the Sim1:Cre mouse presented a novel opportunity to precisely manipulate LEC L2 output to the hippocampus.

Finally, Chapter 4 presented an experiment where adeno-associated virus encoding the tetanus toxin light chain was injected into the superficial LEC of a cohort of Sim1:Cre mice, which effectively suppressed output from LEC L2 to the dentate gyrus. Subsequently, the performance of these mice on a novel object recognition task and a series of associative recognition memory tasks was examined. Given the profound associative recognition memory impairment observed after whole lesions of the LEC (see Section 1.5.2 of the General Introduction) and evidence that LEC L2 pathology contributes to memory impairment in

human and animal models of age-related cognitive decline (see Section 1.5.5 of the General Introduction), it was hypothesised that projections to the hippocampus from LEC L2 may be critical for associative recognition memory. Indeed, suppression of this pathway impaired performance on an episodic memory task which requires recognition of novel object-place-context configurations. Further, Sim1:Cre mice injected with tetanus toxin demonstrated impaired novel object recognition and less robust recognition of novel object-place configurations in comparison to controls. However, suppression of LEC L2 output to the hippocampus did not impair recognition of novel object-context configurations, which suggests object and context information is integrated elsewhere within the network. Overall, this experiment demonstrated that input from LEC L2 into the hippocampus is required for episodic memory in mice, and may help support novel object recognition.

5.2 Implications for Episodic Memory Circuitry

Overall, the experiments presented in this thesis provide new evidence that the laminar components of superficial LEC make distinct contributions to episodic memory processes. These findings suggest that input from LEC L2 into the DG is critical for episodic memory and contributes to novel object recognition, but is not required for integrating object and context information. Further, these findings suggest that input from LEC L3 into CA1 of the hippocampus modulates spatial tuning in place cells when the environments contains objects, and may support a neural mechanism for object-place memory. Like previous research, these data are inconsistent with the predictions of the parallel processing model; both behavioural experiments (Chapter 2 and 4) provide evidence that the superficial LEC contributes to the integration of spatial and non-spatial content of an episode.

These findings are consistent with the models proposed by Knierim & Hamilton (2011) and Deshmukh & Knierim (2011), which posit that the LEC attends to the non-spatial attributes

of an episode, yet still maintains spatial representations of local landmarks. Indeed, these data suggest that the superficial LEC plays a critical role in processing information about local cues, but may be less involved in processing global information, such as context. Further, these findings are consistent with lesion experiments which reported that LEC lesions only produced mild impairments in novel context recognition (Hunsaker et al. 2013), and the observation that impaired performance on a scene-based contextual memory task is driven by damage to the deep, not superficial LEC (Yoo & Lee, 2017). However, the present finding of impaired object-place-context memory after selective suppression of LEC L2 input into the hippocampus does suggest that some contextual information is processed within this part of the circuit.

Conversely, the data presented in this thesis are difficult to reconcile with the 'contextual gating' hypothesis proposed by Hayman & Jeffrey (2008). Specifically, their model suggests that LEC L2 input into the DG/CA3 provides non-spatial contextual information to the hippocampus, which then modulates the activity of place cells to induce remapping in response to environmental changes. The present finding of intact object-context recognition after selective suppression of projections from LEC L2 might suggest that contextual representations are generated elsewhere in the circuit, or this information reaches the hippocampus via projections from MEC L2. This latter possibility would be consistent with reports of impaired contextual memory after damage to the MEC (Suh et al. 2011; Hunsaker et al. 2013; Kitamura et al. 2014; Yoo & Lee, 2017). Notably, context is a broad term in episodic memory research, and while the experiments presented in this thesis define context using visual and tactile environmental cues, other associative memory tasks use other aspects of an experience, such a temporal attributes or behavioural saliency (eg. Kart-Teke et al. 2009; Komoroswki et al. 2009). If different types of contextual information are processed by various parts of the circuit, it is possible that a different pattern of impairment would emerge after suppression of LEC L2 using a different paradigm. Further, it is possible that these

representations reach the hippocampus via communication with LEC L3 or deep LEC (Yoo & Lee, 2017). Unfortunately, the behavioural paradigm used in the examination of place cell activity across the proximodistal axis of CA1 did not incorporate a contextual component, therefore it is not possible to further speculate to what extent contextual information might be encoded by LEC L3, nor whether input from LEC L3 modulates the remapping of place cells in response to contextual change.

Importantly, there is strong interconnectivity between the superficial LEC and the MEC. The superficial LEC projects to the superficial and deep layers of MEC, and the superficial MEC further projects to LEC L2 and L5 (Section 1.2.1 of the General Introduction). The findings reported in Chapter 2 and Chapter 4 may reveal something about communication between the two regions of superficial entorhinal cortex. It is possible that projections to superficial MEC from LEC L2/L3 may contain information about local cues in the environment, which are incorporated in the representations of the environment projected to the hippocampus from MEC L2/L3. This organisation would predict similar patterns of remapping across the proximodistal axis of CA1, as reported in Chapter 2, as information about objects in space would reach the hippocampus via both regions of entorhinal cortex. Further, this organisation would predict the mild impairment in the novel object-place recognition task, as observed in Chapter 4, given that some information about the location of objects in the environment would reach MEC via LEC L3, and therefore indirectly reach CA1. Conversely, some aspects of associative recognition memory might be supported by intact projections from MEC L2 to the hippocampus. Indeed, Tennant et al. (2018) recently reported impaired recognition of a novel object location after selective inactivation MEC L2 stellate cells. Therefore, it is possible that the integration of spatial and non-spatial information in the LEC is a product of laminar communication between the superficial MEC and LEC, and further

152

elucidation of the functional connectivity between these adjacent structures will be critical for establishing a network which underlies episodic memory.

Further, it is interesting to consider how the data presented in this thesis would fit into a model of microcircuitry in the LEC which supports episodic memory. In the MEC, the hippocampus feeds back information to MEC L5, which projects back to MEC L3, and receives input from MEC L2 (See Fig. 1.1, General Introduction). Further, within MEC L5, L5b receives the majority of feedback from the hippocampus and input from MEC L2 stellate cells, rendering it well-situated for integrating information from the hippocampus and superficial MEC within the circuit (Surmeli et al. 2015). Currently, it is unknown whether the circuit is similarly organised in the LEC, but it is likely that the superficial and deep layers of LEC communicate (see Van Strien et al. 2009; Witter et al. 2017). If information is similarly integrated in LEC L5b, this layer may make important contributions to an episodic memory circuit. This notion is consistent with impaired performance on context-based tasks after lesions of deep LEC (Yoo & Lee, 2017). Further, it would suggest that episodic memory impairment after suppression of LEC L2 fan cells is a result of reduced signalling between LEC L2 and the hippocampus *and* between LEC L2 and L5b. Future experiments elucidating the microcircuitry of the LEC and identifying tools for selective manipulation of deep LEC will be critical for understanding how the findings presented in this thesis fit into a model of episodic memory in an entorhinal-hippocampal circuit.

5.3 Methodological Implications and Future Work

This thesis presents the first use of a molecular tool to selectively manipulate a discrete sub-population of neurons within a layer of the LEC and measure the behavioural consequences. Recently, this approach has become more common in research which examines the functional circuitry of MEC (Suh et al. 2011; Kitamura et al. 2014; Tennant et al. 2018),

and similar techniques might be used more frequently in the future study of the LEC. Our findings complement previous research which used non-specific lesions of LEC or hippocampus to identify associative recognition memory impairments after widespread disruption to this network (Langston & Wood, 2010; Wilson et al. 2013a, 2013b) and research which has examined the role of the reelin signalling pathway from entorhinal cortex to hippocampus in spatial memory and age-related cognitive decline (Stranahan et al. 2011a; 2011b). With the Sim1:Cre line, future behavioural experiments could build on our finding of impaired episodic memory after suppression of LEC L2a. For example, given evidence that the DG is involved in distinguishing between overlapping experiences (see Colgin et al. 2008; Yassa & Stark, 2011), it would be interesting to examine whether input from LEC L2 into the DG contributes to the capacity to discriminate between episodes with overlapping features.

Further, the use of transgenic mice could be enormously valuable for future in-vitro electrophysiology experiments. Cre-dependent virus which encodes excitatory or inhibitory compounds could be used in conjunction with paired recordings of cells in-vitro to further elucidate the microcircuitry of the LEC and progress the understanding of connectivity between the superficial LEC and MEC. Specifically, as discussed in Section 5.4 of this chapter, it would be interesting to examine the existence and nature of connectivity between superficial and deep LEC. Identifications of mouse lines which provide genetic access to discrete sub-populations of LEC L3 and L5 would permit examination of any interaction between neurons in LEC L2, L3 and L5. This work could elucidate how the LEC processes the perceptual information entering the LEC from the PER in conjunction with output from the hippocampus, which may underlie recognition of novel versus familiar configurations of object-place-context.

Finally, the recent development of sophisticated activity markers which can be packaged into adeno-associated virus (eg. Sorensen et al. 2016; Lee et al. 2017) presents the novel opportunity to precisely label neurons which are active during behaviour with a high

degree of temporal sensitivity, and then examine their electrophysiological properties and connectivity in-vitro. By combining the use of these markers and behaviour in wild-type mice, this technique could further elucidate which components of the network are contributing to episodic memory. For example, active neurons could be labelled during different associative recognition memory tasks, and then the properties and connectivity of the labelled populations with could be examined in-vitro. These types of experiments would build on the findings presented in this thesis and perhaps substantiate some of the ideas about the underlying network presented in the discussion.

5.4 Concluding Remarks

Overall, this thesis presents two lines of evidence which indicate that discrete projections from the superficial layers of the LEC to the hippocampus make distinct contributions to episodic memory processes. Specifically, LEC L2 is required for associating object-place-context information and contributes to novel object recognition. In contrast, LEC L3 drives spatial tuning in the hippocampus in relation to objects in the environment, and might contribute to object-place memory. Together, these findings begin to tease apart entorhinal-hippocampal circuitry which underlies associative recognition memory.

References

Aggleton, J. P., & Brown, M. W. (1999). Episodic memory, amnesia, and the hippocampal anterior thalamic axis. *Behavioral and Brain Sciences, 22,* 425-489.

Ainge, J.A., Heron-Maxwell, C., Theofilas, P., Wright, P., de Hoz, L., & Wood, E. R. (2006). The role of the hippocampus in object recognition in rats: examination of the influence of task parameters and lesion size. *Behavioural Brain Research, 167(1),* 183-195.

Ainge, J. A., Tamosiunaite, M., Woergoetter, F., Dudchenko, P. A. (2007). Hippocampal CA1 place cells encode intended destination on a maze with multiple choice points. *Journal of Neuroscience, 27(36),* 9769-9779.

Albasser, M. M, Poirier, G. L., & Aggleton, J. P. (2010) Qualitatively different modes of perirhinal-hippocampal engagement when rats explore novel vs familiar objects as revealed by c-fos imaging. *European Journal of Neuroscience, 31 (1),* 134-147.

Annese, J., Schenker-Ahmed, N. M., Bartsch, H., Maechler, P., Sheh, C., Thomas, N., Kayano, J., Ghatan, A., Bresler, N., Frosch, M. P., Klaming, R., & Corkin, S. (2014). Postmortem examination of patient H.M.'s brain based on histological sectioning and digital 3D reconstruction.

Babb, S. J., & Crystal, J. D. (2005). Discrimination of what, when, and where: Implications for episodic-like memory in rats. *Learning and Motivation,* 36(2), 177-189.

Barker, G. R. I., & Warburton, E. C. (2011). When is the hippocampus involved in recognition memory? *The Journal of Neuroscience, 31(29),* 10721-10731.

Basu, J., Zaremba, J. D., Cheung, S. K., Hitti, F. L., Zemelman, B. V., Losonczy, A. & Siegelbaum, S. A. (2016). Gating of hippocampal activity, plasticity, and memory by entorhinal cortex long-range inhibition. *Science, 351(6269),* doi:10.1126/science.aaa5694.

Belblidia, H., Abedlouadoud, A., Jozet-Alves, C., Dumas, H., Freret, T., Leger, M., & Schumann-Bard, P. (2015). Time decay of object, place and temporal order memory in a paradigm assessing simultaneously episodic-like memory components in mice. *Behavioural Brain Research, 286,* 80-84. doi: 10.1016/j.bbr.2015.02.043.

Brown, M. W., & Aggleon, J. P. (2001). Recognition memory: What are the roles of the peririhinal cortex and the hippocampus? *Nature Reviews Neuroscience, 13,* 987-994.

Brun, V. H., Otnaess,. K., Molden, S., Steffenach, H-A., Witter, M. P., Moser, M-B., & Moser, E. I. (2002). Place cells and place recognition maintained by direct entorhinal-hippocampal circuitry. *Science, 296(5576),* 2243-2246.

Brun, V. H., Solstad, T., Kjelstrup, K. B., Fhyn, M., Witter, M. P., Moser, E. I., & Moser, M-B. (2008). Progressive increase in grid scale from dorsal to ventral medial entorhinal cortex. *Hippocampus, 18(12),* 1200-1212.

Burke, S. N., Maurer, A. P., Nematollahi, S., Uprety, A. R., Wallace, J. L., & Barnes, C. A. (2011). The influence of objects on place field expression and size in distal hippocampal CA1. *Hippocampus,21(7),* 783-801.

Burwell, R. D. (2000). The parahippocampal region: Corticocortical connectivity. *Annals of the New York Academy of Sciences, 911,* 25-42.

Burwell, R. D., & Amaral, D. G. (1998). Cortical afferents of the perirhinal, postrhinal, and entorhinal cortice of the rat. *Journal of Comparative Neurology, 398(2)*, 179-205.

Burwell, R. D., Saddoris, M. P., Bucci, D. J., & Wiig, K. A. (2004). Corticohippocampal contributions to spatial and contextual learning. *The Journal of Neuroscience, 24(15)*, 3826-3836.

Bussey, T. J., Duck, J., Muir, J. L., & Aggleton, J. P. (2000). Distinct patterns of behavioural impairments resulting from fornix transection or neurotoxic lesions of the perirhinal and posthrinal cortices in the rat. *Behavioural Brain Research, 111(1-2),* 187-202.

Caballero-Bleda, M. & Witter, M. P. (1993). Regional and laminar organization of projections from the presubiculum, and parasubiculum to the entorhinal cortex: An anterograde tracing study in the rat. *The Journal of Comparative Neurology, 328,* 115-129.

Canto, C. B. & Witter, M. P. (2012a). Cellular properties of principal neurons in the rat entorhinal cortex. I. The lateral entorhinal cortex. *Hippocampus*, *22(6)*, 1256-1276.

Canto, C. B. & Witter, M. P. (2012b). Cellular properties of principal neurons in the rat entorhnal cortex II. The medial entorhinal cortex. *Hippocampus, 22(6),* 1277-1299.

Canto, C. B., Wouterlood, F. G., & Witter, M P. (2008). What does the anatomical organisation of the entorhinal cortex tell us? *Neural Plasticity,* 1-18, http://dx.doi.org/10.1155/2008/381243.

Cappaert, N. L. M., Van Strien, N. M., & Witter, M. P. (2014). *Hippocampal Formation,* The Rat Nervous System (4th Edition). Amsterdam: Elsevier, Academic Press. 511-573.

Chin, J., Massaro, C. M., Palop, J. J., Thwin, M. T., Yu, G-Q., Bien-Ly, N., Bender, A., & Mucke, L. (2007). Reelin depletion in the entorhinal cortex of human amyloid precursor protein transgenic mice and humans with Alzheimer's disease. *Journal of Neuroscience, 27(11),* 2727-2733. doi: https//doi.org/10.1523/jneurosci.3758-06.2007.

Clark, R.E., Zola, S. M., & Squire, L. R. (2000). Impaired recognition memory in rats after damage to the hippocampus. *Journal of Neuroscience, 20,* 8853-8860.

Clayton, N. S., Bussey, T. J., Emery, N. J., & Dickinson, A. (2003). Prometheus to Proust: the case for behavioural criteria for mental time travel. *Trends in Cognitive Neuroscience,* 7(10), 436-437.

Clayton, N. S. & Dickinson, A. (1998). Episodic-like memory during cache recovery by scrub jays. *Nature, 395,* 272-274.

Colgin, L. L., Moser, E. I., & Moser, M-B. (2008). Understanding memory through hippocampal remapping. *Trends in Neurosciences, 31(9),* 469-477.

Corkin, S., Amaral, D. G., Gonzalez, R. G., Johnson, K. A., & Hyman, B. T. (1997). H.M.'s medial temporal lobe lesion: findings from magnetic resonance imaging. *The Journal of Neuroscience, 17(10),* 3964-3979.

Davis, K. E., Easton, A., Eacott, M. J., & Gigg, J. (2013). Episodic-like memory for what-where-which occasion is selectively impaired in the 3xTgAD mouse model of Alzheimer's disease. *Journal of Alzheimer's Disease, 33 (3)*, 681-698. doi: 103233/JAS-2012-121543.

Day, M., Langston, R., & Morris, R. G. M. (2003). Glutamate-receptor-mediated encoding and retrieval of paired-associate learning. *Letters to Nature, 424,* 205-209.

Dere, E., Huston, J. P., & De Souza Silva, M. A. (2005). Episodic-like memory in mice: Simultaneous assessment of object, place and temporal order memory. *Brain Research Protocols,* 16, 10-19.

Derdikman, D., & Moser, E. I. (2014). Spatial maps in the entorhinal cortex and adjacent structures, in D. Derdikman & J. J. Knierim (Eds.), Space, Time and Memory in the Hippocampal Formation (pp. 107-125): Springer.

Deshmukh, S. S., Johnson, J. L., & Knierim, J. J. (2012). Perirhinal cortex represents nonspatial, but not spatial, information in rats foraging in the presence of objects: Comparison with lateral entorhinal cortex. *Hippocampus, 22,* 2045-2058.

Deshmukh, S. S. & Knierim, J. J. (2013). Influence of local objects on hippocampal representations: Landmark vectors and memory. *Hippocampus, 23(4),* 253-267.

Deshmukh, S. S., & Knierim, J. J. (2011). Representation of non-spatial and spatial information in the lateral entorhinal cortex. *Frontiers in Behavioural Neuroscience*, 5, 1-13.

Devito, L. M., & Eichenbaum, H. (2010). Distinct contributions of the hippocampus and medial prefrontal cortex to the 'what-where-when' components of episodic-like memory in mice. *Behavioural Brain Research, 215(2),* 318-325.

Dolorfo, C. L., & Amaral, D. G. (1998a). Entorhinal cortex of the rat: topographic organization of the cells of origin of the perforant path projection to the dentate gyrus. *398(1),* 25-48.

Dolorfo, C. L., & Amaral, D. G. (1998b). Entorhinal cortex of the rat: Organization of intrinsic connections. *The Journal of Comparative Neurology, 398(1),* 49-82.

Eacott, M. J., & Easton, A. (2010). Episodic memory in animals: Remembering which occasion. *Neuropsychologia*, 48, 2273-2280.

Eacott, M. J., & Norman, G. (2004). Integrated memory for object, place and context in rats: a possible mode of episodic-like memory? *Journal of Neuroscience,* 24(8), 1948-1953.

Eichenbaum, H. (2014). Time cells in the hippocampus: a new dimension for mapping memories. *Nature Reviews Neuroscience, 15,* 732-744.

Eichenbaum, H., Sauvage, M., Fortin, N., Komorowski, R., & Lipton, P. (2012). Towards a functional organisation of episodic memory in the medial temporal lobe. Neuroscience & Biobehavioral Reviews, 36, 1597-1608.

Ennaceur, A., & Delacour, J. (1988). A new one-trial test for neurobiological studies of memory in rats. 1: Behavioral data. *Behavioural Brain Research, 31(1)*, 47-59.

Ennaceur, A., Neave, N., & Aggleton, J. P. (1996). Neurotoxic lesions of the perirhinal cortex do not mimic the behavioural effects of fornix transection in the rat. *Behavioural Brain Research, 80(1-2),* 9-25.

Fellini, L., & Morellini, F. (2013). Mice create what-where-when hippocampus-dependent memories of unique experiences. *The Journal of Neuroscience, 33(3),* 1038-1043.

Ferbinteanu, J., Holsinger, R. M. D., & McDonald, R. J. (1999). Lesions of the medial or lateral performant path have different effects on hippocampal contributions to place learning and on fear conditioning to context. *Behavioural Brain Research, 101,* 65-84.

Ferry, B., Ferreira, G., Traissard, N. & Majchrzak, M. (2006). Selective involvement of the lateral entorhinal cortex in the control of the olfactory memory trace during conditioned odor aversions in the rat. *Behavioural Neuroscience, 120(5)*: 1180-1186.

Ferry, B., Herbeaux, K., Javelot, H.& Majchrzak, M. (2015). The entorhinal cortex is involved in conditioned odor and context aversions. *Frontiers in Neuroscience, 2(9),* 342. doi: 10.3389/fnins.2015.00342.

Fortin, N. J., Wright, S. P., & Eichenbaum, H. (2004). Recollection-like memory retrieval in rats is dependent on the hippocampus. *Nature, 431,* 188-191.

Forwood, S. E., Winters, B. D., & Bussey, T. J. (2005). Hippocampal lesions that abolish §spatial maze performance spare object recognition memory at delays of up to 48 hours. *Hippocampus, 15,* 347-355.

Frank, L. M., Brown, E. N., & Wilson, M. (2001). Trajectory encoding in the hippocampus and entorhinal cortex. *Neuron, 27(1),* 169-178.

Fujimaru, Y. & Kosaka, T. (1996). The distribution of two calcium binding proteins, calbindin D-28K and parvalbumin, in the entorhinal cortex of the adult mouse. *Neuroscience Research, 24(4),* 329-343.

Garden, D. L. F., Dodson, P. D., O'Donnel, C., White, M. D., & Nolan, M. F. (2008). Tuning of synaptic integration in the medial entorhinal cortex to the organization of grid cell firing fields. *Neuron, 60(5),* 875-889.

Gaskin, S., Tremblay, A., & Mumby, D. G. (2003). Retrograde and anterograde object recognition. *Hippocampus, 13(8)*, 962-969.

Germroth, P., Schwerdtfeger, W. K., & Buhl, E. H. (1989). Morphology of identified entorhinal neurons projecting to the hippocampus. A light microscopical study combining retrograde tracing and intracellular injection. *Neuroscience, 30(3)*, 683-691.

Gilbert, P. E., Kesner, R. P., & Lee, I. (2001). Dissociating hippocampal subregions: double dissociation between dentate gyrus and CA1. *Hippocampus, 11(6)*, 626-636.

Gomez-Isla, T., Price, J. L., McKeel, D. W., Morris, J. C., Growdon, J. H., & Hyman, B. T. (1996). *Journal of Neuroscience, 16(14),* 4491-4500.

Good, M. A., Barnes, P., Staal, V., McGregor, A., & Honey, R.C. (2007). Context- but not familiarity-dependent forms of object recognition are impaired following excitotoxic hippocampal lesions in rats. *Behavioural Neuroscience, 121(1),* 218-233.

Gould, T. J., Heman, K. L., Mesches, M. H., Young, D. A., Rose, .G. M., & Bickford, P. C. (2002). Effects of hippocampal lesions on patterned motor learning in the rat. *Brain Research Bulletin, 58(6),* 581-586.

Griffen, A. L., Eichenbaum, H., & Hasselmo, M. E. (2007). Spatial representations of hippocampal CA1 neurons are modulated by behavioural context in a hippocampus- dependent memory task. *The Journal of Neuroscience, 27,* 2416-2423.

Haberly, L. B., & Price, J. L. (1978). Association and commissural fiber systems of the olfactory cortex of the rat. I. Systems originating in the piriform cortex and adjacent areas. *Journal of Comparative Neurology, 178 (4)*, 711-740.

Hafting, T., Fhyn, M., Molden, S., Moser, M-B., & Moser, E. I. (2005). Microstructure of a spatial map in the entorhinal cortex. *Nature, 436,* 801-806.

Hales, J. B., Schlesiger, M. I., Leutgeb, J. K., Squire, L. R., Leutgeb, S., & Clark, R. E. (2014). Medial entorhinal cortex lesions only partially disrupt hippocampal place cells and hippocampus-dependent place memory. *Cell Reports, 9(3),* 893-901.

Hamam, B. N., Kennedy, T. E., Alonso, A., Amaral, D. G. (2000). Morphological and electrophysiological characteristics of layer V neurons of the rat medial entorhinal cortex. *The Journal of Comparative Neurology, 418,* 457-472.

Hammond, R. S., Tull, L. E., Stackman, R.W. (2004). On the delay-dependent involvement of the hippocampus in memory. *Neurobiology of Learning & Memory, 82(1)*, 26-34. doi: 10.1016/j.nlm.2004.03.005.

Hargreaves, E. L., Yogaranasimha, D., & Knierim, J. J. (2005). Cohesiveness of spatial and directional representations recorded from neural ensembles in the anterior thalamus, parasubiculum, medial entorhinal cortex and hippocampus. *Hippocampus, 17,* 826-841.

Hartzell, A. L., Burke, S. N., Hoang, L. T., Lister, J. P., Rodriguez, C. N. & Barnes, C. A. (2014). Transcription of the immediate-early gene *Arc* in CA1 of the hippocampus reveals activity differences along the proximodistal axis that are attenuated by advanced age. *Journal of Neuroscience, 33(8),* 3424-3433.

Hayman, R. M. & Jeffrey, K. J. (2008). How heterogenous place cell responding arises from homogenous grid – A contextual gating hypothesis. *Hippocampus, 18(12),* 1301-1313.

Henriksen, E. J., Colgin, L. L., Barnes, C. A., Witter, M. P., Moser, M.B., & Moser, E. I. (2010). Spatial representation along the proximodistal axis of CA1. *Neuron, 68(1),* 127-37. doi: 10.1016/j.neuron.2010.08.042.

Hunsaker, M. R., Chen, V., Trant, G. T., & Kesner, R. P. (2013). The medial and lateral entorhinal cortex contribute to contextual and item recognition memory: A test of the binding of items and context model. *Hippocampus, 23,* 380-391.

Hunsaker, M. R., Mooy, G. G., Swift, J. S., & Kesner, R. P. (2007). Dissociations of the medial and lateral perforant path projections into dorsal DG, CA3, CA1 for spatial and nonspatial (visual object) information processing. *Behavioural Neuroscience, 121(4)*, 742-750.

Hunsaker, M. R., Rosenberg, J. S., & Kesner, R. P. (2008). The role of the dentate gyrus, CA3a,b, and CA3c for detecting spatial and environmental novelty. *Hippocampus, 18(10)*, 1064-1073.

Insausti, R., Herrero, M. T., Witter, M. P. (1997). Entorhinal cortex of the rat: Cytoachitectonic subdivisions and the origin and distribution of cortical efferents *Hippocampus, 7(2)*, 146-183. doi: 10.1002/(SICI)1098-1063(1997)7:2<146::AID-HIPO4>3.0.CO;2-L.

Ito, H. T., & Schuman, E. M. (2012). Functional division of hippocampal area CA1 via modulatory gating of entorhinal cortical inputs. *Hippocampus, 22(2),* 372-387.

Jessberger, S.; Clark, R. E., Broadbent, N. J., Clemenson, G. D., Consiglio, A., Lie, D. C., Squire, L. R., & Gage, F. H. (2009). Dentate gyrus-specific knockdown of adult neurogenesis impairs spatial and object recognition memory in adult rats. *Learning & Memory, 16(2)*, 147-154. doi: 10.1101/lm.1172609.

Johnson, A., & Redish, A. D. (2007). Neural ensembles in CA3 transiently encode paths forward of the animal at decision point. *Journal of Neuroscience, 27(45)*, 12176-12189.

Jones, B. F. & Witter, M. P. (2007). Cingulate cortex projections to the parahippocampal region and hippocampal formation in the rat. *Hippocampus, 17,* 957-976.

Jung, M. W., Wiener, S. I., & McNaughton, B. L. (1994). Comparison of spatial firing characteristics of units in dorsal and ventral hippocampus of the rat. *The Journal of Neuroscience, 14(12),* 7347-7356.

Kart-teke, E., De Souza Silva, M. A., Huston, J. P., & Dere, E. (2006). Wistar rats show episodic-like memory for unique experiments. *Neurobiology of Learning and Memory, 85(2)*, 173-182.

Keene, C. S., Bladon, J., McKenzie, S., Liu, C. D., O'Keefe, J. & Eichenbaum, H. (2016). Complementary functional organization of neuronal activity patterns in the perirhinal, lateral entorhinal, and medial entorhinal cortices. *The Journal of Neuroscience, 36(13),* 3660-3675.

Kerr, K. M., Agster, K. L., Furtak, S. C., & Burwell, R. D. (2007). Functional neuroanatomy of the parahippocampal region: The lateral and medial entorhinal areas. *Hippocampus, 17(9)*, 697-708.

Kesner, R. P., Ravidrathan, A., Jackson, P., Giles, R., & Chiba, A.A. (2001). A neural circuit analysis of visual recognition memory: role of the perirhinal, medial, and lateral entorhinal cortex. *Learning & Memory, 8(2)*, 87-95. doi: 10.1101/lm.29401.

Khan, U. A., Liu, L., Provenzano, F. A., Berman, D. E., Profaci, C. P., Sloan, R., Mayeux, R., Duff, K. E., Small, S. A. (2014). Molecular drives and cortical spread of lateral entorhinal cortex dysfunction in preclinical Alzheimer's disease. *Nature Neuroscience, 17(2)*, 304-311.

Kitamura, T., Pignatelli, M., Suh, J., Kohara, K., Yoshiki, A., Abe, K., & Tonegawa, S. (2014). Island cells control temporal association memory. *Science, 343 (6173)*, 896-901.

Kjelstrup, K. B., Solstad, T., Brun, V. H., Hafting, T., Leutgeb, S., Witter, M. P., Moser, E. I., & Moser, M-B. (2008). Finite scale of spatial representation in the hippocampus. *Science, 321(5885),* 140-143.

Kloosterman, F., Van Haeften. T., Witter, M. P., Lopes Da Silva, F. H. (2003). Electrophysiological characterization of interlaminar entorhinal connections: an essential link for re-entrance in the hippocampal entorhinal system. *European Journal of Neuroscience, 18(11),* 3037-3052.

Knierim, J. J., & Hamilton, D. A. (2011). Framing spatial cognition: Neural representations of proximal and distal frames of references and their roles in navigation. *Physiological Reviews, 91(4),* 1245-1279.

Knierim, J. J., Lee, I., & Hargreaves, E. L. (2006). Hippocampal place cells: Parallel input streams, subregional processing, and implications for episodic memory. *Hippocampus,* 16, 755-764.

Kohler, C. (1986). Intrinsic connections of the retrohippocampal region in the rat brain. II. The medial entorhinal area. *Journal of Comparative Neurology, 246(2)*, 149-169.

Kohler, C. (1988). Intrinsic connections of the retrohippocampal region in the rat brain. III. The lateral entorhinal area. *Journal of Comparative Neurology, 271, (2),* 208-228.

Komorowski, R. W., Manns, J. R., & Eichenbaum, H. (2009). Robust conjunctive item-place coding by hippocampal neurons parallels learning what happens where. *Journal of Neuroscience, 29(31),* 9918-9929.

Kondo, H. & Witter, M. P. (2014). Topographic organisation of orbitofrontal projections to the parahippocampal region in rats. *Journal of Comparative Neurology, 522(4),* 772-793.

Kosel, K. C., Van Hoesen, G. W., & West, J. R. (1981). Olfactory bulb projections to the parahippocampal area of the rat. *Journal of Comparative Neurology, 198(3)*, 467-482. Ku, S-P., Nakamura, N. H., Maingret, N., Mahnke, L., Yoshida, M. & Sauvage, M. M. (2017). Regional specific evidence for memory-load dependent activity in the dorsal subiculum and the lateral entorhinal cortex. *Frontiers in Systems Neuroscience,* doi: https://doi.org/10.3389/fn-sys.2017.00051.

Kropff, E., Carmichael, J. E., Moser, M. B., & Moser, E. I. (2015). Speed cells in the medial entorhinal cortex. *Nature, 523,* 419-424.

Ku, S-P., Nakamura, N. H., Maingret, N., Mahnke, L., Yoshida, M., & Sauvage, M. M. (2017). Regional specific evidence for memory-load dependent activity in the dorsal subiculum and lateral entorhinal cortex. *Frontiers in Systems Neuroscience, 11(30),* https://doi.org/10.3389/fnsys.2017.00051

Kubie, J. L., & Ranck, J. B. (1983). Sensory-behavioural correlates of individual hippocampal neurons in three situations: Space and Context. In W. Seifert (Ed.), Neurobiology of the Hippocampus (433-447): Academic Press: New York, New York.

Kuruvilla, M. V. & Ainge, J. A. Lateral entorhinal cortex lesions impair local spatial frameworks. *Frontiers in Systems Neuroscience, 11(30),* doi: 10.3389/fnsys.2017.00030.

Langston, R. F., & Wood, E. R. (2010). Associative recognition and the hippocampus: Differential effects of hippocampal lesions on object-place, object-context, and object- place-context memory. *Hippocampus, 20(10),* 1139-1153.

Larkin, M. C., Lykken, C., Tye, L. D., Wickelgren, J. G., & Frank, L. M. (2014). Hippocampal outputarea CA1 broadcasts a generalized novelty signal during an object-place recognition task. *Hippocampus, 24(7),* 773-783.

Lee, I., Hunsaker, M. R., & Kesner, R.P. (2005). The role of hippocampal subregions in detecting spatial novelty. *Behavioral Neuroscience, 119(1),* 145-153.

Lee, I., Yoganarasimha, D, Rao, G., & Knierim, J. J. (2004). Comparison of population coherence of place cells in hippocampal subfields CA1 and CA3. *Nature, 430,* 456-459.

Leitner, F. C., Melzer, S., Lutcke, H., Pinna, R., Seeburg, P. H., Helmchen, F., & Monyer, H. (2016). Spatially segregated feedforward and feedback neurons support differential odor processing in the lateral entorhinal cortex. *Nature Neuroscience.* doi:10.1038/nn.4303.

Lenck-Santini, P.P., Rivard, B., Muller, B. U., & Poucet, B. (2005). Study of CA1 place cell activity and exploratory behaviour following spatial and nonspatial changes in the environment. *Hippocampus, 15(3),* 356-369.

Leutgeb, S., Leutgeb, J. K., Barnes, C. A., Moser, E. I., & McNaughton, B. L., & Moser, M-B. (2005b). Independent codes for spatial and episodic memory in hippocampal neuronal ensembles. *Science, 309,* 619-623.

Leutgeb, J. K., Leutgeb, S.., Treves, A., Meyer, R., Barnes, C. A., McNaughton, B. L., Moser, M-B., & Moser, E. I. (2005a). Progressive transformation of hippocampal neuronal representations in 'morphed' environments. *Neuron, 48(2),* 345-358.

Leutgeb, S., Leutgeb, J. K., Treves, A., Moser, M-B., & Moser, E. I. (2004). Distinct ensemble codes in hippocampal areas CA3 and CA1. *Science, 305 (5688),* 1295-1298.

Link, E., Edelmann, L., Chou, J. H., Binz, T., Yamasaki, S., Eisel, U., Baumen, M., Sudhof, T.C., Niemann, H., & Jahn, R. (1992). Tetanus toxin action: Inhibition of neurotransmitter release linked to synaptobrevin proteolysis. *Biomedical and Biophysical Research Communications, 189 (2),* 1017-1023.

Lu, L., Igarashi, K. M., Witter, M. P., Moser, E. I. & Moser, M-B. (2015). Topography of place maps along the CA3-toCA2 axis of the hippocampus. *Neuron, 87(5),* 1078-1092.

Lu, L., Leutgeb, J. K., Tsao, A., Henriksen, E. J., Leutgeb, S., Barnes, C. A., Witter, M. P., Moser, M-B., & Moser, E. I. (2013). Impaired hippocampal rate coding after lesions of the lateral entorhinal cortex. *Nature Neuroscience, 16,* 1085-1093.

Maass, A., Schutze, H., Speck, O., Yonelinas, A., Tempelmann, C., Heinze, H-J., Berron, D., Cardenas-Blanco, A., Brodersen, K. H., Stephan, K. E. & Duzel, E. (2014). Laminar activityin the hippocampus and entorhinal cortex related to novelty and episodic encoding. *Nature Communications, 5,* doi:10.1038/ncomms6547.

Macdonald, C. J., Lepage, K. Q., & Eden, U. T., & Eichenbaum, H. (2011). Hippocampal 'time cells' bridge the gap in memory for discontiguous events. *Neuron, 71(4),* 571-573.

Mallory, C. S., Hardcastle, K., Bant, J. S., & Giocomo, L. M. (2018). Grid scale drives the scale and long-term stability of place maps. *Nature Neuroscience, 21,* 270-282.

Manns, J. R., Howard, M.W., & Eichenbaum, H. (2007). Gradual changes in hippocampal activity support remembering the order of events. *Neuron, 56(3),* 530-540.

Masurkar, A. V., Srinivas, K. V., Brann, D. H., Warren, R., Lowes, D. C., & Siegelbaum, S. A. (2017). Medial and lateral entorhinal cortex differentially excite deep versus superficial CA1 pyramidal neurons. *Cell Reports, 18(1),* 148-160.

Matthiasen, M. L., Hansen, L., & Witter, M. P. (2015). Insular projections to the parahippocampal region in the rat. *Journal of Comparative Neurology, 523,* 1379-1398.

McClure, C., Cole, K.L.H., Wulff, P., Klugmann, M., & Murray, A. J. (2011). Production and titreing of recombinant adeno-associated viral vectors. *Journal of Visualised Experiments,* 57, 3348. doi: 10.3791/3348.

McNaughton, B. L., Battaglia, F. P., Jensen, O., Moser, E. I., & Moser, M.B. (2006). Path integration and the neural basis of the 'cognitive map'. *Nature Reviews Neuroscience, 7,* 663-678.

Moita, M. A. P., Rosis, S., Zhou, Y., LeDoux, J., & Blair, H. T. (2004). Putting fear in its place: Remapping of hippocampal place cells during fear conditioning. *Journal of Neuroscience, 24(31),* 7015-7023.

Moser, E. I., Kroff, E., & Moser, M-B. (2008). Place cells, grid cells, and the brains spatial representation system. *Annual Review of Neuroscience, 31,* 69-89.

Muller, R. U. & Kubie, J. L. (1987). The effects of changes in the environment on the spatial firing of hippocampal complex-spike cells. *The Journal of Neuroscience, 7(7),* 1951-68.

Mumby, D. G., Glenn, M. J., Nesbitt, C., & Kyriazis, D. A. (2002). Dissociation in retrograde memory for object discriminations and object recognition in rats with perirhinal cortex damage. *Behavioural Brain Research, 132(2),* 215-226.

Murray, E. A., Bussey, T. J., & Saksida, L. M. (2007). Visual perception and memory: A new view of medial temporal lobe function in primates and rodents. *Annual Review of Neuroscience, 30,* 99-122.

Murray, A. J., Sauer, J-F., Riedel, G., McClure, C., Ansel, L., Cheyne, L., Bartos, M., Wisden, W., & Wulff, P. Parvalbumin-positive CA1 interneurons are required for spatial working but not for reference memory. *Nature Neuroscience, 14,* 297-299. doi:10.1038/nn.2751.

Naber, P. A., Caballero-Bleda, M., Jorritsma-Byham, B., & Witter, M. P. (1997). Parallel input to the hippocampal memory system through peri- and postrhinal cortices. *Neuroreport, 8,* 2617-2621.

Naber, P. A., Lopes da Silva, F. H., & Witter, M. P. (2001). Reciprocal connections between the entorhinal cortex and hippocampal fields CA1 and the subiculum are in register with the projections from CA1 to the subiculum. *Hippocampus, 11(2),* 99-104.

Nakamura, N. H., Flasbeck, V., Maingret, N., Kitsukawa, T. & Sauvage. (2013). Proximodistal segregation of nonspatial information in CA3: Preferential recruitment of a proximal CA3-distal CA1 network in nonspatial recognition memory. *The Journal Neuroscience, 33(28)*, 11506-11514.

Nakazawa, Y., Pevzner, A., Tanaka, K. Z., & Wiltgen, B. J. (2016). Memory retrieval along the proximodistal axis of CA1. *Hippocampus, 26(9),* 1140-1148.

Neunnebel, J. P., & Yoganarasimha, D., Rao, G. & Knierim, J. J. (2013). Conflicts between local and global spatial frameworks dissociate neural representations of the lateral and medial entorhinal cortex. *The Journal of Neuroscience, 33(22),* 9246-9258.

Norman, G. & Eacott, M. J. (2005). Dissociable effects of lesions to the perirhinal cortex and the postrhinal cortex on memory for context and objects in rats. *Behavioral Neuroscience, 119(2),* 557-566.

O'Keefe, J. (1976). Place units in the hippocampus of the freely moving rat. *Experimental Neurology, 51(1),* 78-109.

O'Keefe, J., & Conway, D. H. (1978). Hippocampal place units in the freely moving rats: Why they fire where they fire. *Experimental Brain Research, 31(4),* 573-590.

O'Keefe, J., & Dostrovsky, J. (1971). The hippocampus as a spatial map: Preliminary evidence from unit activity in the freely-moving rat. *Brain Research, 34,* 171-175.

O'Keefe, J., & Nadek, L. (1978). The Hippocampus as a Cognitive Map. Oxford University Press.

Olsen, G. M., Ohara, S., Lijima, T., & Witter M. P. (2017). Parahippocampal and retrosplenial connections of rat posterior parietal cortex. *Hippocampus, 27(4)*, 335-358.

Olton, D. S., Branch, M., & Best, P. J. (1978). Spatial correlates of hippocampal unit activity. *Experimental Neurology, 58(3),* 387-409.

Pilkiw, M., Insel, N., Cui, Finney, C., Morissey, M. D. & Takehara-Nishiuchi, K. (2017) Phasic and tonic neuron ensemble codes for stimulus-environment conjunctions in the lateral entorhinal cortex. *eLife.* DOI: 10.7554/eLife.28611.001.

Ramsden, H. L., Surmeli, G., McDonagh, S. G., & Nolan, M. F. (2015). Laminar and dorsoventral molecular organization of medial entorhinal cortex revealed by large-scale analysis of gene expression. *PLOS Computational Biology,* https://doi.org/10.1371/journal.pcbi.1004032.

Rodo, C., Sargolini, F., & Save, E. (2017). Processing of spatial and non-spatial information in rats with lesions of the medial and lateral entorhinal cortex: Environmental complexity matters. *Behavioural Brain Research, 320,* 200-209.

Save, E., Poucet, B., Foreman, N., & Buhot, M. C. (1992). Object exploration and reactions to spatial and nonspatial changes in rats following damage to parietal cortex or hippocampal formation. *Behavioural Neuroscience, 106(3)*, 447-456.

Savelli, F., Yoganarasima, D., & Knierim, J. J. (2008). Influence of boundary removal on the spatial representations of the medial entorhinal cortex. *Hippocampus, 18,* 8455-8466.

Save, E. & Sargolini, F. (2017). Processing of spatial and non-spatial information: Contribution of lesion studies. *Frontiers in System Neuroscience,* https://doi.org/10.3389/fnsys.2017.00081

Schiavo, G., Benfenati, F., Poulain, B., Rossetto, O., Polverino de Laureto, P., DasGupta, B.R., & Montecucco, C. (1992). Tetanus and botulinum-B neurotoxins block neurotransmitter release by proteolytic cleavage of synaptobrevin. *Nature, 359,* 832-835.

Schmidt, B., Satvat, E., Argraves, M., Markus, E. J., & Marrone, D. F. (2012). Cognitive demands induce selective hippocampal reorganization: *Arc* expression in a place and response task. *Hippocampus, 22(11),* 2114-2126.

Scaplen, K. M., Ramesh, R. N., Nadvar, N., Ahmed, O. J. & Burwell, R. D. Inactivation of the lateral entorhinal area increases the influence of visual cues on hippocampal place cell activity. *Frontiers in Systems Neuroscience, 11 (40),* doi: 10.3389/fnsys.2017.00040.

Scoville, W. B., & Milner, B. (1957). Loss of recent memory after bilateral hippocampal lesions. *Journal of Neurology, Neurosurgery, & Psychiatry, 20,* 11-21.

Shipton, O.A., El-Gaby, M., Apergis-Schoute, J., Diesseroth, K., Bannerman, D. M., Paulsen, O., & Kohl, M. M. (2015). Left-right dissoctiaton of hippocampal memory processes in mice. *PNAS, 11,* 15238-15243, doi: 10.1073/pnas.1405648111.

Skaggs, W. E., & McNaughton, B. L. (2006). Spatial firing properties of hippocampal CA1 populations in an environment contains two visually identical regions. *The Journal of Neuroscience, 18(2)),* 8455-8466.

Smith, D. M., & Mizumori, S. J. Y. (2006). Learning-related development of context-specific neuronal responses to places and events: The hippocampal role in context processing. *Journal of Neurosience, 26(12),* 3154-3163.

Solstad, T., Boccara, C. N., Kropff, E., Moser, M-B., & Moser, E. I. (2008). Representation of geometric borders in the entorhinal cortex. *Science, 322,* 1865-1868.

Solstad, T., Moser, E. I., & Moser, E. I. (2006). From grid cells to place cells: A mathematical model. *Hippocampus, 16,* 1026-1031.

Spiers, H. J., Burgess, N., Hartley, T., Vargha-Khadem, F., & O'Keefe, J. (2001). Bilateral hippocampal pathology impairs topographical and episodic memory by not visual pattern matching. *Hippocampus, 11(6),* 715-725.

Spiers, H. J., Burgess, N., Maguire, E. A., Baxendale, S. A., Hartley, T., Thompson, P. J., & O'Keefe, J. (2001). Unilateral temporal lobectomy patients show lateralized topographical and episodic memory deficits in a virtual town. *Brain, 124(12),* 2476-2489.

Spiers, H. J., Maguire, E. A., & Burgess, N. (2001). Hippocampal amnesia. *The Neural Basis of Cognition, 7(5),* 357-382.

Steffenach, H-A., Witter, M., Moser, M-B., & Moser, E-I. (2005). Spatial memory in the rat required the dorsolateral band of the entorhinal cortex. *Neuron, 45(7)*, 301-313.

Stranahan, A. M., Haberman, R.P., & Gallagaher, M.(2011a). Cognitive decline is associated with reduced reelin expression in the entorhinal cortex of aged rats. *Cerebral Cortex, 21(2)*, 392-400. doi: 10.1093/cercor/bhq106.

Stranahan, A. M., Mattson, M. P. (2010). Selective vulnerability of neurons in layer II of the entorhinal cortex during aging and Alzheimer's disease. *Neural Plasticity,* doi:10.1155/2010/108190.

Stranahan, A. M., Salas-Vaga, S., Jiam, N. T., & Gallagher, M. (2011b). Interference with reelin signalling in the lateral entorhinal cortex impairs spatial memory. *Neurobiology of Learning & Memory, 96(2),* 150-155. doi: 10.1016/j.nlm.2011.03.009.

Suddendorf, T., & Busby, J. (2003). Mental time travel in animals? Trends in Cognitive Sciences, 7, 391-396.

Suddendorf, T., & Corballis, M. C. (2007). The evolution of foresight: What is mental time travel, and is it unique to humans? Behavioral and Brain Sciences, 30, 299-313.

Suh, J., Rivest, A. J., Nakashiba, T., Tominaga, T., Tonegawa, S. (2011). Entorhinal cortex layer III input to the hippocampus is critical for temporal association memory. *Science, 334(6061),* 1415-1420.

Surmeli, G., Marcu, D. C., McClure, C., Garden, D. L. F., Pastoll, H., & Nolan, M. F. Molecularly defined circuitry reveals input-output segregation in deep layers of the medial entorhinal cortex. *Neuron, 88(5),* 1040-1053.

Tahvildari, B., & Alonso, A. (2005). Morphological and electrophysiological properties of lateral entorhinal cortex layers II and III principal neurons. *Journal of Comparative Neurology, 491(2),* 123-140.

Tanninen, S. E., Morissey, M. D. & Takaehara-Nishiuchi, K. (2013). Unilateral lateral entorhinal inactivation impairs memory expression in trace eyeblink conditioning. *PLoS One, 8(12)*, doi: 10.1371/journal.pone.0084543.

Tang, Q., Ebbese, C L., Sanguinetti-Scheck, J. I., Preston-Ferrer, P., Gundfinger, A., Winterer, J.,Beed, P., Ray, S., Naumann, R., Schmitz, D., Brecht, M., & Burgalossi, A. (2015). Anatomical organisation and spatiotemporal firing patterns of layer 3 neurons in the rat medial entorhinal cortex. *Journal of Neuroscience, 35(36)*, 12346-12354.

Tamamaki, N., & Nojyo, Y. (1995) Preservation of topography in the connections between the subiculum, field CA1, and the entorhinal cortex in rats. *Journal of Computational Neurology, 353,* 379-390.

Taube, J. S. (1998). Head direction cells and the neurophysiological basis for a sense of direction. *Progress in Neurobiology, 55,* 225-256.

Tennant, S. A., Fischer, L., Garden, D. L. F., Gerlei, K. Z., Martinez-Gonzalez, C., McClure, C., Wood, E., & Nolan, M. F. (2018). Stellate cells in the medial entorhinal cortex are required for spatial learning. *Cell Reports, 22(5),* 1313-1324.

Tolman, E. C. (1948). Cognitive maps in rats and men. *Psychological Review, 55*(4), 189-208

Tsao, A., Moser, M-B., & Moser E.I. (2013). Traces of experience in the lateral entorhinal cortex. *Current Biology, 23,* 399-405.

Tulving, E. (1983). Elements of episodic memory. Oxford: Claredon.

Tulving, E. (1985). Memory and consciousness. *Canadian Psychology,* 26, 1-12.

Van Cauter, T., Camon, J., Averabe, A., Eduayen, C., Sargolini, F., & Save, Etienne. (2012). Dstinct roles of medial and lateral entorhinal cortex in spatial cognition. *Cerebral Cortex, 23,* 451-459. doi: 10.1093/cercor/bhs033.

Van Cauter, T., Poucet, B., & Save, E. (2008). Unstable CA1 place cells representation in rats with entorhinal cortex lesions. *European Journal of Neuroscience, 27(8),* 1933-1946.

Van Haeften, T., Baks-te-Bulter, L., Goede, P. H., Wouterlood, F. G., & Witter, M. P. (2003). Morphological and numerical analysis of synaptic interactions between neurons in deep and superficial layers of the entorhinal cortex of the rat. *Hippocampus, 13(8),* 943-952.

Van Groen, T., & Wyss, J. M. (1992). Connections of the retrosplenial dysgranular cortex in the rat. *Journal of Comparative Neurology, 315(2)*, 200-216.

Van Strien, N. M., Cappaert, N. L., & Witter, M. P. (2009). The anatomy of memory: an interactive overview of the parahippocampal-hippocampal network. *Nature Reviews Neuroscience, 10(4),* 272-282.

Varga, C. Lee, S. Y., & Soltesz, I. (2010). Target-selective GABAergic control of entorhinal cortex output. *Nature Neuroscience, 13,* 822-824.

Vargha-Khadem, F., Gadian, D. G., Watkins, K. E., Connelly, A., Van Paescheen, W., & Mishkin, M. (1997). Differential effects of early hippocampal pathology on episodic and semantic memory. Science, 277, 376-380.

Veyrak, A., Allerborn, M., Gros, A., Michon, F., Raguet, L., Kenney, J., Godinot, F., Thevent, M., Garcia, S., Messaoudi, B., Laroche, S., & Ravel, N. (2015). Memory of occasional events in rats: Individual episodic memory profiles, flexibility, and neural substrate. *Journal of Neuroscience, 35(19),* 7575-7586.

Wan, H., Aggleton, J. P., & Brown, M. W. (1999). Differential contributions of the hippocampus and perirhinal cortex to recognition memory. *The Journal of Neuroscience, 19,* 1142-1148.

Wilson, D. I. G., Langston, R. F., Schlesiger, M. I., Wagner, M., Watanabe, S. & Ainge, J. A. (2013a). Lateral entorhinal cortex is critical for novel object-context recognition. *Hippocampus, 23(5),* 352-366.

Wilson, D. I. G, Watanabe, S., Milner, H., & Ainge, J. A. (2013b). Lateral entorhinal cortex is necessary for associative but not nonassociative recognition memory. *Hippocampus, 23 (12),* 1280-1290.

Winters, B. D. & Bussey, T. J. (2005). Glutamate receptors in perirhinal cortex mediate encoding, retrieval, and consolidation of object recognition memory. *The Journal of Neuroscience, 25(17),* 4243-4251.

Winters, B. D., Forwood, S. E., Cowell, R. A., Saksida, L. M., & Bussey, T. J. (2004). Double dissociation between the effects of peri-postrhinal tests of object recognition and spatial memory: Heterogeneity of function within the temporal lobe. *The Journal of Neuroscience, 24,* 5901-5908.

Witter, M. P., Naber, P. A., van Haeften, T., Machielsen, W. C. M., Rombouts, S. A. R. B., Barkhof, F., Scheltens, P., & Lopes da Silva, F. (2000). Cortico-hippocampal communication by way of parallel parahippocampal-subicular pathways. *Hippocampus, 10*, 398-410.

Witter, M. P. (2007). The perforant path: projections from the entorhinal cortex to the dentate gyrus. *Progress in Brain Research, 163,* 43-61.

Witter, M. P., & Amaral, D. G. (2004). The hippocampal region. The Rat Nervous System, 637-703.

Witter, M. P., Doan, T. P., Jacobsen, B., Nilssen, E. S., & Ohara, S. (2017). Architecture of the entorhinal cortex: A review of entorhinal anatomy in rodents with some comparative notes. *Frontiers in Systems Neuroscience,* https://doi.org/10.3389/fnsys.2017.00046.

Witter, M. P., Naber, P. A., van Haeften, T., Machielsen, W. C. M., Rombouts, S. A. R. B., Barkhof, F., Scheltens, P., & Lopes da Silva, F. H. (2000a). Cortico-hippocampal communication by way of parallel parahippocampal-subicular pathways. *Hippocampus, 10*, 398-410.

Wood, E. R., & Dudchenko, P. A., & Eichenbaum, H. (1999). The global record of memory in hippocampal neuronal activity. *Nature, 397,* 613-616.

Wood, E. R., Dudchenko, P. A., & Robitesk, R. J., & Eichenbaum, H. (2000). Hippocampal neurons encode information about different types of memory episodes occurring in the same location. *Neuron, 27(3),* 623-633.

Wouterlood, F. G., Hartig, W., Bruckner, G., & Witter, M. P. (1995). Parvalbumin-immunoreactive neurons in the entorhinal cortex of the rat: localisation, morphology, connectivity, and ultrastructure. *Journal of Neurocytology, 24(2)*, 135-153.

Yassa, M. A. & Stark, C. E. L. (2011). Pattern separation in the hippocampus. *Trends in Neurosciences, 34(10),* 515-525.

Yogaranashima, D. Rao, G., & Knierim, J. J. (2011). Lateral entorhinal neurons are not spatially selective in cue-rich environments. *Hippocampus, 12,* 1263-1374.

Yoo, S. & Lee, I. (2017). Functional double dissociation within the entorhinal cortex for visual scene-dependent choice behaviour. *eLife,* doi: 107554/eLife.21543.001.

Young, B. J., Otto, T., Fox, G. D., & Eichenbaum, H. (1997). Memory representations within the parahippocampal region. *Journal of Neuroscience, 17(13),* 5183-5195.

Xiang, J. Z. & Brown, M. W. (1999). Differential neuronal responsiveness in primate perirhinal cortex and hippocampal formation during performance of a conditional visual discrimination task. *The Journal of Neuroscience, 11,* 3715-3724.

Zhu, X. O., McCabe, B. J., Aggleton, J. P., & Brown, M. W. (1997). Differential activation of the rat hippocampus and perirhinal cortex by novel visual stimuli and a novel environment. *Neuroscience Letters, 229,* 141-143.

Zola-Morgan, S., Squire, I. R., Amaral, D. G., Susuki, W. A. (1989). Lesions of the perirhinal and parahippocampal cortex that spare the amygdala and hippocampal formation produce severe memory impairments. *The Journal of Neuroscience, 9,* 4355-4370.

Appendix A

Proportion of Remapping Cells by Individual Animal

Table A.2

Proportions of place cells which demonstrated a remapping response to object displacement

Animal	Drive Location	Number of Remapping Cells	Proportion (%)
15048	Distal CA1	25/75	33.3
15056	Distal CA1	19/46	41.3
15049	Distal CA1	40/106	45.3
17047	Distal CA1	3/3**	100.0
15099	Distal CA1	1/3**	33.3
15049	Proximal CA1	13/23	56.5
15096	Proximal CA1	11/27	40.7
15098	Proximal CA1	0/2**	0.0

Note: Animals with implants which yielded < 5 cells are denoted by a double asterisk (**). Animal 15049 had bilateral implants across hemispheres, with drives aimed at distal and proximal CA1, respectively. All proportion values are rounded to the nearest decimal point.

Proportion of Types of Remapping by Individual Animal

Table A.3

Proportions of place cells which demonstrated each type of remapping

Animal	Drive Location	Novel Location	Disrupted	New Field/ Field Shift	Lost Field
15048	Distal CA1	52.0	12.0	12.0	24.0
15056	Distal CA1	31.6	15.8	15.8	36.8
15049	Distal CA1	25.0	22.5	35.0	17.5
17047	Distal CA1	33.3	0.0	0.0	66.6
15099	Distal CA1	0.0	0.0	100.0	0.0
15049	Proximal CA1	30.8	30.8	15.4	23.1
15096	Proximal CA1	27.3	36.4	27.3	9.1
15098	Proximal CA1	0.0	0.0	0.0	0.0

Note: Animals with implants which yielded < 5 cells are denoted by a double asterisk (**). Animal 15049 had bilateral implants across hemispheres, with drives aimed at distal and proximal CA1, respectively. All values are rounded to the nearest decimal point.

Appendix C

Proportion of Trace Cells by Individual Animal

Table A.3

Proportions of place cells which demonstrated trace firing in response to object displacement

Animal	Drive Location	Number of Trace Cells	Proportion (%)
15048	Distal CA1	10/75	13.3
15056	Distal CA1	9/46	19.6
15049	Distal CA1	20/106	18.9
17047	Distal CA1	1/3**	33.3
15099	Distal CA1	2/3**	66.7
15049	Proximal CA1	7/23	30.4
15096	Proximal CA1	4/27	14.8
15098	Proximal CA1	0/2**	0.0

Note: Animals with implants which yielded < 5 cells are denoted by a double asterisk (**). Animal 15049 had bilateral implants across hemispheres, with drives aimed at distal and proximal CA1, respectively. All proportion values are rounded to the nearest decimal point.

Appendix D

Proportion of Trace Cells Types by Individual Animal

Table A.3

Proportions of cells which demonstrated each type of trace behaviour

Animal	Drive Location	Proportion of Misplace Cells	Proportion of Remap & Trace	Proportion of Trace
15048	Distal CA1	30.0	40.0	30.0
15056	Distal CA1	22.2	44.4	33.3
15049	Distal CA1	60.0	30.0	20.0
17047	Distal CA1	0.0	0.0	100.0
15099	Distal CA1	0.0	50.0	50.0
15049	Proximal CA1	42.9	42.9	14.3
15096	Proximal CA1	75.0	25.0	0.0
15098	Proximal CA1	0.0	0.0	0.0

Note: Animals with implants which yielded < 5 cells are denoted by a double asterisk. Animal 15049 had bilateral implants across hemispheres, with drives aimed at distal and proximal CA1, respectively. Two cells recorded from animal 15049 demonstrated misplace and trace behaviour. All values are rounded to the nearest decimal point.

Appendix E

Borders of the Lateral Entorhinal Cortex Along the Dorsoventral Axis
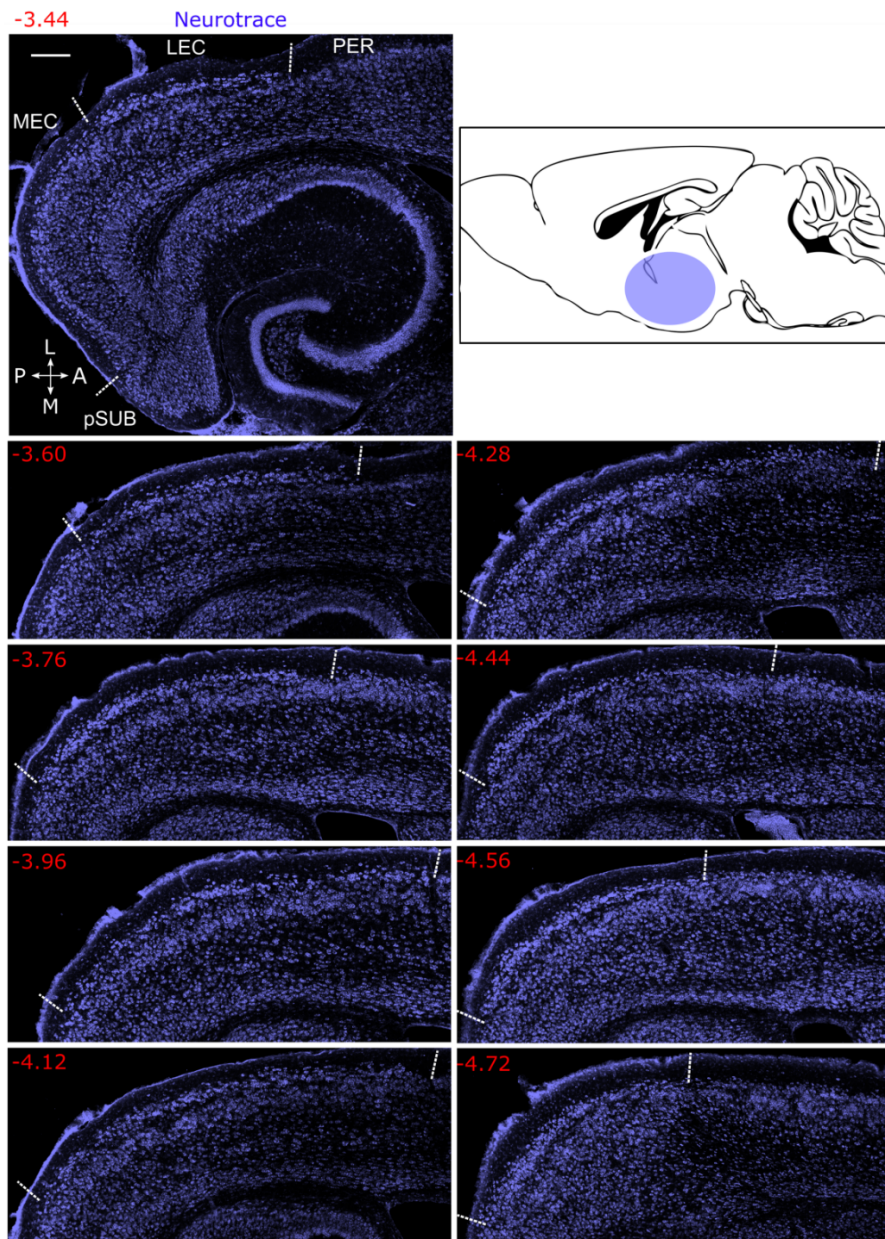

Figure A.1: Borders of the lateral entorhinal cortex along the dorsoventral axis. White lines indicate LEC borders in horizontal brain sections. Scale bar indicates 250 μm. Red digits indicate coordinates in mm from bregma. Neurons are counterstained with Neurotrace (violet). Most extreme dorsal (-3.28) and ventral (-4.88, -5.02) are not displayed. Top Right: Purple overlay indicates approximate location of LEC in a mouse brain. Abbrevations: PER, perirhinal cortex; LEC, lateral entorhinal cortex; MEC, medial entorhinal cortex; pSUB, parasubiculum.

Appendix F

Summary of Analysis Post Exclusion of Damaged Tissue

Table A.5

Summary of analysis post exclusion of damaged tissue

Task	TeLC x̄ D'	GFP x̄ DI'	TeLC v GFP
NOR	0.21	0.40	$P = 0.011$*
OP	0.04	0.09	$P = 0.404$
OC	0.10	0.15	$P = 0.258$
OPC	-0.05	0.12	$P = 0.009$**

Note: Columns labelled 'TeLC x̄ D'' and 'GFP x̄ DI'' contain average discrimination ratios for each task. Column labelled 'TeLC v GFP' contains *P* values for a univariate ANOVA comparing discrimination ratios with group (TeLC or GFP) as a between-subjects factor. Asterisks indicates values of statistical significance (* = $P < 0.05$, ** = $P < 0.01$).